TÉCNICO LISBOA

Synthesis and Characterization of Novel Monophasic Hybrid Membranes of Cellulose Acetate by Co-polymerization with Tetraethyl Orthosilicate and 3-(Aminopropyl)triethoxysilane

Miguel Alexandre Nobre Figueiredo Lopes

Thesis to obtain the Master of Science Degree in

Chemical Engineering

Supervisors: Dr. Mónica Cristina Faria Besteiro, IST-UL
Dr. Maria Clara Henriques Baptista Gonçalves, IST-UL

Examination Committee

Chairperson: Full Prof. Francisco Manuel Da Silva Lemos
Supervisor: Dr. Mónica Cristina Faria Besteiro, IST-UL
Members of the Committee: Dr. Ana Sofia de Oliveira Figueiredo
Dr. Mónica Cristina Faria Besteiro

July 2021

Acknowledgments

First, I would like to thank my mentors for their support throughout this journey. Not only did they transmit knowledge, but they also put my academic, personal, and emotional skills to the test. I would also like to emphasize the support of all the students in the membrane laboratory at the Instituto Superior Técnico de Lisboa.

To my parents, and friends, who were my rock and source of unconditional support. Finally, and perhaps the most special thanks, to my grandmother, who raised and educated me to pursue and conquer my dreams. Although she's no longer present, I dedicate this work to you, and from the bottom of my heart, thank you.

Abstract

Cellulose acetate membranes were one of the pioneer membranes targeted for structural modifications. In this work, hybrid membranes of cellulose acetate, silica, and amine, were synthesized by the phase inversion method and sol-gel process, in an acidic medium. Various molar compositions, of unfunctionalized silica and functionalized silica with amine, of 100/0, 95/5, 90/10, 80/20, 70/30, and 50/50 were tested. Morphological characterization via SEM proves the linear increase in the total membrane thickness with the increase in the molar amine content, and that the silica-amine functionalization did not affect the membranes' skinned asymmetric character. SEM images prove the presence of clusters in the active layer that influence the hydraulic permeability but do not affect the thickness of the membrane. Furthermore, clusters present on the bottom layer have no impact on mechanical properties. Mechanical properties show that the Young modulus increases and the rupture elongation decrease as the amine content increases, while the rupture strength remains constant. Permeation tests reveal an increase in hydraulic permeability with increasing amine content and with decreasing number of clusters and their total area in the active layer. In terms of molecular exclusion rate, it decreases with the introduction of amine. For higher compositions than A90/10 the MWCO increases and then decreases from A80/20to A70/30, remaining constant afterward. Amine functionalization, under pH$<$5, translates into an increase in hydraulic permeability when compared to cellulose acetate and cellulose acetate, and silica membranes. In terms of applicability in blood purification treatments, synthesized amine membranes have great potential.

Keywords

Cellulose acetate, Silica, Amine, Membrane Functionalization, Sol-Gel

Resumo

Membranas de acetato de celulose foram pioneiras no âmbito de modificações estruturais. Neste trabalho, membranas híbridas de acetato de celulose, sílica e amina, foram sintetizadas, pelo método de inversão de fases e processo sol-gel, em meio ácido, com composições molares, de sílica não funcionalizada e sílica funcionalizada com amina, 100/0, 95/5, 90/10, 80/20, 70/30 e 50/50. A caracterização morfológica via SEM comprova o aumento linear da espessura da membrana com o aumento de amina, e que a funcionalização não afetou a assimetria das membranas. Imagens SEM comprovam a presença de clusters na camada ativa que influenciam a permeabilidade hidráulica. Clusters presentes na camada porosa não têm impacto nas propriedades mecânicas. As propriedades mecânicas revelam que o módulo de Young aumenta e o alongamento de rutura diminui à medida que o conteúdo de amina aumenta, enquanto a resistência à rutura permanece constante. Testes de permeabilidade revelam um aumento da permeabilidade hidráulica com o aumento do grupo amina, com a diminuição do número de clusters e da área total por eles ocupado na camada ativa. Funcionalização com o grupo amina traduz-se num aumento da permeabilidade quando comparada a membranas de acetato de celulose e acetato de celulose com sílica. Em termos da taxa de exclusão molecular, diminui com a introdução da amina. Para composições superiores a A90 / 10, o MWCO aumenta, diminuindo de A80 / 20 para A70 / 30, permanecendo constante posteriormente. Em termos de aplicabilidade em tratamentos de purificação do sangue, as membranas com funcionalizadas com amina apresentam potencial.

Palavras Chave

Acetato de celulose, Sílica, Amina, Funcionalização de membranas, Sol-Gel

Contents

1 Introduction **1**

1.1 Separation Processes with Membranes . . . 3

1.2 Market for Separation Processes with Membranes . . . 5

1.3 Separation Processes where the Driving Force is Pressure . . . 6

1.4 Principles of Ultrafiltration . . . 7

1.4.1 Factors for Quantifying the Performance of an Operation in UF . . . 8

1.4.2 Transport Phenomena in Ultrafiltration . . . 9

1.4.3 Solutions and Limit Flow . . . 10

2 State of Art **11**

2.1 Polymeric Cellulose Acetate Membranes . . . 13

2.2 Membrane Functionalization . . . 13

2.2.1 TEOS Functionalization . . . 14

2.2.2 APTES Functionalization . . . 15

2.3 The Sol-Gel Process . . . 15

2.4 Main Purposes of the Present Work . . . 16

2.4.1 Chronic Kidney Disease . . . 18

2.4.1.A End-Stage Renal Disease . . . 18

2.4.2 Hemodialysis Process Overview . . . 19

3 Materials and Methods **21**

3.1 Experimental Methodology . . . 23

3.2 Membranes Synthesis . . . 23

3.2.1 Casting Solutions Preparation . . . 23

3.2.2 Membranes Manual Casting . . . 25

3.2.3 Membranes Selection and Cutting . . . 28

3.3 Permeation Unit . . . 29

3.3.1 Ultra-filtration Set-up . . . 29

3.3.2 Membranes Compaction . . . 31

3.3.3 Pump Calibration . . . 31
3.4 Permeation Performance Experiments . . . 32
3.4.1 Hydraulic Permeability . . . 32
3.4.2 Salts Rejection Coefficient . . . 33
3.4.2.A Salts Concentration Measurement . . . 33
3.4.3 Molecular Weight Cut-Off . . . 35
3.4.3.A Total Organic Carbon and Concentration Measurement . . . 35
3.5 Membrane Characterization Techniques . . . 37
3.5.1 Membranes Drying . . . 37
3.5.2 Field Emission Gun Scanning Electron Microscopy-FEGSEM . . . 38
3.5.3 Mechanical Properties . . . 38
4 Results and Discussion **39**
4.1 Membrane Characterization Techniques . . . 41
4.1.1 FEGSEM . . . 41
4.1.1.A Cross-Section . . . 43
4.1.1.B Active layer . . . 46
4.1.1.C Bottom Layer . . . 47
4.1.2 Mechanical Properties . . . 48
4.2 Permeation Performance . . . 51
4.2.1 Hydraulic Permeability . . . 51
4.2.1.A Permeated Deionized Water Fluxes . . . 51
4.2.1.B Hydraulic Permeability . . . 52
4.2.1.C Membrane Resistance . . . 56
4.2.2 Salts Rejection Coefficient . . . 57
4.2.2.A Permeated Salts Fluxes . . . 57
4.2.2.B Rejection Factor . . . 58
4.2.3 MWCO . . . 59
4.2.3.A Permeated PEGs and Dextran Fluxes . . . 59
4.2.3.B Rejection Factor for PEGs and Dextran . . . 61
4.2.3.C MWCO Determination . . . 61
4.3 Pore Size . . . 66
5 Conclusion **67**
5.1 Future Work Proposals . . . 71
Bibliography **73**

A Membrane Selection 81

B Pump Calibration 85

C Temperature Correction of the Permeate Fluxes 87

D Linear Regressions to Calculate Hydraulic Permeability 89

E Salts Concentration Measurement Calibration Lines 95

F Total Organic Carbon Calibration Lines 97

List of Figures

1.1 Classification of membranes according to their form of synthesis 4
1.2 Global membrane separation technology market size, by process, from 2016 to 2027 in billion USD 5
1.3 Global membrane separation technology market share, by application, in 2019 6
1.4 Gradation of solute separation in membrane separation processes that use pressure as a driving force 7
1.5 Examples of variant substances shown in approximate correspondence to the pore size of the membrane separation method that may be employed 7
1.6 Ultrafiltration operation scheme 8
1.7 Ultrafiltration factors for quantifying the performance of an operation 8
1.8 Permeation flux as a function of applied pressure for a pure solvent (A) and a solution (B) 10

2.1 Molecular structure of cellulose composed of glucose monomers and molecular structure of cellulose acetate produced by acetylation of cellulose followed by acid hydrolysis . . . 13
2.2 Silica monomers and possible structures after sol-gel condensation reaction 14
2.3 APTES organometallic precursor structure 15
2.4 Illustration of the two steps of the sol-gel process for the TEOS metal alkoxide precursor . 16
2.5 Different ways of the sol-gel process considering the final application 16
2.6 Schematic diagram of a membrane in hemodialysis process 19

3.1 Experimental methodology flowchart 23
3.2 Casting solution homogenization 24
3.3 Casting glass (yellow arrow), casting knife (orange arrow) and casting knife gap (red arrow) 25
3.4 Casting knife 26
3.5 Casting glass (between the red square), casting knife holding positions (green circles) and casting direction (yellow arrow) 27
3.6 Membrane hybrid flat-sheet disposition for cutting 28

3.7 Membrane cutting step. Metallic cutting circular impression is visible on the left-side. . . . 28
3.8 Ultrafiltration Set-Up . . . 29
3.9 Ultra-filtration Set-up components . . . 30
3.10 UF set-up wrapped in aluminum foil, left side (green arrow), to prevent bacterial and fungi growth, right side . . . 30
3.11 Ultra-filtration module . . . 31
3.12 CRISON CONDUCTIMETER GLP 32 . . . 34
3.13 SHIMADZU Total Organic Carbon Analyzer . . . 36

4.1 Schematic representation for the interpretation and discussion of the experimental results obtained . . . 41
4.2 SEM microphotographs of the active layer (a), porous layer (b), cross section (c), at an energy of 15.0 kV and resolution x10000, x10000 and x800, respectively, for A100/0 (d), A95/5 (e), A90/10 (f), A80/20 (g), A70/30 (h) and A50/50 (i) membranes composition . . . 42
4.3 SEM microphotographs of the active layer (a), porous layer (b), cross section and complete cross section (c), at an energy of 15.0 kV and resolution x2000, x2000 and x800, respectively, for A100/0 (d), A95/5 (e), A90/10 (f), A80/20 (g), A70/30 (h) and A50/50 (i) membranes composition . . . 44
4.4 SEM microphotographs of the active layer (a), porous layer (b), cross section and complete cross section (c), at an energy of 15.0 kV and resolution x2000, x2000 and x800, respectively, for A80/20 (g), A70/30 (h) and A50/50 (i) membranes composition, being the white arrows the clusters structures . . . 45
4.5 Effect of the presence of the TEOS functional group and TEOS/APTES functionalization on membrane total thickness . . . 46
4.6 Membranes' number of clusters on the active layer . . . 46
4.7 Relationship between the number of clusters and the total area occupied by these structures for the top layer . . . 47
4.8 Relationship between the number of clusters and the total area occupied by these structures for the bottom layer . . . 47
4.9 Mechanical properties as a function of membranes' composition . . . 48
4.10 Mechanical properties comparison between the current work (C) and published work (P) . 49
4.11 Relationship between clusters properties and mechanical properties . . . 50
4.12 Average values of the permeated deionized water fluxes, of the first, second and third experiments, as a function of the imposed TMP, for the tested membranes . . . 51
4.13 Hydraulic permeability for the tested membranes . . . 52

4.14 Comparison of the behaviour, of current work with published work, of the hydraulic permeability for monophasic hybrid membranes . . . 53
4.15 Comparison between works of the relationship of hydraulic permeability mechanical properties . . . 54
4.16 Relationship between hydraulic permeability and clusters' properties . . . 56
4.17 Comparison of the corrected permeate fluxes of the reference salts, obtained at TMP=1 bar and feed rate of 180 L/h, with the DI water permeate corrected fluxes obtained at TMP=1 bar and feed rate of 150 L/h . . . 58
4.18 Rejection coefficients for reference salts . . . 58
4.19 Comparison of the permeate flux of a polymer solution from 300 to 40000 Da at TMP=1 bar and feed-rate of 180 L/h, with the flow of DI water permeated at TMP=1 bar and feed-rate of 150 L/h , for the tested compositions . . . 60
4.20 Summary of the rejection coefficients for the various solutions of PEGs and Dextran in MilliQ water for the tested compositions . . . 61
4.21 MWCO determination for A100/0 . . . 62
4.22 MWCO determination for A95/5 . . . 62
4.23 MWCO determination for A90/10 . . . 63
4.24 MWCO determination for A80/20 . . . 63
4.25 MWCO determination for A70/30 . . . 63
4.26 MWCO determination for A50/50 . . . 64
4.27 Summary of calculated MWCO values for tested membranes . . . 64
4.28 MWCO for the tested membranes . . . 65
4.29 Size pore determination based on the MWCO . . . 66

A.1 Representation of the active layer facing top (orange arrow), with a protective surface (red arrow) and areas that should be excluded from the cut (boxes in black) . . . 82
A.2 Representation a), b) and c) scenarios, respectively . . . 83

B.1 Pump Calibration for membranes CA, A100/0-1-1, A95/5-1-2, A90/10-1-4 and A80/20-1-4, together with filter paper, using DI water . . . 86
B.2 Pump Calibration for membranes A70/30-1-5 and A50/50-1-6, together with filter paper, using DI water . . . 86

D.1 J_{pw} as a function of TMP, for the first, second and third experiment, for the CA membrane 90
D.2 J_{pw} as a function of TMP, for the first, second and third experiment, for the A100/0-1-1 membrane . . . 90

D.3 J_{pw} as a function of TMP, for the first, second and third experiment, for the A95/5-1-2 membrane . . . 91
D.4 J_{pw} as a function of TMP, for the first, second and third experiment, for the A90/10-1-4 membrane . . . 91
D.5 J_{pw} as a function of TMP, for the first, second and third experiment, for the A80/20-1-2 membrane . . . 92
D.6 J_{pw} as a function of TMP, for the first, second and third experiment, for the A70/30-1-5 membrane . . . 92
D.7 J_{pw} as a function of TMP, for the first, second and third experiment, for the A50/50-1-6 membrane . . . 93

E.1 NaCl conductivity as a function of the concentration calibration line . . . 95
E.2 Na_2SO_4 conductivity as a function of the concentration calibration line . . . 96
E.3 $MgCl_2$*$6H_2O$ conductivity as a function of the concentration calibration line . . . 96
E.4 $MgSO_4$*$7H_2O$ conductivity as a function of the concentration calibration line . . . 96

F.1 PEG 400 Total Carbon as a function of the concentration . . . 98
F.2 PEG 3000 Total Carbon as a function of the concentration . . . 98
F.3 PEG 6000 Total Carbon as a function of the concentration . . . 99
F.4 PEG 10000 Total Carbon as a function of the concentration . . . 99
F.5 PEG 20000 Total Carbon as a function of the concentration . . . 99
F.6 PEG 350000 Total Carbon as a function of the concentration . . . 100
F.7 Dextran 40000 Total Carbon as a function of the concentration . . . 100

List of Tables

1.1 Membranes' process classification according to the respective driving force 3
1.2 Summary of current materials used to make membranes 4
1.3 Types of modules and corresponding compatibility with membranes separation processes 4
1.4 Comparison between different modules configurations 5

3.1 Materials used in the preparation of the casting solutions. 24
3.2 Membranes' acronyms and casting solution massic composition 25
3.3 Acronym's designation based on the casting solution molar composition (%) 25
3.4 Membranes used during the permeation experiments 32
3.5 Reference salts used to determinate the salts rejection coefficient 33
3.6 Standard solutions used for the automatic CRISON CONDUCTIMETER GLP 32 calibration 34
3.7 Polymers used to determine the MWCO 35
3.8 Reagents used for the membranes drying process 37
3.9 Solvent-exchanged drying process with respective day, solution and time 37
3.10 Dry membranes used for morphological and topographic study via FEGSEM technique . 38

4.1 Mean values of membrane thickness, and respective standard deviation, calculated by the ImageJ image analysis program, for the cross-section images at a resolution of x800. 44
4.2 Mean values of membrane resistance and respective standard deviation for tested membranes 57
4.3 Permeate fluxes obtained at TMP=1 bar and feed rate of 180 L/h, for PEGs and Dextran, corrected for a temperature of 25ºC 60

Acronyms

APTES - 3-(Aminopropyl)triethoxysilane

A - Clusters total area

CA - Cellulose Acetate

CAGR - Compound Annual Growth Rate

C_f - Feed concentration

CKD - Chronic kidney disease

C_p - Permeate concentration

DI - Deionized

ED - Electrodialysis

ESRD - End-Stage Renal Disease

FESEM - Field Emission Gun-Scanning Electron Microscopy

f - Rejection Factor

GFR - Glomerular Filtration Rate

GS - Gas Separation

HD - Hemodialysis

H_2O_d - Deionized water

IC - Inorganic Carbon

J_{pw} - Flux of pure water in the permeate

L - Membranes thickness

l - Pore length

L_p - Hydraulic permeability

MF - Microfiltration

MW - Molecular Weight

MWCO - Molecular Weight Cut-Off

N_c - Number of clusters

NF - Nanofiltration

PBUT - Protein Bound Uremic Toxin

PD - Peritoneal dialysis

PEG - Polyethyleneglycol

R_m - Membrane's resistance

RO - Reverse Osmosis

r - Pore Radium

Std - Standard deviation

TEOS - Tetraethyl orthosilicate

TMP - Transmembrane Pressure

TC - Total Carbon

TOC - Total Organic Carbon

UF - Ultrafiltration

UFM - Ultrafiltration Module

USD - United States Dollars

η - Solvent's viscosity

ε - Porosity

1

Introduction

Contents

1.1 Separation Processes with Membranes 3
1.2 Market for Separation Processes with Membranes 5
1.3 Separation Processes where the Driving Force is Pressure 6
1.4 Principles of Ultrafiltration 7

1.1 Separation Processes with Membranes

For the last century populational growth has shown astonishing records of 4.6 to 7 billion people [1]. This crescent growth boosted the accelerated use of separation processes using membranes in many fields of the industry. Separation processes, coupled with membranes, has numerous applications [2] [3], standing out:

- Chemical industry (petrochemicals and fine chemistry)
- Food industry
- Pharmaceutical and biotechnology
- Environmental applications
- Wastewater treatment.

In a separation process using membranes there's always a membrane between two phases. The phase, located upstream, is called the feed. By applying a driving force in the feed, some of its components are forced through the membrane, thus a separation process occurs. The flux of mass that goes through (downstream) is called the permeate, being the reminisce part called the concentrate.

Several driving forces are used to make a separation happen. Classification of different processes using membranes and respective driving forces [4] can be consulted in the next table.

Table 1.1: Membranes' process classification according to the respective driving force

Driving Force	Process
Pressure	-Reverse Osmosis (RO) -Nanofiltration (NF) -Ultrafiltration (UF) -Microfiltration (MF)
Partial Pressure	-Gas Separation (GS) -Vapor Permeation
Concentration	-Dialysis -Membrane Extraction
Electric Potential	-Electrodialysis (ED) -Membrane Electrolysis

Due to the variety of different membrane separation processes, nowadays, there's a variety of membranes on the market. One membrane only it's not enough to cover all applications of a given process, on the other hand, is also expected to be able to respond to different practical situations. Therefore, in the past few years, membranes development has been the focus in terms of constituent materials and manufacturing techniques that, for most of the cases, can provide "tailor-made" features for a specific application. Table 1.2 sums the main materials from which membranes are currently made of [4] [5].

Table 1.2: Summary of current materials used to make membranes

Membranes Types	Materials
Inorganic	Porous glass, ceramics, graphite, metal oxides
Modified Natural Materials	Cellulose acetate, cellulose acetobutyrate, regenerated cellulose, cellulose nitrate
Synthetic	Aromatic polyamides, vinyl polymers, polyvinyl acetate, sulfonated polyester, polyolefins

Classification of membranes [5] [6] [7], considering their form of synthesis, a subject that has quite different approaches according to authors, is illustrated by fig. 1.1.

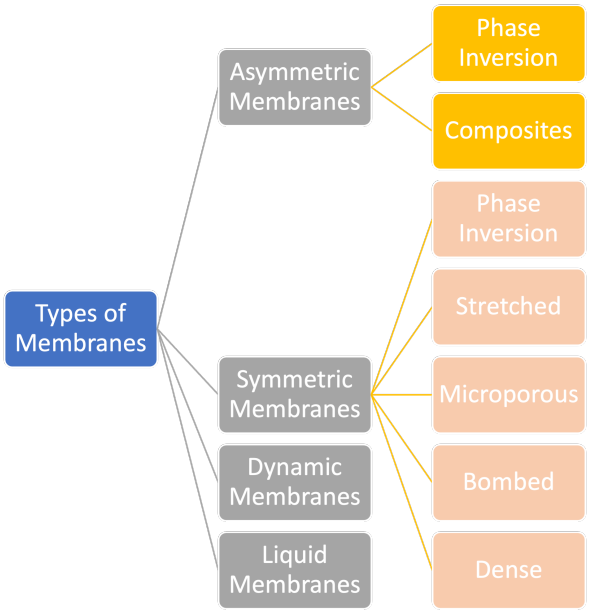

Figure 1.1: Classification of membranes according to their form of synthesis

Membrane modules are of fundamental significance as it is within the modules that membranes are accommodated. These modules are available in five basic configurations [5]: hollow fibers, spirals, tubular, flat, and capillary. In general, the following classification can be considered for the compatibility between modules and operations.

Table 1.3: Types of modules and corresponding compatibility with membranes separation processes

Type of Modules	Process Compatibility
Spiral Wound	RO, GS and UF
Hollow Fibers	RO and GS
Flat Sheet	RO, UF, ED and MF
Tubular	RO, UF and MF
Capillary	UF and MF

The type of module to be used is determined by economic factors, of greater weight, type of final application, fouling, cleaning, operating costs, among others. The comparison of different modular configurations can be found in the table below [4] [5].

Table 1.4: Comparison between different modules configurations

	Tubular	Flat	Spiral	Capillary	Hollow Fibers
Packing Density	Low	——————————>			Very High
Investment/Area cost	High	——————————>			Low
Fouling Tendency	Low	——————————>			Very High
Cleaning	Easy	——————————>			Difficult
Operation Costs	High	——————————>			Low
Membrane Replacement	Yes	Yes	No	No	No

1.2 Market for Separation Processes with Membranes

Separation processes with membranes have a stand on various industrial applications, as stated in section 1.1. They make possible the supply of potable water to millions of people, all around the world, and guarantee the survival of chronic kidney disease patients that resort to hemodialysis treatment.

The global membrane separation technology market size was estimated at 17.9 billion united states dollars (USD) in 2019 and is expected to register a compound annual growth rate (CAGR) of 11.7% from 2020 to 2027 [8]. Global market size forecast, from 2016 to 2027, can be seen on the next figure.

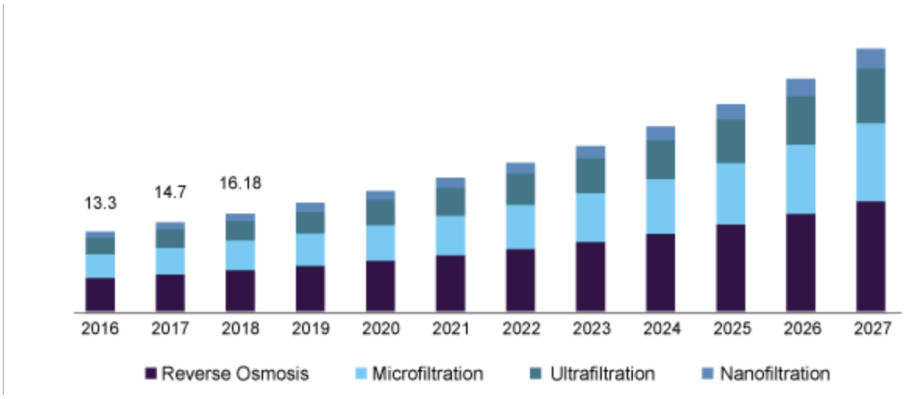

Figure 1.2: Global membrane separation technology market size, by process, from 2016 to 2027 in billion USD [8]

By the year of 2019, some membranes' applications were the main reason for this constant market growth, as represented in fig. 1.3.

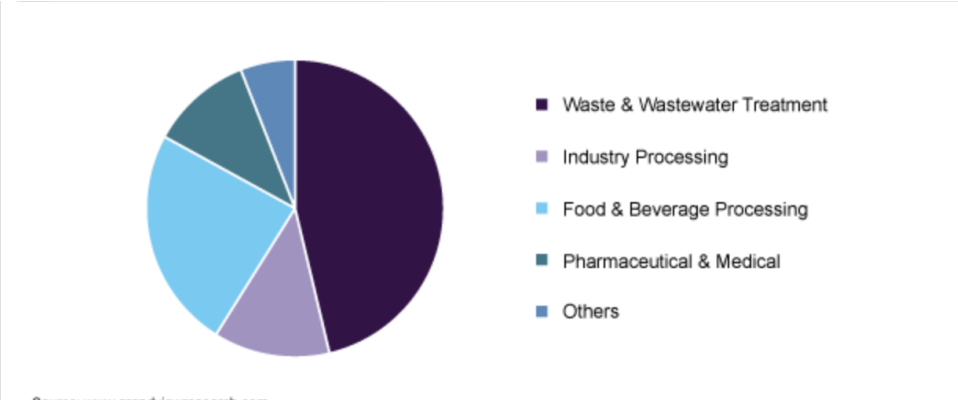

Figure 1.3: Global membrane separation technology market share, by application, in 2019 [8]

Key market drivers for membrane separation processes increase were [9]:

- Water Wastewater Treatment - continuous and increasing population increases the demand for water [1]. Thus, membranes separation technology in water wastewater treatment plants are used for microbial removal, desalination of sea water, sewage treatment, wastewater treatment of water from industries, processing of natural mineral water, production of potable water, and treatment of brackish water. The two major membrane processes used for water wastewater treatment include RO and NF
- Food Beverage - disposal regulations and wastewater treatment are strictly correlated to this type of industry, with greater emphasis on the processes of RO, NF, UF, MF, along with some of the less used technologies such as pervaporation, gas transfer, and membrane distillation
- Medical Pharmaceutical - artificial kidneys transplant, blood oxygenators, and controlled release drug delivery system, using membranes, that is expected to continue to grow at a relatively high rate in microfiltration membranes

Recent studies, [8] [9], also show that medical and pharmaceutical devices the application with one of greatest growing interest since 1998.

1.3 Separation Processes where the Driving Force is Pressure

According to section 1.2, MF, UF, NF and RO are technologies of greatest interest and growth in terms of the market-size.

Microfiltration, ultrafiltration, nanofiltration, and reverse osmosis are conceptually similar processes,

where the driving force for mass transfer across the membrane is pressure, the notable difference between them being the dimensions of the ”pores” and the nature of the membranes used.

Regarding the particle sizes separated by MF, UF, NF, and RO, there is not a very rigid boundary between each of the processes. Your choice strongly depends on the size of the solutes to be separated and the final application. A global scale of separation of solutes, and some substances, allows establishing some correspondence with the pore sizes of a membrane, and the separation method that may be employed, as shown in fig. 1.4 and fig. 1.5, respectively.

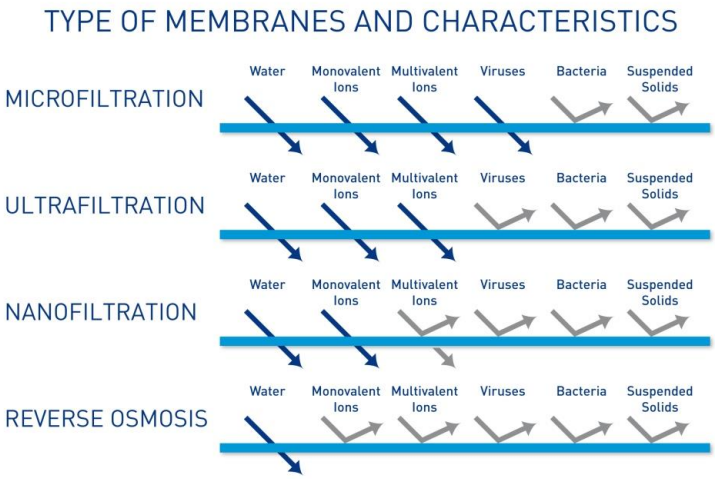

Figure 1.4: Gradation of solute separation in membrane separation processes that use pressure as a driving force [10]

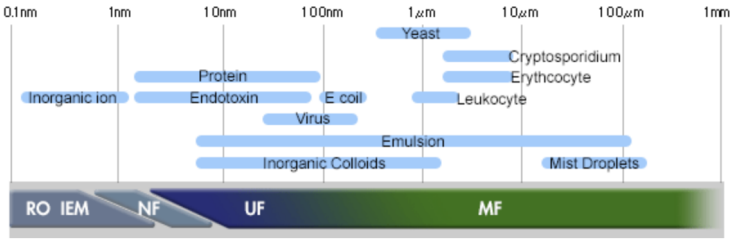

Figure 1.5: Examples of variant substances shown in approximate correspondence to the pore size of the membrane separation method that may be employed [11]

1.4 Principles of Ultrafiltration

Ultrafiltration is a membrane separation process where the driving force is pressure. It can be used to concentrate or fractionate macromolecular solutions that are generally aqueous, homogeneous, or not.

When the objective is to concentrate the solution to be treated, which circulates through the compartment subject to the highest pressure (feed compartment), it splits into two new streams: one that crosses the membrane and exits enriched in solvent (permeate), through the compartment that has the lowest pressure, and another that comes out of the other end of the feeding compartment and that comes enriched in solute(s), the concentrate. When two or more solutes are fractionated, they are distributed through the permeate and the concentrate in greater or lesser amounts according to their characteristics and the selectivity of the membrane.

The UF process can be outlined, in a very simple way, according to fig. 1.6.

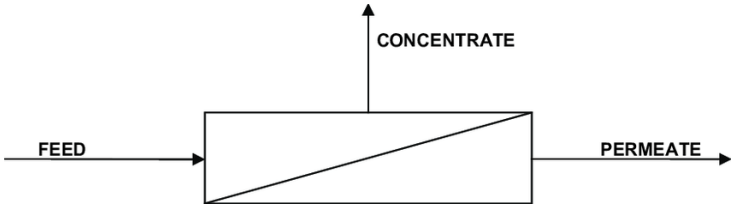

Figure 1.6: Ultrafiltration operation scheme [5]

1.4.1 Factors for Quantifying the Performance of an Operation in UF

The performance of an ultrafiltration operation can be evaluated on three factors. These factors, as shown in fig. 1.8, allow a summary evaluation of the ultrafiltration membrane, also giving back some parameters regarding its performance.

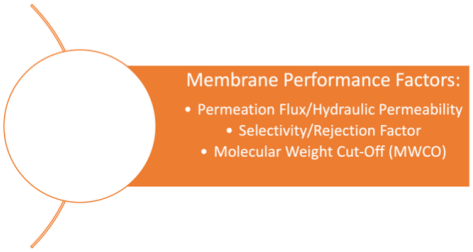

Figure 1.7: Ultrafiltration factors for quantifying the performance of an operation

Permeation flux is the volume of fluid that passes through the membrane per unit of time and unit area and is easily measurable. Knowing the permeation area, that is, the area where the mass transfer occurs, we obtain the hydraulic permeability (L_p) value. Hydraulic permeability, in a sense, measures how easily a membrane allows a given solvent to pass through.

Selectivity is a measure of the relative permeation flow rates of different components across the membrane. The rejection factor (f) is the fraction of solute contained in the feed that is retained by the

membrane. A so-called ideal membrane has a high selectivity, or rejection, and a high permeation flux. However, in general, when trying to maximize one of these factors, the other reduces.

Regarding molecular weight cut-off (MWCO), this is data that the manufacturer generally provides, but it has only a reference meaning. It is determined by passing over the membrane certain reference solutes with increasing molecular weight (MW) that will or will not be retained by the membrane. Despite varying within the scientific community, MWCO is the molecular weight of the solute that is 90% retained by the membrane. This method is disputed as it has several limitations. Reference solutes that are most used are proteins as they have a small molecular weight dispersion unlike, for example, dextran or polyethyleneglycol (PEG) which have a large molecular weight dispersion around an average value. The MWCO value is not an intrinsic membrane property like hydraulic permeability and selectivity. This parameter depends on the rejection coefficient, concentration polarization, chemical nature, and spatial conformation of the macromolecule used as a reference solute, the nature of the solvent, among others.

1.4.2 Transport Phenomena in Ultrafiltration

Ultrafiltration membranes can be considered a porous media, and the rejection of certain species depends essentially on their shape and the dimensions of the solutes contained therein, concerning the size of the pores. For these membranes, solvent transport is proportional to the applied pressure, according to the following equation,

$$J_{pw} = L_p TMP \tag{1.1}$$

where J_{pw} is the solvent flux, L_p is the hydraulic permeability and TMP the applied transmembrene pressure.

There is similarity between eq. (1.1) and the Hagen-Poiseuille equation for flow in porous media, eq. (1.2), in which η is the solvent's viscosity, ε the porosity and r and l the radius and length of the pore.

$$J_{pw} = \frac{\varepsilon r^2}{8l} \frac{TMP}{\eta} \tag{1.2}$$

This relationship directly links hydraulic permeability to structural parameters of the membrane (intrinsic). Thus, the inverse of hydraulic permeability represents the resistance that the membrane has to permeation, R_m, which is called membrane resistance. Equation (1.1) can now be written in the following form:

$$J_{pw} = \frac{TMP}{R_m} \tag{1.3}$$

1.4.3 Solutions and Limit Flow

The permeation linearity, eq. (1.2), disappears when these membranes permeate solutions instead of pure solvents. In the case of solutions, when the operating pressure increases, at first, there is a slow permeation flow increase. As the TMP progresses, the flux increases more and more until it stabilizes at a given value, a value called the permeation limit flux. Upon reaching this value, any pressure increase is useless and only results in wasted energy as the permeation flux value does not change, as shown in the next figure.

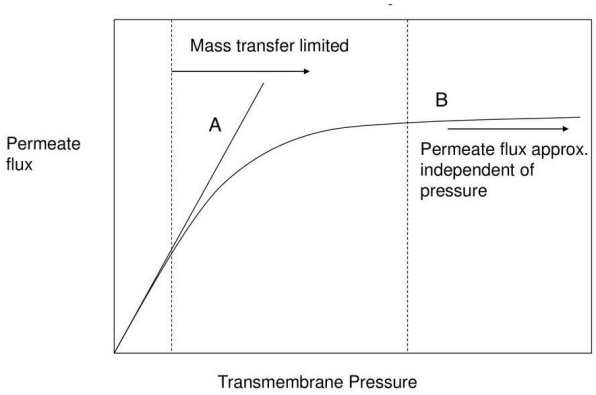

Figure 1.8: Permeation flux as a function of applied pressure for a pure solvent (A) and a solution (B) [5]

For a given solution with a given concentration, the limiting flux is higher if the circulation velocity (or mass transfer coefficient) is higher. On the other hand, for the same mass transfer value, the flow limit is higher for more dilute solutions.

2

State of Art

Contents

2.1 Polymeric Cellulose Acetate Membranes 13

2.2 Membrane Functionalization 13

2.3 The Sol-Gel Process 15

2.4 Main Purposes of the Present Work 16

2.1 Polymeric Cellulose Acetate Membranes

As one of the most abundant organic compounds in the biosphere [12], cellulose is a linear homopolymer composed of D-anhydro glucopyranose units linked by β-(1-4) glycosidic bonds. Cellulose acetate (CA) membranes were developed in the 1960s and were the first type of membranes used in desalination units [13] [14]. Cellulose diacetate, or commonly as cellulose acetate, is obtained by acetylation of cellulose followed by acid hydrolysis, to lower the acetyl degree. First, all the -OH groups are converted to acetate groups, CH_3COO^-, when the cellulose is transformed into cellulose triacetate. Thereafter, C3 is hydrolyzed, given back -OH groups freedom to react. The following figure shows that cellulose is formed from β-glucose, resulting in -CH_2OH lateral groups above and below, which alternate between successive rings. This rigid structure is preserved in CA.

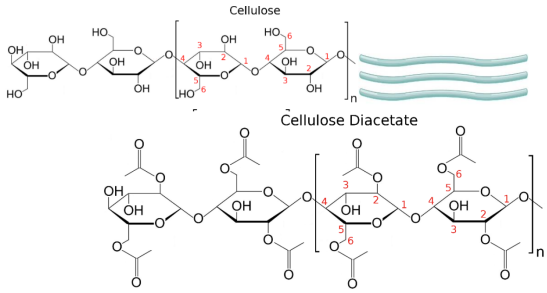

Figure 2.1: Molecular structure of cellulose composed of glucose monomers and molecular structure of cellulose acetate produced by acetylation of cellulose followed by acid hydrolysis [15]

CA membranes have been widely used in ultra and microfiltration processes due to their natural abundance, superior film-forming ability, low price, moderate resistance to chlorinated agents, good biocompatibility, good fouling resistance, and their hydrophilic nature [16] [17]. Furthermore, they played a key role in wastewater treatment plants [18], gas separation [19], blood purification [20] [21] and other bioprocesses [22] [23]. However, despite the numerous advantages of pure cellulose acetate membranes, there are some limitations, such as poor mechanical properties and low chemical resistance. Under more adverse operating conditions, such as high temperatures or low pH, the CA polymer hydrolysis occurs, compromising the chemical, physical structure, and thermal stability.

2.2 Membrane Functionalization

To overcome the various limitations imposed by cellulose acetate membranes, several techniques, such as physical blending with the modifying agent (additive), chemical grafting, and surface modification [24], were investigated to alter and enhance pure CA membranes.

The functionalization of membranes appears, then, as an efficient strategy, as it allows the mixture of organic polymer with inorganic materials, as it de-promotes biofouling by increasing anti-adhesion surfaces [25], controlling bacterial growth [26], and improves stable performances [27]. Inorganic additives, or composites, such as zeolite [28], transition metal complex [29], silver [30], silica [31], titania [32], fluorite [33], are commonly used and incorporated into the polymer-based membrane casting solution.

2.2.1 TEOS Functionalization

The matrix reinforcement of pure cellulose acetate membranes with silica has been accomplished by the addition of silica nanoparticles. Its synthesis can be done by various techniques such as flame spray pyrolysis [26], chemical vapor deposition [34], microemulsion [35], ball mill grinding [36], and sol-gel process [37], being the last method, most used due to its simplicity and control.

Taking the sol-gel process as a starting point, hybrid CA-SiO_2 membranes result from two reactions, hydrolysis, and condensation, in that order. The hydrolysis reaction of silica precursors, such as tetraethyl orthosilicate (TEOS), gives rise to $Si(OH)_4$ "monomers", as follow:

$$Si(OCH_2CH_3)_4 + 4H_2O \mapsto Si(OH)_4 + 4CH_3CH_2OH \tag{2.1}$$

These monomers, later, can react by condensation reactions,

$$Si(OH)_4 + Si(OH)_4 \rightarrow Si_2O(OH)_6 + H_2O \tag{2.2}$$

forming molecules that can form chains, rings, and finally a three-dimensional structure [15], as illustrated in the following figure.

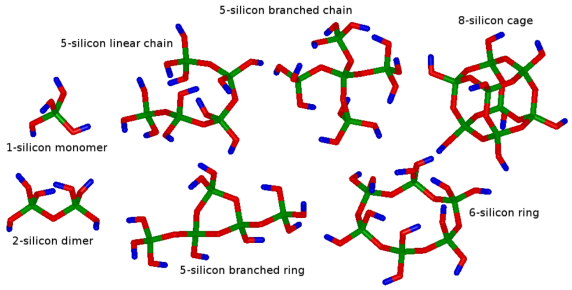

Figure 2.2: Silica monomers and possible structures after sol-gel condensation reaction [15]

2.2.2 APTES Functionalization

Amines are intermediate compounds in various chemical processes [38] due to their basic and nucleophilic character, which makes them quite versatile and reactive compounds [39]. Taking advantage of the ability of primary amines to complex metal ions, commercial cellulose acetate membranes surface was modified with amine groups, aiming at complexation of gadolinium (III) [40], chromium [41] and arsenic [42], aiming for new properties.

Amine functionalization is done by adding an organometallic compound with an amine end-group, as is the case with 3-(aminopropyl)triethoxysilane (APTES). The polymerization complexity is thus amplified, as the amine can undergo hydrolysis and condensation, like TEOS, but with an aliphatic chain (non-hydrolysable Si-C bond), resulting in a more complex, open, and less dense structure. The hydrolysis and condensation reactions are described below, in order.

$$(CH_3CH_2O)_3Si(CH_2)_3NH_2 + 3H_2O \rightarrow (OH)_3Si(CH_2)_3NH_2 + 3CH_3CH_2OH \tag{2.3}$$

$$H_2N(CH_2)_3Si(OH)_3 + (OH)_3Si(CH_2)_3NH_2 \rightarrow H_2N(CH_2)_3Si(OH)_2O(OH)_2Si(CH_2)_3NH_2 + H_2O \tag{2.4}$$

Structurally, fig. 2.3, the APTES precursor enriches the membrane surface chemistry and its complexity, which will impact the permeation properties.

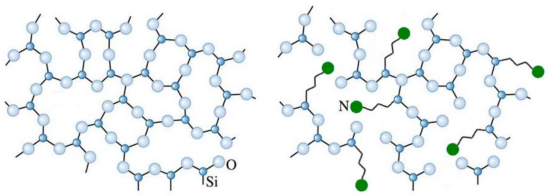

Figure 2.3: APTES organometallic precursor structure [15]

2.3 The Sol-Gel Process

The sol-gel process was first described in 1864 by Ebelmen who observed the hydrolysis and condensation of silicic acid. The proper choice of precursors is fundamental in the membrane synthesis process. Two types of precursors can be used, salts such as chlorides, nitrates, sulfides, etc., and alkoxides. Alkoxides are the type of precursors most used in the sol-gel process and are formed by removing a proton from the hydroxyl group of an alcohol. Metal alkoxides, such as TEOS, are commonly used due to their reactivity with water, which promotes hydrolysis reactions.

The sol-gel process takes place in two steps: i) hydrolysis, in which -OR groups of the precursor are replaced by -OH groups, and ii) condensation, where a polymeric condensation occurs with the release of water or alcohol, as illustrated in the following figure.

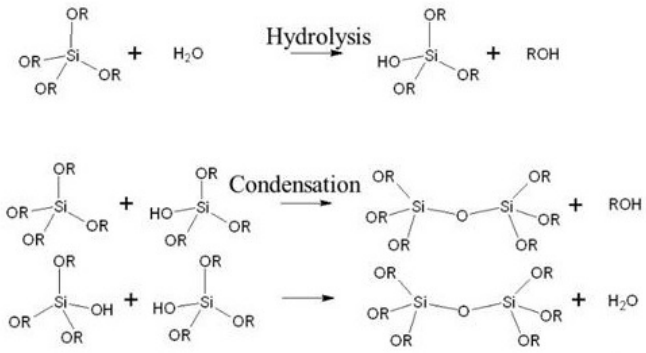

Figure 2.4: Illustration of the two steps of the sol-gel process for the TEOS metal alkoxide precursor [43]

This process can be carried out in several ways, considering the final application, varying only the method and conditions of preparation, fig. 2.5. Among the final applications, the production of films, thin or thick, fibers, ceramics, nanoparticles, among others, stands out.

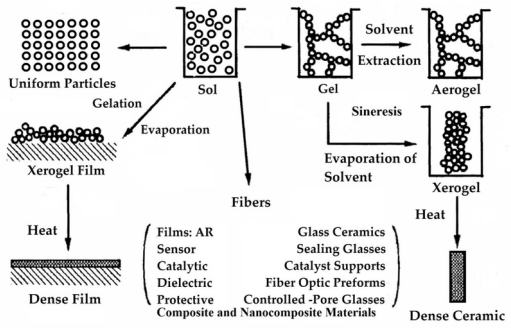

Figure 2.5: Different ways of the sol-gel process considering the final application [44]

2.4 Main Purposes of the Present Work

Functionalization of cellulose acetate membranes with silica has proven to be an upgrade from the traditional pure cellulose acetate membranes in the most diverse applications. To highlight, there is the application of these hybrid membranes in blood purification treatments. Permeation studies reveal that the integration of silica into CA membranes results in high flux UF membranes with enhanced mass transfer properties, “imitating” the metabolic functions of the kidney [20]. Furthermore, these membranes fully permeated urea and have a total rejection of albumin, while being non-hemolytic, in other words, blood compatible [20].

However, there are some limitations of nowadays membranes in protein bound uremic toxin (PBUT) filtration in chronic kidney disease (CKD) and end stage renal disease (ESRD) patients. PBUTs have MWs below 500 Da, being very difficult to remove in dialysis processes due to their great affinity with human blood proteins, in particular with human serum albumin [45]. The non-complete removal, or deficient removal, of these toxic proteins leads to the worsening of the renal patient's condition, and recent studies reveal that PBUT are correlated with increased patient mortality in dialysis treatments [46].

Thus, in this work, within the scope of the dissertation of the master's thesis, is presented the synthesis of new hybrid CA/SiO_2, taking advantage of the upgrade of permeation properties, mechanical properties, and applicability to purification treatments of this functionalization, by adding the amine group to the structure of these membranes. Functionalization with NH_2 from the APTES precursor reveals to improve the structure of membranes, as already mentioned, and may be a way to improve the permeation and mechanical properties of CA/SiO_2 membranes. Also, amine is present in numerous biological reactions in the human body and is also present in proteins. This property may be relevant for the removal of toxic components in the blood, particularly in the case of PBUTs. Information and results obtained may eventually provide a technological advance in membranes and their possible applicability to current problems, such as water treatment or blood purification in patients with kidney disease, thus providing a better quality of life to the human being. The main objectives of this work are:

- Incorporate silica into the polymer matrix of the pure cellulose acetate membrane, in-situ, by adding the precursor tetraethylorthosilicate, TEOS, allowing the Si-O-C covalent bond

- Functionalization of the cellulose acetate/silica membrane, by the addition of amine from the precursor 3-(aminopropyl)triethoxysilane, APTES

- Study the morphology of the synthesized membranes in order to characterize the structure of the membrane with the addition of amine, by Field Emission Gun-Scanning Electron Microscopy (FEGSEM);

- Study the changes in the mechanical properties of CA/SiO_2 membranes with the introduction of the amine group

- To characterize the permeation performance of synthesized membranes by studying the permeation of pure water, salt rejection, and determination of the molecular exclusion ratio of increasing molecular weight polymeric solutes

2.4.1 Chronic Kidney Disease

CKD is characterized by the gradual and irreversible loss of renal function over time in which the blood filtration capabilities and elimination of products of human metabolisms, such as urea, creatinine, uric acid, etc., regulation of mineral salts and water level are compromised. Kidney function, and consequently the presence of CKD, can be assessed in two ways: kidney damage (albuminuria) or by the decreased kidney function (GFR) [47]. Renal function, in the vast majority of cases, is assessed by the GFR, which is detected for creatinine, in blood tests, and which takes into account sex, age, race, clinical and family history, geographic location, among others [48]. Chronic kidney disease is a general term for heterogeneous disorders affecting the structure and function of the kidney [49] and has become a massive public health issue since 75 million people [50] suffer from CKD in Europe, whilst the worldwide frequency has been estimated to 700-800 million people [51] [52] with a projection that CKD will become the 5th cause of death globally in 2040 [53].

2.4.1.A End-Stage Renal Disease

ESRD is diagnosed when at least 15%, or less, of normal kidney functions are assured, i.e, kidney failure. Kidney transplant is the first option in this scenario which only a small percentage of patients could get, as it increases the average life expectancy of the patient, reduces complications, and increases the quality of life [54].

When kidney transplantation is not possible, the patient resorts to dialysis treatments, with two types of techniques that take into account the patient's lifestyle, clinical history, geographical, financial, and personal conditions. Peritoneal dialysis (PD) consists of a cleansing fluid that flows through a tube (catheter) into part of your abdomen. The lining of your abdomen (peritoneum) acts as a filter and removes waste products from your blood [55]. After a set period, the fluid with the filtered waste products flows out of your abdomen and is discarded. Hemodialysis (HD) is another type of dialysis and would be one of the options beside transplant and PD. It involves pumping a patient's blood through an external circuit for filtration before it is pumped back into the body. A typical hemodialysis schedule is three sessions per week, for 3-5 hours per session at a medical facility and represents around 90% of all dialysis patients [56].

2.4.2 Hemodialysis Process Overview

Dialysis is a chemical potential gradient-based separation process [57]. This conceptual idea was first described and mentioned by Graham in which a semi-permeable barrier was used, aiming at the selective transport of elements in a solution [58] [59]. This process contains two main streams on different sides of the membrane: dialyzer, one containing higher amount of targeted chemicals (patient's blood) and another with zero or lower concentrations (dialyzing fluid or dialysate), as shown in section 2.4.2, where the left side describes the blood side of the membrane, and the right side shows the dialysate side of the process. P1 and P2 describe pressure within the blood and dialysate side, respectively. Due to the difference in chemical potential, solutes in blood move through the membrane to the dialysate.

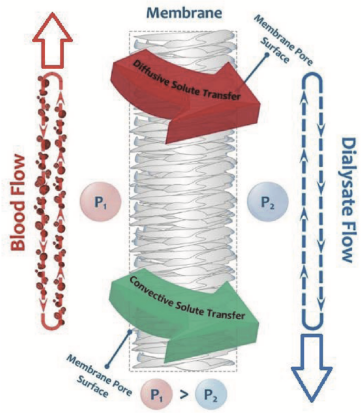

Figure 2.6: Schematic diagram of a membrane in hemodialysis process [57]

HD aims to remove toxins and extra water from the body of patients with kidney failure.

3

Materials and Methods

Contents

3.1 Experimental Methodology 23
3.2 Membranes Synthesis 23
3.3 Permeation Unit 29
3.4 Permeation Performance Experiments 32
3.5 Membrane Characterization Techniques 37

3.1 Experimental Methodology

Experimental protocols followed the working flowchart in fig. 3.1, commonly used for academic and scientific purposes, enabling better understanding and communication.

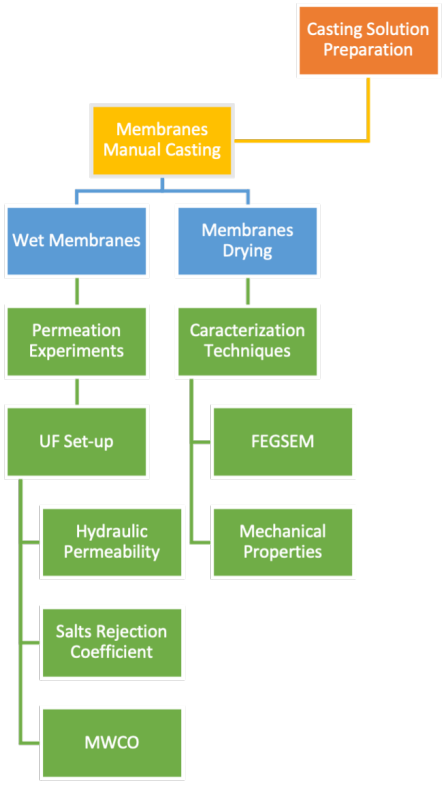

Figure 3.1: Experimental methodology flowchart

3.2 Membranes Synthesis

3.2.1 Casting Solutions Preparation

The preparation of pure cellulose acetate membranes and hybrid monophasic membranes followed the phase inversion method [60] coupled to sol-gel techniques [44]. For the functionalized hybrid monophasic membranes, organic content, cellulose acetate, (95%wt), and the inorganic content (5%wt) was kept constant in the casting solution composition, where the molar composition of non functionalized silica and silica functionalized with amine vary.

Sol-gel reactions were promoted on plastic reaction vessels at room temperature. The first step comprises the membrane matrix, by adding cellulose acetate and a two-solvent mixture, formamide, and

acetone, to promote miscibility. Into this mixture, alkoxide precursors, such as TEOS and APTES were added. To promote hydrolysis/condensation of the alkoxide precursors *in situ*, deionized (DI) water, and nitric acid were added too. To achieve a pH media of 2/3, a sample of all casting solutions were tested on dip in pH stripes to know the number of exact drops of nitric acid to be added to the casting solution.

All materials used for the casting solutions preparation are resumed in the next table.

Table 3.1: Materials used in the preparation of the casting solutions.

Compound	Chemical Formula	Manufacture	Lot	MW (g/mol)	Assay (%)
Cellulose Acetate	$C_{10}H_{16}O_8$	Sigma Aldrich	MKCD7419	~30.000	100
Formamide	CH_3NO	Carlo Erba	P7A004057G	45.02	≥99.5
Acetone	CH_6O	José M.G Dos Santos, LDA	915013.01633	58.08	99,7
TEOS	$Si(OC_2H_5)4$	Sigma Aldrich	STBB4542	208.33	98
APTES	$C_9H_23NO_3Si$	Sigma Aldrich	BCBK8161V	221.37	≥98
Nitric Acid	HNO_3	José M.G Dos Santos, LDA	27.6843001	63.01	>60

Homogenization of the casting solutions was made by a PSELECTA AGIMATIC-N magnetic agitator for 24 h and 300 rpm, at room temperature, with isolation with duct-tape to prevent the matrix leakage by evaporation, as shown in fig. 3.2.

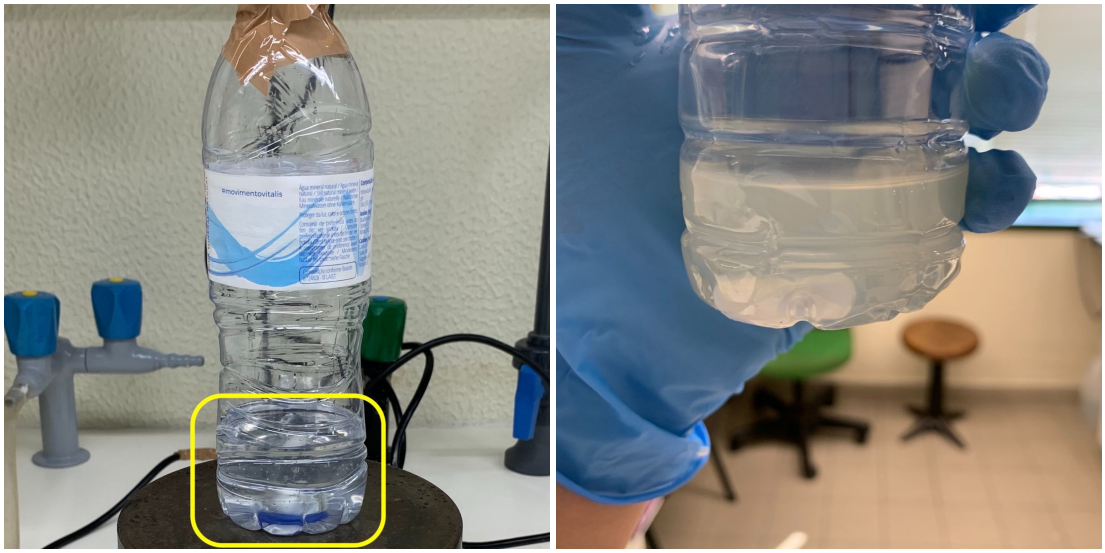

(a) Casting solution (inside yellow square) reaction vessel under a PSELECTA AGIMATIC-N magnetic agitator and isolation

(b) Casting solution

Figure 3.2: Casting solution homogenization

Membranes' acronyms and casting solution compositions are exhibited in table 3.2. Acronyms mirror the membranes' molar composition, as presented in table 3.3, and reflect the final membranes composition.

Table 3.2: Membranes' acronyms and casting solution massic composition

Acronyms/Compounds	CA	A100/0	A95/5	A90/10	A80/20	A70/30	A50/50
CA	16.40	16.40	16.40	16.40	16.40	16.40	16.40
Formamide	29.00	29.00	29.00	29.00	29.00	29.00	29.00
Acetone	51.10	51.10	51.10	51.10	51.10	51.10	51.10
TEOS	-	3.00	2.85	2.70	2.40	2.10	1.50
APTES	-	0.00	0.16	0.32	0.64	0.96	1.60
DI water	-	0.5	0.5	0.5	0.5	0.5	0.5
HNO_3	-	3-4 drops	2 drops	8 drops	12 drops	19-20 drops	33 drops
pH	-	2-3					

Table 3.3: Acronym's designation based on the casting solution molar composition (%)

Acronyms	CA	A100/0	A95/5	A90/10	A80/20	A70/30	A50/50
CA	0.032	0.032	0.032	0.032	0.031	0.031	0.031
SiO_2	0.000	0.830	0.790	0.750	0.660	0.580	0.410
SiO_2-$(CH_2)_3NH_2$	0.000	0.000	0.042	0.082	0.166	0.248	0.410
SiO_2 + SiO_2-$(CH_2)_3NH_2$	0.000	0.830	0.832	0.832	0.826	0.828	0.820
Non-functionalized-SiO_2 /Total SiO_2 (i.e. TEOS/TEOS+APTES)	0.000	100	95	90	80	70	50
Amine-functionalized silica /Total SiO_2 (i.e. APTES/TEOS+APTES)	0.000	0.00	5	10	20	30	50

3.2.2 Membranes Manual Casting

After a 24 h period of complete homogenization, stated in 3.2.1, the casting solution is poured into a gap of the casting knife, that is on top of the casting glass, as shown in fig. 3.3.

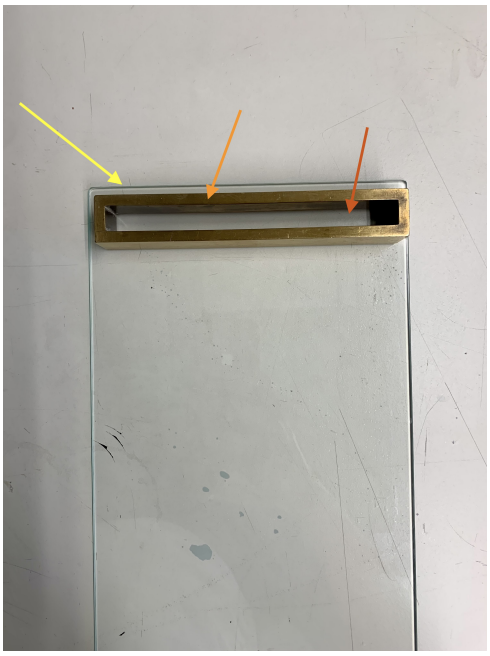

Figure 3.3: Casting glass (yellow arrow), casting knife (orange arrow) and casting knife gap (red arrow)

The casting knife, of 250 μm thickness, is used to spread the casting solution across the casting glass in a uniform way. Some careful steps must be taken into account since casting errors can have a huge impact on the final synthesized membrane. First, the casting glass must be properly cleaned, before use, with dish soap and water and ending with acetone cleanse. This ensures that no cross-contamination will take place. Secondly, the casting knife needs to be cleaned before and after use. The cleaning process needs to be done very carefully since sharp/hard cleaning objects can deform the material, fig. 3.4, making impressions on the membrane at the time of casting. Water and acetone cleanse are enough to remove any trace of casting solution from previous uses.

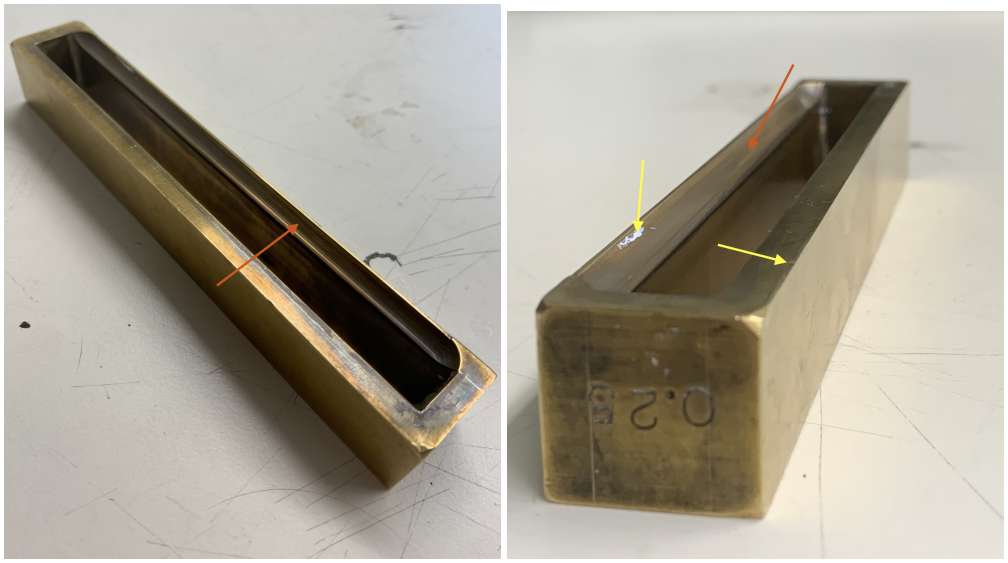

(a) Casting knife 250 μm thickness that enables spreading (orange arrow)

(b) Marked impressions (yellow arrow)

Figure 3.4: Casting knife

The casting knife should be at the top of the casting glass, and, at the moment of pouring the casting solution, the quantity added throughout the gap must be the same to achieve a uniform membrane thickness. Afterwards, the knife should be dragged, holding the two green positions shown in fig. 3.5, vertically from top to bottom, at a controlled and uniform pace, ensuring a rectangular form and absence of accumulation of casting solution on the glass.

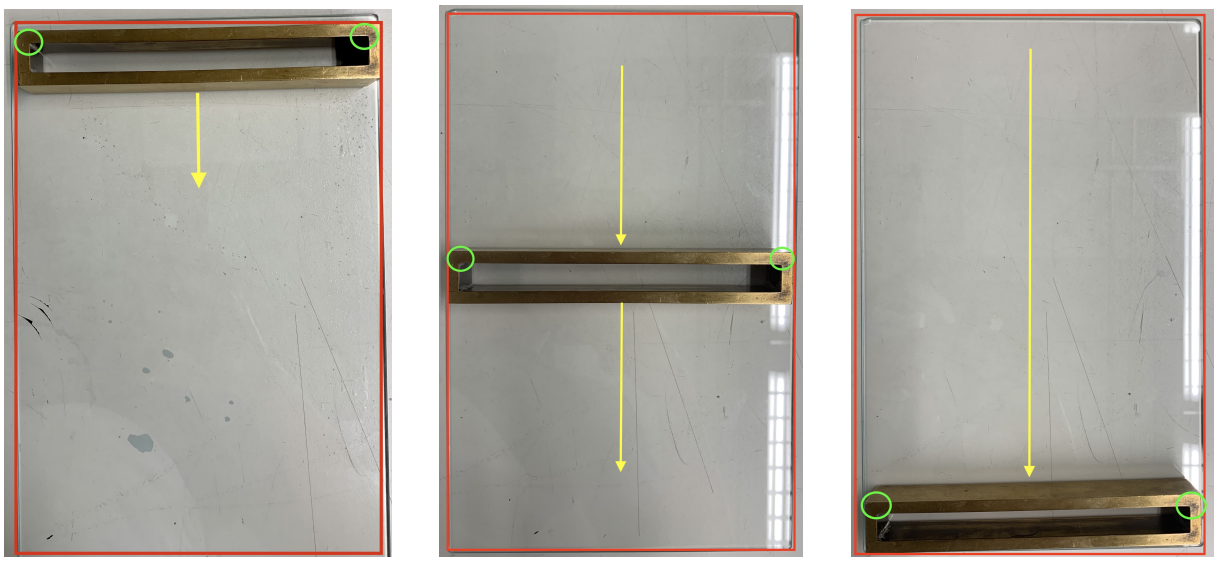

Figure 3.5: Casting glass (between the red square), casting knife holding positions (green circles) and casting direction (yellow arrow)

Concluding this step, a 30 s evaporation process starts. During this time, acetone (solvent) evaporates from the top of the membrane making the concentration of polymer increase in that area, thus forming the active layer of the casted membrane (in contact with air).

After the 30 s period, the casting glass is poured into a coagulation bath, with DI water at low temperature (between 2-3°C), which promotes the solvent exchange with the membrane's matrix and the bath. Formamide, which is in solution, circulates counter-current with water, which will be a part of that matrix. For this purpose, in a bin, filled with DI water, ice must be added to achieve low temperatures. At the pouring moment all the ice must be moved to one of the sides of the bin, ensuring that no ice particles collide with the casting glass that could dent the casted membrane. All this process is done at room temperature and enables the synthesis of asymmetric membranes, in which the top layer, or active layer, is the one that contacted with air and the bottom part, porous layer, the one that contacted with the casting glass.

Between 20 to 30 min membranes begin to self-detached from the glass. At this point, membranes should be marked, with the corresponding nomenclature, at one of the corners of the top layer (layer facing the air), thus, the active layer is signaled. From this, membranes should be stored, in previously washed containers, in cooled DI water at 5°C and stored in a refrigerator.

For each membrane composition one batch was made, resulting in five to eight flat sheets membranes with dimensions of approximately 20 cm (width) x 30 cm (height) each [61]. Therefore, membranes

acronyms, from now on, will also reflect the batch and flat sheet number, i.e, A100/0-1-1 is the membrane with composition stated in section 3.2.1, batch number one and flat sheet produced number one.

3.2.3 Membranes Selection and Cutting

Prior to permeation experiments, section 3.4, wet membranes must be properly selected and cut. Membrane selection is further discussed on appendix A. After selection, the flat sheet must be placed on top of a protective surface (red arrow) with the active layer facing top (orange arrow), as shown in fig. 3.6.

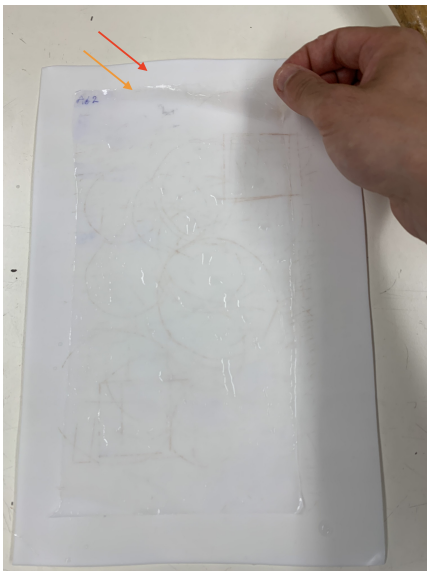

Figure 3.6: Membrane hybrid flat-sheet disposition for cutting

A cutting metallic instrument, with the same diameter as the ultrafiltration module (UFM) permeation area, is placed on top of the chosen area, fig. 3.7. By manual force, using a hammer, the selected area is cut.

Figure 3.7: Membrane cutting step. Metallic cutting circular impression is visible on the left-side.

All cut membranes should be stored, in previously washed containers, in cooled DI water at 5°C and stored in a refrigerator. The cutting process must be done on a steady-firm table and furthest away, possible, from any electronic and breakable equipment, given that vibrations produce during the manual cut (via hammer) can break or decalibrate the latter.

3.3 Permeation Unit

Not knowing the characteristics of hydraulic permeability, salt rejection coefficient and MWCO, the synthesized wet membranes were characterized in an ultrafiltration set-up.

3.3.1 Ultra-filtration Set-up

The UF set-up global view is represented in fig. 3.8.

Figure 3.8: Ultrafiltration Set-Up

It's composed, fig. 3.9, by and ISGEV AS71B4 pump (A) coupled to a MOVITRAC LTE SEW EURODRIVE power source (B), that makes the centrifugal paws rotate and sets the pump position rotating frequency. The feed solution tank (C), with a capacity for 5 L, it's pumped through the feed line (white arrow) throughout the ultrafiltration five modules, displayed in series (D). Each UFM has an outlet line, or permeate exit (red arrows). At the end of the UFM set-up there's a manometer (F). Transmembrane pressure, or TMP, and the feed-rate are controlled by a cut-valve (G) and rotameter (H) (in %, that measure the cut-vale opening). The non-permeated solution, or concentrate, goes back to the feed tank (C) through the concentrated line (black arrow).

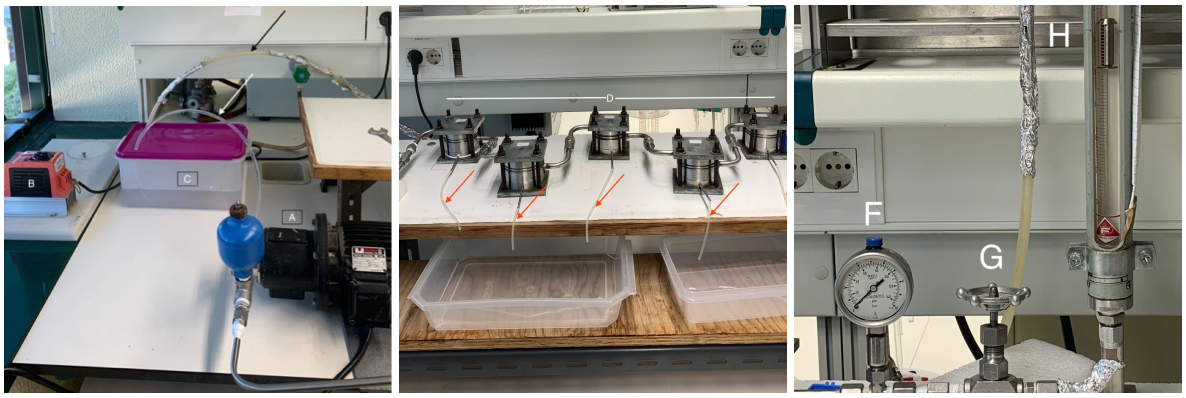

Figure 3.9: Ultra-filtration Set-up components

It's very important that all inlets and outlets are protected fun direct sunlight exposure. UV radiation is one of many sources for bacterial and fungi growth [62], clearly visible in fig. 3.10. Therefore, all lines from the UF set-up were wrapped with aluminum foil to prevent this to happen.

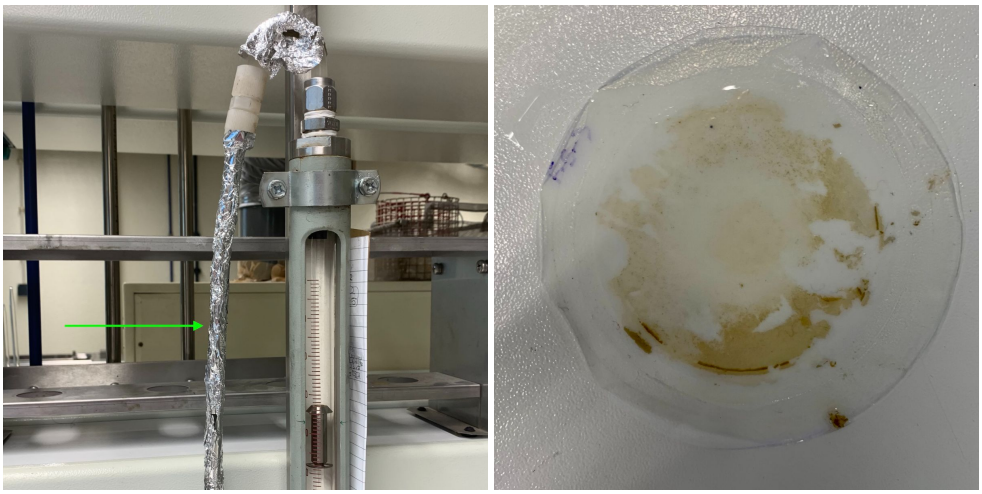

Figure 3.10: UF set-up wrapped in aluminum foil, left side (green arrow), to prevent bacterial and fungi growth, right side

The UFMs were developed at Instituto Superior Técnico, Lisboa, Portugal, following the original design by Dr. Matsuura and Dr. Souririjan of Ottawa, Canada, National Investigation Council [63]. It's composed by, fig. 3.11, an inlet line (green arrow), permeate (red arrow) and concentrate outlet (orange arrow). Part A (porous plate) and part B (O-ring structure) are detachable components and where filter paper and membranes are accommodated (in this order), on top of part A, with the membrane active layer facing top and porous part facing bottom. The UFM permeation area, orange circle, is 13.2 cm^2.

Figure 3.11: Ultra-filtration module

3.3.2 Membranes Compaction

When membranes are under pressure reorganization of polymeric chains occurs, which leads to the change in the membrane structure with the formation of uniform pores [64]. In other words, for the same membrane, measuring permeate fluxes at different times will lead to different values. To prevent this, pressure must be applied until a steady-state value is obtained, which confirms that compaction was achieved.

Compaction, for all tested membranes, was made during 3 hours at 3.0 bar (pressure 20% higher than the maximum pressure used during the permeation experiments) to ensure the formation of uniform rigid pores and a steady permeate flux. Furthermore, this process ensures that membranes, together with the filter papers, do not move within the permeation cell as well to remove the excess air and any trace quantity of solvent present in the membrane surface.

3.3.3 Pump Calibration

A permeation flux is the volume of fluid that goes through the membrane, per unit of time and unit of permeation area, and it is easily measured. As stated in 3.3.1, the UF set-up does not have a flowmeter, therefore direct measuring feed-rates is not possible. Thus, calibration lines were drawn to see how the flow-rate varies according to the pump position. For this purpose, tests were carried out, without any transmembrane pressure, with the aid of a beaker and a stopwatch. Three-time measurements were made, for six different pump positions, for a volume of 0.3 L of water exiting the concentrate line. For

each pump position, a set of three volumetric flow-rates was calculated, by dividing the target volume (0.3 L) by the respective time (h). Finally, for each position, a pondered average of the volumetric flow-rate was calculated as well the correspondent standard deviation. All the calibration lines can be consulted in appendix B.

3.4 Permeation Performance Experiments

Permeation experiments were carried out on the ultrafiltration set-up described in section 3.3.1 to quantify the membranes performance. Table 3.4 sums up all membranes that underwent permeation experiments.

Table 3.4: Membranes used during the permeation experiments

Membranes	
Group 1	**Group 2**
CA	A70/30-1-5
A100/0-1-1	
A95/5-1-2	
A90/10-1-4	A50/50-1-6
A80/20-1-2	

3.4.1 Hydraulic Permeability

The hydraulic permeability (L_p) represents the membrane's ability to permeate pure water. To quantify this parameter, it is necessary to know how the flux of permeated water, (J_{pw}), in kg/h m^2, varies according to the transmembrane pressure imposed, (TMP), in bar. This correlation is verified by the following equation:

$$L_p = \frac{J_{pw}}{TMP} \tag{3.1}$$

Under ultrafiltration conditions, water fluxes were obtained at a feed rate of 150 L/h and a pressure gradient of 0.5, 1, 1.5, 2, and 2.5 bar. The permeates were collected into a cup and then weighed on a Sartorius BASIC B 120 S analytical balance for greater accuracy ($\pm$0.00001 g), as well the permeation time was taking into account, using a digital chronometer. For each experiment, a linear regression was made, as shown by eq. (3.1). Given that the slope represents the hydraulic permeability, for each composition, a three-pondered average was made and the respective standard deviation (Std) calculated. Since permeation tests were carried out during different days and temperatures, all fluxes were corrected to a temperature of 25°C, according to the equations on appendix C.

3.4.2 Salts Rejection Coefficient

The rejection factor can be described as the fraction of solute, present on the feed solution, restrained by the membrane. The definition of rejection factor, f, is

$$f = \frac{C_f - C_p}{C_f} \times 100 \tag{3.2}$$

being C_f and C_p the feed and permeate concentration, respectively, in ppm. This factor, defined by eq. (3.2), can be also called the apparent rejection factor, once it depends on variables that can be easily measured.

Permeation experiments were carried out at constant pressure and feed-rate (1 bar and 192 L/h respectively). The used salts were sodium chloride (NaCl), sodium sulfate (Na_2SO_4), magnesium chloride hexahydrate ($MgCl_2$*$6H_2O$), and magnesium sulfate heptahydrate ($MgSO_4$*$7H_2O$), given that they are reference solutes. All of the used salts can be consulted on the next table.

Table 3.5: Reference salts used to determinate the salts rejection coefficient

Compound	Chemical Formula	Manufacture	Lot	MW (g/mol)	Assay (%)
Sodium Chloride	NaCl	Merck	K39723604 908	58.44	$\geq$99.5
Sodium Sulfate	Na_2SO_4	Scharlau Chemie S.A.	SO06671000	142,04	$\geq$99
Magnesium Chloride Hexahydrate	$MgCl_2$*$6H_2O$	Merck	TA523833 O14	202,30	$\geq$99
Magnesium Sulfate Heptahydrate	$MgSO_4$*$7H_2O$	Merck	A217086 026	246,48	$\geq$99.5

Feed solutions were prepared with deionized water (H_2O_d) and a concentration of 600 ppm. Deionized water is used because it's ions free. Prior to the salt dissolution, all the reference salts were weighted and put inside a stove, at 60°C for 30 minutes, to remove impurities and water content.

Before starting permeation tests, the feed solution conductivity was read 10 times, afterwards, circulated throughout the UF set-up for 30 minutes. For each membrane composition, three permeates were collected. Each permeate went to a conductimeter, see section 3.4.2.A, where conductivity was read 10 times. After every single reading, the equipment reading cells were cleaned with DI water. For each conductivity read a concentration was calculated, using the calibration lines, thus being possible the calculus of and average rejection factor and respective standard deviation. Finished a permeation test, the feed solution was cleaned and filled with DI water, that was circulated throughout out the UF set-up, for 1 h, to make sure there was no influence between tests.

3.4.2.A Salts Concentration Measurement

Salt concentration, on both feed and permeate, was measured by conductivity using a CRISON CONDUCTIMETER GLP 32, as shown in fig. 3.12, having a reproducibility of $\pm$0.1% and a reading error

$\leq$0.5% [65].

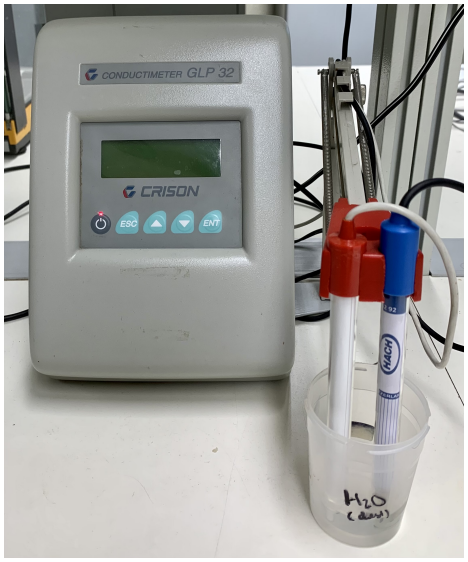

Figure 3.12: CRISON CONDUCTIMETER GLP 32

Before using the conductimeter, the user or if asked by the equipment itself, needs to be calibrated. Calibration is automatic and it's done in two steps. According to the user's manual [65], two standard- are needed: First Standard Solution of 1413 μS/cm and Second Standard Solution of 1288 μS/cm. Used standard solutions for the equipment calibration are shown in the following table.

Table 3.6: Standard solutions used for the automatic CRISON CONDUCTIMETER GLP 32 calibration

Compound	Manufacture	Lot	Conductivity (25°C) (mS/cm)
Potassium Chloride	VWR PROLABO	11C280028	1.41
Potassium Chloride	VWR PROLABO	11B250021	12.94

For the salt concentration measurement, calibration lines were made for each of the used salts, where a correlation of conductivity as a function of the concentration was obtained. Prior to the salt dissolution, all the reference salts were weighted and put inside a stove at 60°C for 30 minutes. Mother-solutions were made at 2000 ppm and respective dilutions at 1500, 1000, 700, 400, 200, 100 and 60 ppm. Conductivity was read from the least concentrated to the most concentrated, with cleanse with DI water of the reading cells between measurements. For each solution, 10 conductivity values were registered, being possible the calculus of an average and corresponding standard deviation. All conductivity values are automatically corrected to the reference temperature of 25°C. Calibration lines, for the four reference salts, can be consulted in appendix E.

3.4.3 Molecular Weight Cut-Off

The MWCO is the minimum molecular weight, in kDa, where 90% of the solute is rejected by the membrane. For this purpose, polymers with different molecular weights were used to calculate the rejection factor using eq. (3.2).

Permeation experiments were carried out with equal conditions for the salts rejection coefficient, i.e, at constant pressure and feed-rate (1 bar and 192 L/h respectively). The polymers used were PEG 400 Da, 3000 Da, 6000 Da, 10000 Da, 20000 Da, 35000 Da, and Dextran 40000 Da. Polymer data can be consulted in the next table.

Table 3.7: Polymers used to determine the MWCO

Compound	Chemical Formula	Manufacture	Lot	MW (Da)
PEG 4000	$HO(C_2H_4O)_nH$	Merck	MKCJ4921	400
PEG 3000		Merck-Schuchardt	819015	3000
PEG 6000		Merck-Schuchardt	807491	6000
PEG 10000		Merck-Schuchardt	821881	10000
PEG 20000		Fulka	95172	20000
PEG 35000		Merck-Schuchardt	818892	35000
Dextran 40000	$HO(C_6H_{10}O_5)_nH$	Amersham Pharmacia Biotech AB	285740	40000

Feed solutions were prepared with milliQ water and a concentration of 600 ppm. MilliQ water is used because it's organic carbon free. Prior to the polymers' dissolution, all of them were weighted and put inside a stove, at 60°C for 30 minutes, to remove impurities and water content.

After the machine mechanical cleaning, the total organic carbon (TOC) of a blank sample of milliQ water (used to prepare the solution) and a feed sample are read, 5 concordant measurements out of a maximum 10 readings, thus being possible the calculus of an average TOC value and respective standard deviation. Before starting permeation tests, the feed solution was circulated throughout the UF set-up for 30 minutes, afterwards the permeates were collected and TOC values were read with 5 concordant measurements out of a maximum 10. For all feed and permeates TOC values, the blank average TOC result was subtracted. Total organic values are then converted to concentrations, in ppm, using calibration lines, as stated in section 3.4.3.A. Finished a permeation test, the feed solution was cleaned and filled with DI water, that was circulated throughout out the UF set-up, for 1 h, to make sure there was no influence between tests.

3.4.3.A Total Organic Carbon and Concentration Measurement

Blank, feed and permeates TOC were measured using a SHIMADZU Total Organic Carbon Analyzer (TOC-V CSH/CSN), as shown in fig. 3.13, working with the combustion chamber at 680°C and a reconstituted air pressure of 200 kPa.

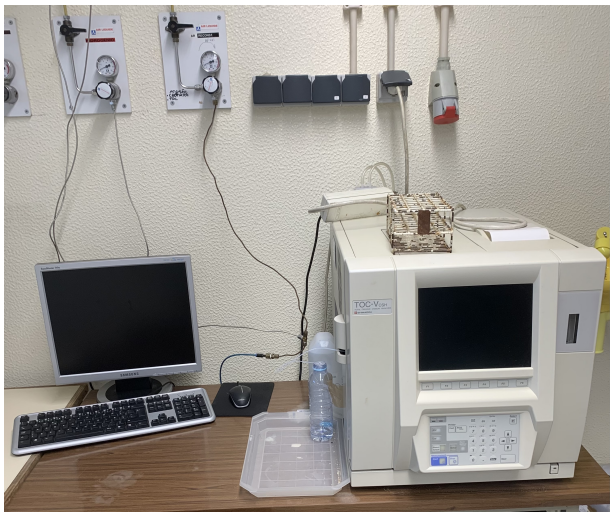

Figure 3.13: SHIMADZU Total Organic Carbon Analyzer

To ensure the concentration calculus of the samples, calibration lines were made for each of the used polymers, where a correlation of total organic carbon as a function of the solute concentration was obtained. Prior to the polymers' dissolution, all of them were weighted and put inside a stove, at 60°C for 30 minutes, to remove impurities and water content. Mother-solutions, in miliQ water, were made at 1000 ppm and respective dilutions at 500, 400, 300, 200, 100, 50 and 25 ppm. Total organic carbon was read from the least concentrated to the most concentrated, considering the best 5 readings out of a maximum of 10, thus being possible the calculation of an average TOC value, for a given concentration, and respective standard deviation. For all total organic carbon values obtained, the blank sample (milliQ water used to prepare the solution) was subtracted. Calibration lines can be consulted in appendix F.

SHIMADZU Total Organic Carbon Analyzer [66] carrier gas is controlled using a pressure regulator (set for 4 bar) and a mass flow controller. Carrier gas flows at 150 mL/min to the combustion tube, which has been filled with an oxidation catalyst and heated to 680°C. The total carbon (TC) of a sample is burned in the combustion tube to form carbon dioxide. The carrier gas, containing the carbon dioxide and other combustion products, flows from the combustion chamber tube to a dehumidifier, where it is cooled and dehydrated. Then, it passes through a halogen scrubber before it reaches the cell of non-dispersive infrared gas analyzer, where the carbon dioxide is detected. The signal forms a peak, and the area of this peak is measured by a processor. The peak area is proportional to the TC concentration of the sample. The inorganic carbon (IC) in TOC analysis refers to carbon contained in the carbon dioxide dissolved in water and that found in carbonates. By acidifying the sample with a small amount of HCl to obtain a pH less than 3, all carbonates produce CO_2 according to the following reactions.

$$Me_2CO_3 + 2HCl \mapsto CO_2 + 2MeCl + H_2O \tag{3.3}$$

$$MeHCO_3 + HCl \mapsto CO_2 + MeCl + H_2O \tag{3.4}$$

The carbon dioxide and dissolved carbon dioxide in the sample are volatilized by bubbling air or a gas that does not contain nitrogen or carbon dioxide through the sample [67].

3.5 Membrane Characterization Techniques

3.5.1 Membranes Drying

Before membrane characterization , stated herein 3.5, wet samples must be cut and dried. The cutting process is described in section 3.2.3.

To maintain chemical properties, pore size and pore distribution, the drying process chosen is a key-factor. Therefore, solvent-exchange adapted method [68] was made in which all the samples were submerged in a two solvent solution for a period of 24 h at room temperature, inside a fume hood. Aiming a completely dried membrane, the last solvent was evaporated in a desiccator coupled with a COMECTA, s.a, 0041615 vacuum pump to avoid any contact with air humidity. All of the reagents used and drying process scheme are presented in table 3.8 and table 3.9, respectively.

Table 3.8: Reagents used for the membranes drying process

Compound	Chemical Formula	Manufacturer	Lot	MW (g/mol)	Assay (%)
Isopropanol	C_3H_8O	Honeywell	H2360	60.11	$\geq$99.8
n-Hexane	C_6H_{14}	Carlo Erba Reagents	P7G039317G	86.00	$\geq$95

Table 3.9: Solvent-exchanged drying process with respective day, solution and time

Day	Solution	Time (h)
1	H_2O_d	24
2	Isopropanol (25% V/V) + H_2O_d (75% V/V)	
3	Isopropanol (50% V/V) + H_2O_d (50% V/V)	
4	Isopropanol (75% V/V) + H_2O_d (25% V/V)	
5	Isopropanol (100% V/V)	
6	Isopropanol (75% V/V) + n-Hexane (25% V/V)	
7	Isopropanol (50% V/V) + n-Hexane (50% V/V)	
8	Isopropanol (25% V/V) + n-Hexane (75% V/V)	
9	n-Hexane (100% V/V)	
10	Desiccator	

Finished the drying process, membranes must be stored in glass containers and away from light. It is important mentioning that membranes handling must be taken into account since, at each passing drying day, they become more fragile and brittle.

3.5.2 Field Emission Gun Scanning Electron Microscopy-FEGSEM

To study the behavior of the introduction of amine in the CA/SiO_2 membranes, and possible morphological and topographic changes, FEGSEM technique was used and performed by the JM-7001F FEG-SEM (JEOL) equipment at an accelerated voltage of 5.0 kV. Before the technique, membranes were dried according to the protocol in section 3.5.1 and cut into smaller pieces (1cmx1cm), and placed in liquid nitrogen to be cut again, so that the cross section was as uniform as possible. Finally, a film of gold and palladium was deposited on the samples so that they could become electrical conductors, as this image acquisition technique is made at the expense of the incidence of an electron beam. Micrographs of the top surface and bottom layer (magnification of x10000) and cross-sections (magnification of x800) were obtained. All dried membranes, which followed the protocol stated in section 3.5.1, that underwent FEGSEM technique are displayed on the next table.

Table 3.10: Dry membranes used for morphological and topographic study via FEGSEM technique

Membranes					
A100/0-1-2	A95/5-1-6	A90/10-1-4	A80/20-1-7	A70/30-1-9	A50/50-1-3

3.5.3 Mechanical Properties

Mechanical properties such as Young modulus, rupture elongation and rupture strength were analysed in a laboratory outside the Instituto Superior Técnico.

4

Results and Discussion

Contents

4.1 Membrane Characterization Techniques 41

4.2 Permeation Performance 51

4.3 Pore Size 66

For the interpretation and discussion of the experimental results, the plan presented in fig. 4.1 was followed. The general morphological characterization of the images obtained via FEGSEM was the first step, followed by a more detailed analysis of the various sections that constitutes the membranes: active layer, porous layer, and cross-section. Mechanical properties of the synthesised membranes were tested to see if amine functionalization brings better results when compared to CA and CA/SiO_2 membranes. Finally, all the results described above will be compared with the permeation properties in order to try to understand the impact of the TEOS and TEOS+APTES groups.

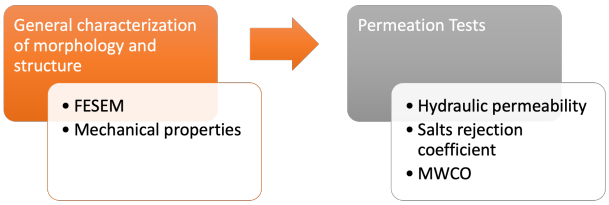

Figure 4.1: Schematic representation for the interpretation and discussion of the experimental results obtained

4.1 Membrane Characterization Techniques

4.1.1 FEGSEM

To assess the structure of the synthetized membranes FEGSEM technique was used. FEGSEM is an indispensable tool to study possible morphological changes caused by the presence of TEOS and TEOS+APTES within the CA matrix.

Membranes synthesized via sol-gel in conjunction with the phase inversion method have two distinct phases: an active layer and a porous layer. Figure 4.2, column (c), shows an active dense top layer and a porous bottom layer in all micrographs, which confirms the integral asymmetric structure and that *in situ* silica and amine-functionalization, CA-SiO_2 and CA-SiO_2-$(CH_3)_3NH_2$ respectively, did not affect the membranes' skinned asymmetric character.

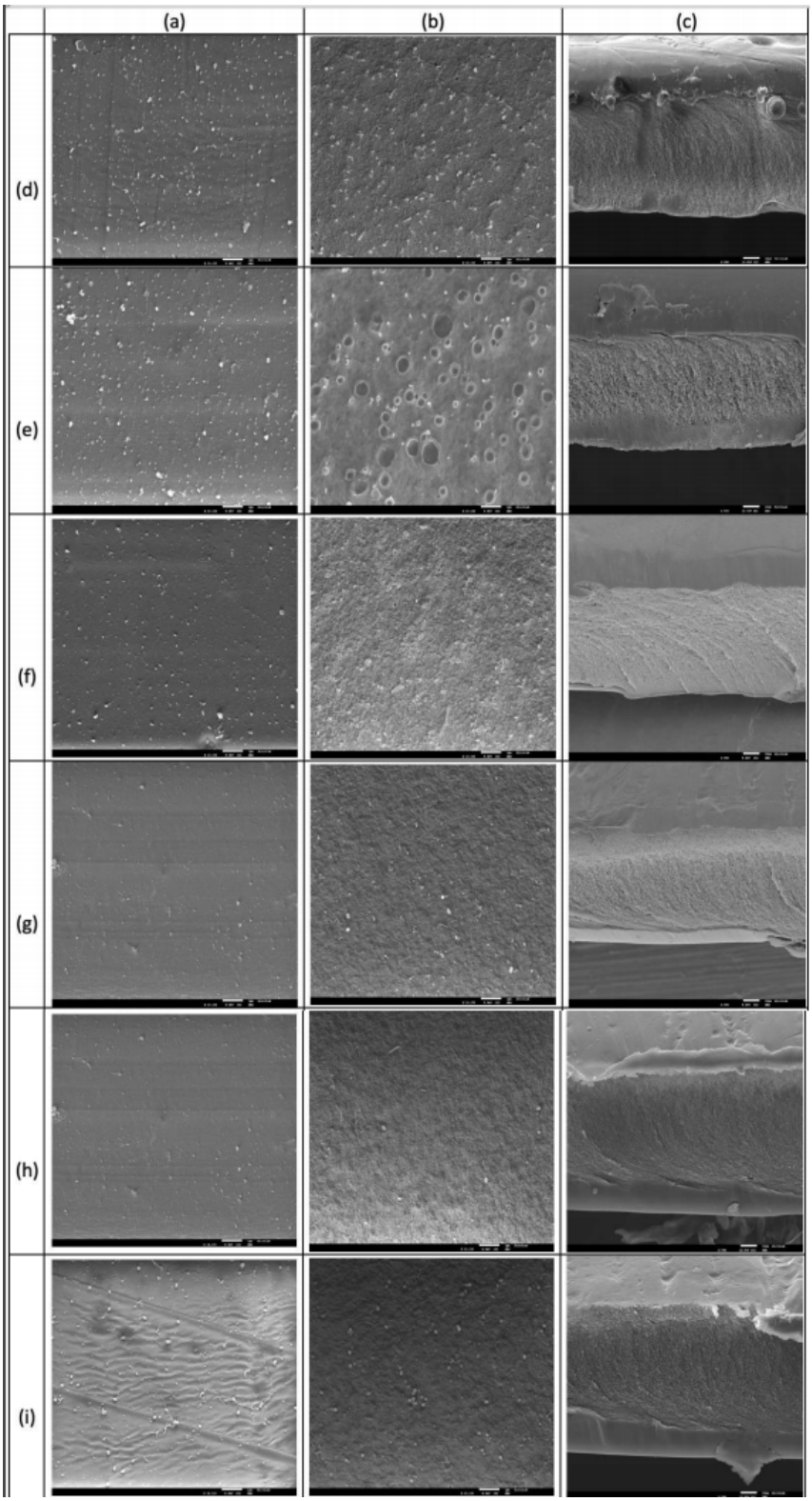

Figure 4.2: SEM microphotographs of the active layer (a), porous layer (b), cross section (c), at an energy of 15.0 kV and resolution x10000, x10000 and x800, respectively, for A100/0 (d), A95/5 (e), A90/10 (f), A80/20 (g), A70/30 (h) and A50/50 (i) membranes composition

With regard to the active layer, fig. 4.2 column (a), and porous layer, fig. 4.2 column (b), the introduction of the functional groups reveals to have a fundamental role in the morphology of the membrane. In all SEM images the presence of white structures/dots can be seen, whose quantity and density varies according to the composition. These structures, from now on, will be called clusters, and will be the target of a more detailed study since the active layer is directly related to hydraulic permeability, rejection of salts and MWCO, while the porous layer has the purpose to confer mechanical strength to the membranes while offering no resistance to permeation of water and reference solutes [69]. It is important to point out that in this work it was not possible to qualitatively and quantitatively analyze the chemistry of the clusters, that is, whether it is polymer, silica and/or amine. In addition, images of the active dense layer have no visible pores at a magnification of x10000, which is expected since the pores of UF membranes are in the range of 2 to 50 nm [20] [70].

4.1.1.A Cross-Section

Images obtained from the cross-section, fig. 4.3, shows that the increase in the molar content of APTES, and consequently the decrease in the molar content of TEOS, does not cause significant morphological differences, at the micrometer scale, in terms of polymer chains density. A95/5 membrane shows a less polymer dense behavior when compared to the others, fig. 4.3 column (a) and (b). For this composition, the cross-sectional images present a greater free space between the polymer chains, which will probably have some effect at the level of the permeation tests. The remaining membranes have similar behavior.

Membrane's composition A80/20, A70/30, and A50/50 show the presence of clusters in their structure, fig. 4.4. Composition A50/50 has, in general, the highest number of these structures, followed by A80/20 and finally A70/30. This behavior is not visible in the remaining compositions.

To evaluate the influence of these functional groups on the total membrane thickness (L), cross-section images from fig. 4.2 column (c) were analyzed via ImageJ, which is an open-source software for processing of scientific images. As all SEM images are accompanied by a scale, in the lower right corner, it is possible to establish a measurement reference. Since for images with a resolution of x800, 170 pixels correspond to 170 μm, it was possible to make three measurements of the membranes' thickness, in three different positions, enabling the calculation of an average value and respective standard deviation, as shown in the next table.

Membranes	L (μm)	std (μm)
A100/0	67	$\pm$1
A95/5	53	$\pm$0.5
A90/10	53	$\pm$1
A80/20	67	$\pm$2
A70/30	68	$\pm$3
A50/50	88	$\pm$1

Table 4.1: Mean values of membrane thickness, and respective standard deviation, calculated by the ImageJ image analysis program, for the cross-section images at a resolution of x800.

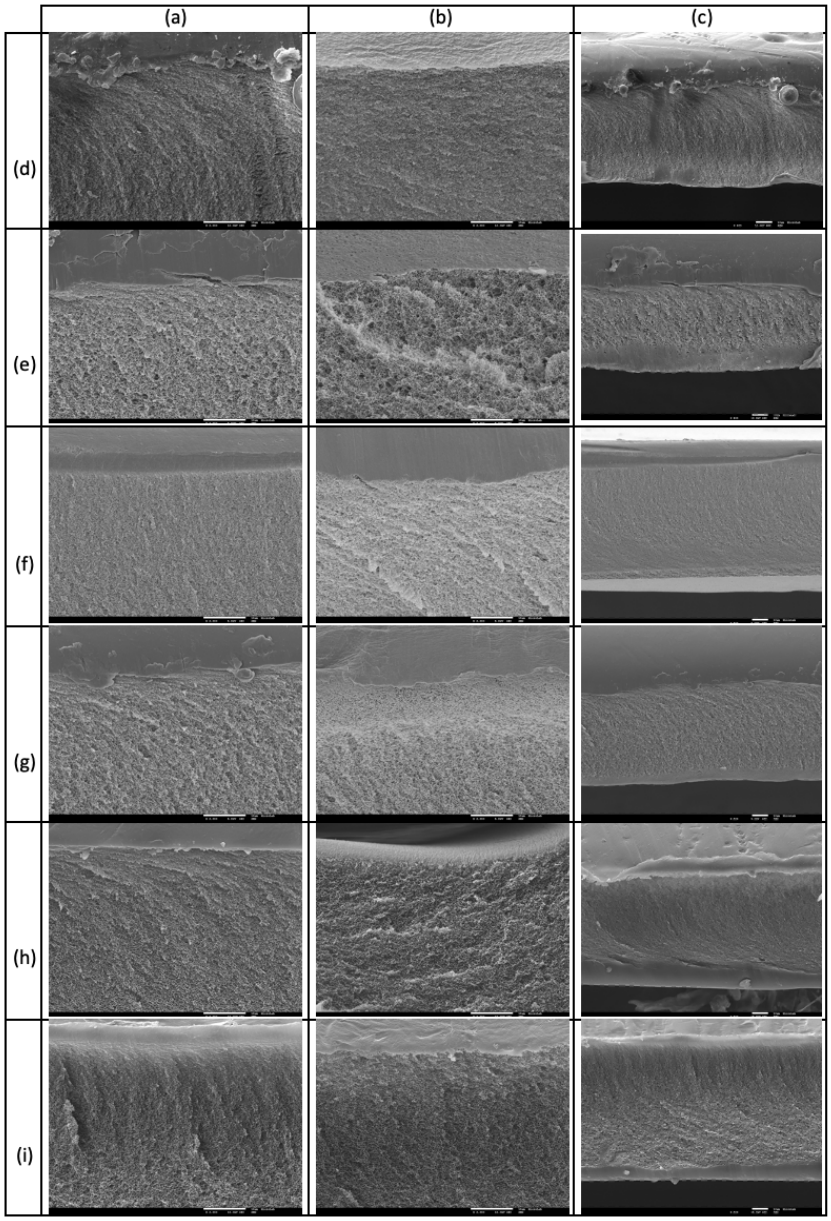

Figure 4.3: SEM microphotographs of the active layer (a), porous layer (b), cross section and complete cross section (c), at an energy of 15.0 kV and resolution x2000, x2000 and x800, respectively, for A100/0 (d), A95/5 (e), A90/10 (f), A80/20 (g), A70/30 (h) and A50/50 (i) membranes composition

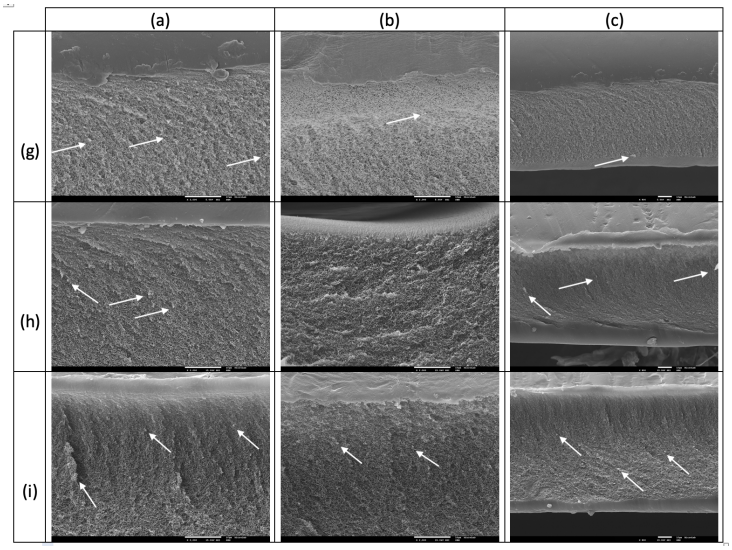

Figure 4.4: SEM microphotographs of the active layer (a), porous layer (b), cross section and complete cross section (c), at an energy of 15.0 kV and resolution x2000, x2000 and x800, respectively, for A80/20 (g), A70/30 (h) and A50/50 (i) membranes composition, being the white arrows the clusters structures

By analyzing fig. 4.5, TEOS/APTES functionalization translates into a 21% decrease in membrane thickness, in the passage from A100/0 to A95/5. This functionalization makes the membrane less thicker. The increase of the molar composition A95/5 to A90/10 has no structural impact whatsoever, which implies that for this range of compositions the functionalization does not entail changes. For compositions above A90/10, a strictly increasing behavior of the membrane thickness is noted. From A90/10 to A80/20, from A80/20 to A70/30, and from A70/30 to A50/50, there is a percentage increase of 8%, 19%, and 29%. This is indicative that the increase in the molar APTES content and the decrease in the TEOS content translates into a thicker membrane. This behavior is expected, since amine functionalization where the casting solution has a pH$<$5, results in a thicker structure [15]. In this set of results, the least thick membrane corresponds to A95/5 and A90/10, both with 53 μm, and the thickest membrane to A50/50 with 83 μm.

Previous works, developed during the master thesis dissertation, show that for a membrane with the same molar content of TEOS (A1-previous work), the total thickness is 53 μm [43], which translates to a difference of 14 μm, with the value of the present work (A100/0). Both membranes were synthesized by the sol-gel method and phase inversion and have the same molar amount of silica precursor. However, the amount of formamide used was lower than in this work. Formamide is considered a swelling agent, since the increase in its quantity, in the casting solution, translates into an increase in the total thickness of the membrane [71]. This is a justification for the differences found between works.

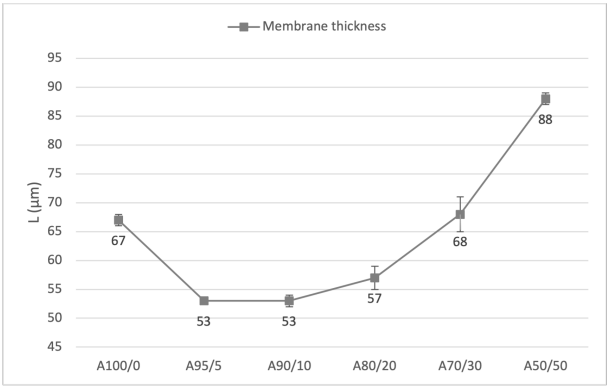

Figure 4.5: Effect of the presence of the TEOS functional group and TEOS/APTES functionalization on membrane total thickness

4.1.1.B Active layer

Images of the active layer (top dense surface) were studied via ImageJ. Two parameters were analyzed: number of clusters (Nc) and total area occupied (A). In terms of number of clusters in the active layer, fig. 4.6, the introduction of the APTES group does not cause major changes in the morphological levels of the membrane, with a decrease from 2106 to 2045 clusters. With the increase in the amine content and the decrease in the silica group, there is a sharp decrease of 58% in the number of clusters, in the transition from composition A95/5 to A90/10. As the SiO_2-NH_2 group, in molar terms, increases, the number of clusters decreases. From composition 90/10 to 80/20 there is a decrease of 21%, and from 80/20 to 70/30 a decrease of 27%. When the molar content of silica and silica functionalized with amine are equal, 50/50, the number of clusters rises from 495 to 821, translating into an increase of 65%. In global terms, increasing the molar content of NH_2 decreases the number of this structures, except for composition 50/50. Composition A100/0 and A70/30 are the ones with the highest and lowest number of clusters, respectively.

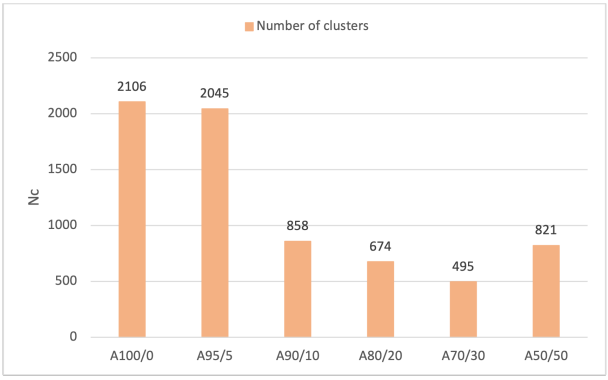

Figure 4.6: Membranes' number of clusters on the active layer

Figure 4.8 relates the total area of clusters, that is, the sum of all areas, with the total number of clusters.

With the introduction of the APTES precursor, the number of clusters decreases from 2106 to 2045, while the total area increases from 4.3 to 4.5 μm^2. This is indicative that for low amine compositions there will be no noticeable differences. However, from composition A95/5 to A90/10, the number of clusters and the total area, in percentage terms, decreases by 58 and 67%, respectively. This is suggestive that for molar contents above 5%, NH_2 plays a fundamental role in decreasing the number and total area occupied by these structures. This behavior continues to be verified for compositions above A90/10, with the exception of the A50/50 composition.

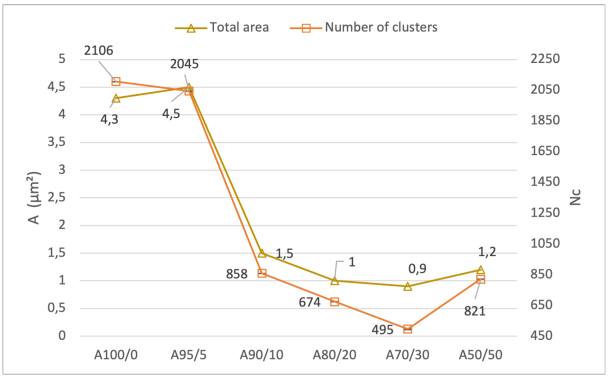

Figure 4.7: Relationship between the number of clusters and the total area occupied by these structures for the top layer

4.1.1.C Bottom Layer

Similar to what was done for the active layer, in the analysis of the porous layer, or bottom layer, the number of clusters and the total area occupied by them will be analyzed, as shown in the following figure.

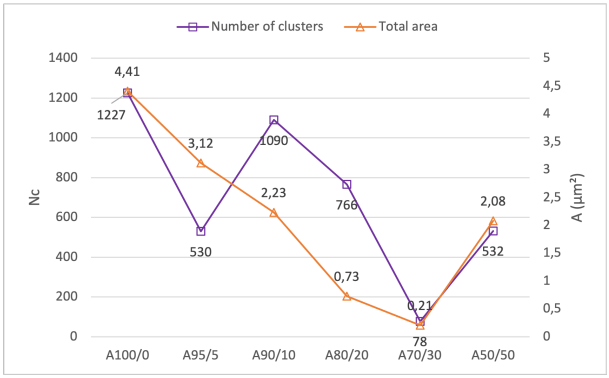

Figure 4.8: Relationship between the number of clusters and the total area occupied by these structures for the bottom layer

Concerning the total area occupied by the clusters, the behavior is strictly increasing with the increase of the propylamine group, except for the passage from A70/30 to A50/50. As for the number of clusters,

the introduction of the NH_2 group results in a sudden decrease of 57%, with an increase of 106% from A95/5 to A90/10, followed by a strictly decreasing behaviour until the transition from A70/30 to A50/50, where the number of these structures increases.

In general, the number of clusters and the area occupied by them decreases with increasing molar content of the APTES precursor, and for TEOS/APTES equimolar compositions, both properties increase. There is a clear deviation from this behaviour, regarding the number of clusters, in the transition from A100/0-A95/5-A-A90/10. This deviation can be explained by the presence of large O-ring-shaped structures, clearly visible in fig. 4.2 column (b) row (e), which may imply a greater difficulty in the formation of clusters.

4.1.2 Mechanical Properties

The following figure condenses the results obtained in the tests of mechanical properties, rupture strength, rupture elongation, and Young's modulus, as a function of membranes composition.

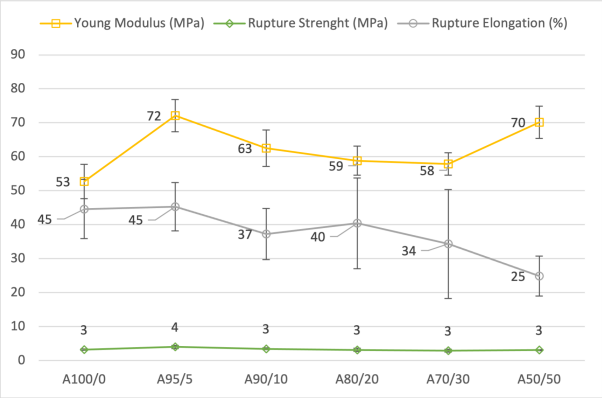

Figure 4.9: Mechanical properties as a function of membranes' composition

With the introduction of the propylamine group in the functionalized membrane of CA/SiO_2 (A100/0 to A95/5), the Young modulus increases from 53 MPa to 72 MPa. As the molar content of APTES increases, this parameter has a strictly decreasing behaviour, except for A50/50 membrane composition. This behaviour is also verified for rupture elongation, except the first two tested compositions whose value is constant. Young modulus, or the modulus of elasticity in tension, is a mechanical property that measures the tensile stiffness of a solid material [72], while elongation at break, also known as fracture strain, is the ratio between changed length and initial length after breakage of the test specimen and expresses the capability to resist changes of shape without crack formation [73].

The higher the modulus of elasticity of the material, the greater the rigidity, the greater the rigidity of

a structure, the more force must be applied to produce a given deformation. That said, amine functionalization (A95/5) makes the membrane more rigid, this being the highest value obtained for Young modulus for all compositions tested. However, and with the increase of this functional group, the membranes become less rigid. As far as rupture elongation, a higher percentage represents a more ductile material, which implies that as the APTES content increases, membranes become less and less ductile. This set of results allow us to state that the introduction of the amine group in the CA/SiO_2 membranes makes the network more closed, denser, with a much higher elongation at rupture point, while the increase of the NH_2 group the overall network becomes more open, less rigid, elongating less at rupture point [15]. This conclusion is supported with the values obtained for the total membrane thickness, via FEGSEM.

The tensile strength results are almost in line with the elongation results. This is expected since for the same Young modulus, the larger is the elongation at rupture point, the larger might be the rupture tensile strength [15].

When these results, (C), are compared with membranes with the same composition, from published works (P), fig. 4.10, there are notable differences in the mechanical properties.

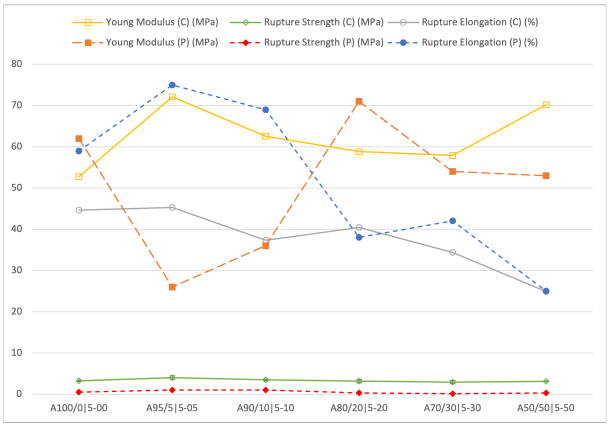

Figure 4.10: Mechanical properties comparison between the current work (C) and published work (P)

As far as rupture strength is concerned, the values of both works are within the same order of magnitude, and those of the published work are slightly higher. For rupture elongation, the values of published work are much higher than current work when comparing membranes of the same composition. This is indicative that P-work membranes exhibit a greater elastomer behavior. However, the behavior/trend of this property throughout the composition, for both works, is similar, excluding the passage A90/10—5-10 to A80/20—5-20. The notable difference is for the Young modulus, in which the behavior is inverse between works, since for amine compositions the overall network initially becomes more open, and tends

to close as the amine composition increases.

It is important to point out, once again, that the membranes, when compared, have the same composition and that they were all synthesized by the sol-gel method coupled with the phase inversion method. The difference in the behavior of the mechanical properties is based on the pH conditions of the casting solution, which in the current work was constant and of 2/3 value, whereas in the published work, the pH is initially acidic and becomes increasingly basic with the increase in the propylamine group. This point of the work, regarding the pH, will be addressed once more, and in more detail, in section 4.2.1.B.

Having analyzed the mechanical properties, it is now important to see the influences that clusters, and their respective properties, may or may not have. This influence can bee seen in the next figure.

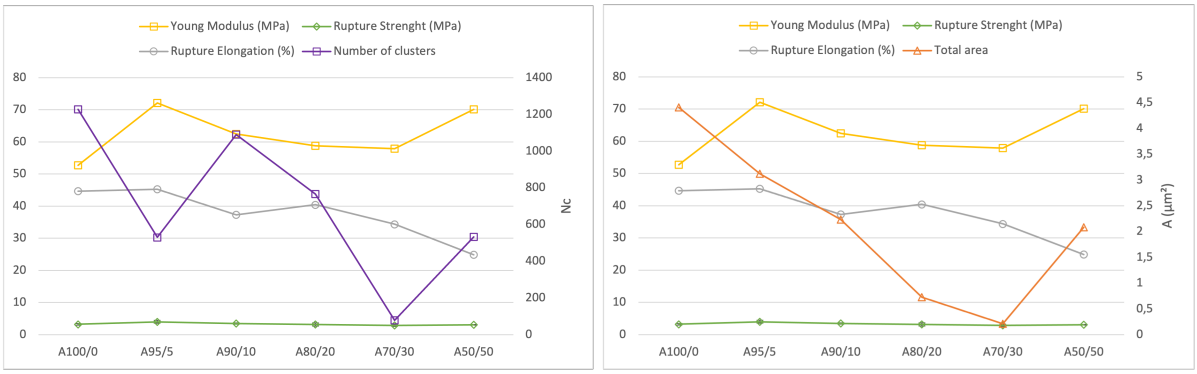

(a) Relationship between number of clusters and mechanical properties of the current work

(b) Relationship between the clusters total area and mechanical properties of the published work

Figure 4.11: Relationship between clusters properties and mechanical properties

The analysis of the figure allows us to conclude that the properties of the clusters do not have any influence on the rupture strength, since its linear behavior along the composition does not vary. For the compositions A100/0 and A95/5, the Young modulus has an inverse behavior with the number of clusters, that is, for contents without amine (A100/0), or with reduced molar composition (A95/5), the Young modulus is favored by the decrease in the number of clusters and by the area occupied by them. However, and with the increase in the molar content of the APTES group, there does not seem to be a direct relationship between the properties of the clusters with the mechanical properties, that is, despite the decreasing trend of mechanical properties, excluding A50/50, the decrease is not explained by the accentuated decrease in the number of clusters and area. In other words, the clusters do not have enough dimensions to cause significant changes in the mechanical properties, with the increase of the amine group.

4.2 Permeation Performance

4.2.1 Hydraulic Permeability

4.2.1.A Permeated Deionized Water Fluxes

Permeation tests were carried for a feed rate of 150 L/h and imposing a gradual TMP. For each composition tested, table 3.4, three experiments were performed, thus being possible the calculation of a average permeated flux, corrected to 25 °C, and corresponding standard deviation, fig. 4.12.

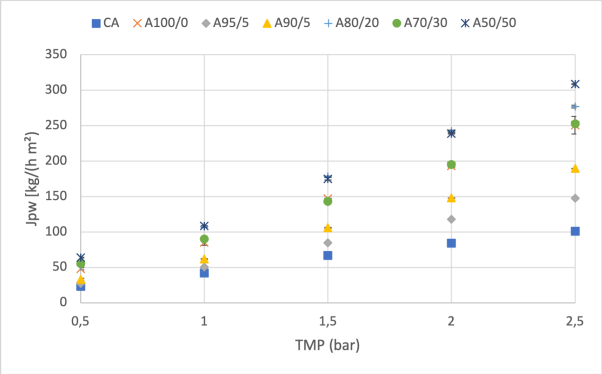

Figure 4.12: Average values of the permeated deionized water fluxes, of the first, second and third experiments, as a function of the imposed TMP, for the tested membranes

It is visible that, for a given composition, the greater the pressure exercised the greater the average permeated flux is. This conclusion is expected due to the direct proportionality between TMP and J_{pw} of eq. (3.1). It's worth mentioning that exists reproducibility between the three experiments. In other words, the standard deviation obtained never surpasses 1.55 kg/h m^2, except for A100/0-1-1 that has the highest values of 4.10, 2.01 and 12.24 kg/h m^2 for TMP of 1.0, 2.0 and 2.5 bar, respectively.

Preliminary analysis of fig. 4.12 allows us to conclude that membrane pairs A100/0 / A70/30 and A80/20 / A50/50 have similar behaviors, except the latter for pressure above 2.0 bar where A50/50 has higher flow value compared to A80/20. It is notorious that the introduction of silica (A100/0) promotes an increase in permeation flux when compared to the CA reference membrane, and that the introduction of the amine group, functionalized with silica, (A95/5 to A50/50) has the same effect, showing the potentiality of this functional group in terms of permeation. Furthermore, for molar compositions of A80/20 and A50/50, flux values are the highest, proving, once again, the potential of functionalization.

4.2.1.B Hydraulic Permeability

Hydraulic permeability is given by the slope of J_{pw} as a function of TMP. For each composition tested, three tests were performed, which implies three linear regressions that can be consulted in appendix D. Equation (3.1) is a good fit for the experimental results since R^2 values are always greater than 0.99. It's worth mentioning that exists reproducibility between the experiments. In other words, the standard deviation (std) obtained never surpasses 0.3 kg/h m^2, excluding membrane composition A100/0, where the std was 3 kg/(h m^2).

Regarding fig. 4.13, hydraulic permeability increases from 42 to 98 kg/(h m^2 bar), in the passage of the pure membrane of CA to A100/0, representing a percentage increase of 133%. This increase it's expected since permeation studies have shown that the integration of silica into CA membranes increases hydraulic permeability [20]. The key factor in changing the behavior of hydraulic permeability occurs when the propyl-amine group is added to single-phase hybrid membranes. After the introduction of the APTES group, the permeability decreases from 98 to 58 kg/h m^2 bar, representing a 41% decrease in the Lp value. This is due to the complexity of surface chemistry, which now has a variety of species (hydroxyl, acetate, silica, and propyl-amine). In this case, inter-molecular bonds squeeze porous diameter, resulting in the observed decrease. With the increase in the amine content, the hydraulic permeability presents a growing behavior, with an increase of 26% and 58%, in the passage from A95/5 to A90/10, and from A90/10 to A80/20, respectively. This suggests that for these ranges of compositions, the additional disorder caused by the propyl-amine chains is sufficient to force the opening of the overall network, producing more empty spaces, which justifies the increase in permeability. Concerning the three final compositions, the hydraulic permeability value tends to stabilize, although there is a small decrease of 14% from A80/20 to A70/30. For this range of molar compositions, hydraulic permeability is (111$\pm$11) kg/h m^2 bar.

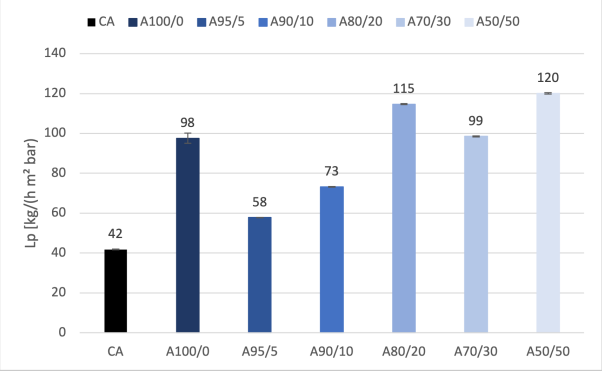

Figure 4.13: Hydraulic permeability for the tested membranes

Hydraulic permeability experiments prove that amine functionalization with hybrid CA/SiO2 membranes

enhances this permeation property, which will be greater the greater the content of the NH_2 group. This functional group shows promising results, as the hydraulic permeability value of A100/0 increases by 17% and 22%, when compared to A80/20 and A50/50, respectively.

Interestingly, the behavior observed is opposite to that reported in published works. The following figure compares the values obtained in the current work against the values obtained by other authors [15]. It is important to mention that the membranes, when compared, have the same composition.

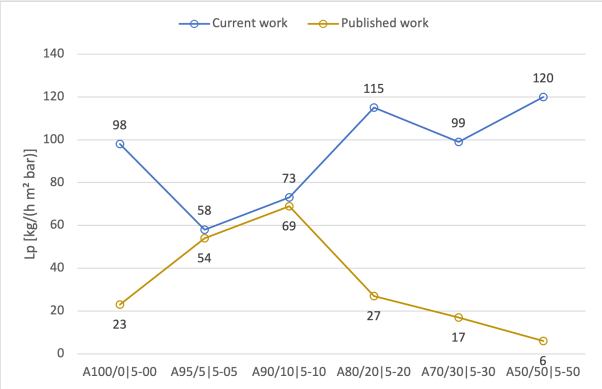

Figure 4.14: Comparison of the behaviour, of current work with published work, of the hydraulic permeability for monophasic hybrid membranes

By analyzing fig. 4.14, there is a big difference between the works regarding hydraulic permeability behavior. This noticeable difference is due to the pH of the casting solution. In the current work, the amount of nitric acid added was such as to reach a pH 2/3 for all the synthesized compositions. In the published work, the number of drops added for the CA/TEOS membrane, 5-00, was six, and for the remaining compositions of CA-SiO_2-NH_2 membranes was nine. The type of structure formed by the membrane to be synthesized depends on the balance between the hydrolysis and condensation steps, which are strongly affected by the pH of the casting solution. For acidic conditions (pH$<$5) condensation only occurs after all of the precursors are hydrolyzed. Thus, an extensive branching and therefore more open, less dense 3D network is produced since most functional groups -OH are available for condensation [15]. For more basic media (pH$>$10), hydrolysis and condensation happen at the same time, with fewer -OH groups being available for the condensation step, resulting in linear, less branched, and denser structures [74].

For membranes with only TEOS (A100/0 and 5-00), there is a difference of 75 kg/h m^2 bar between the two values. This is suggestive that the number of drops added to the casting solution, in the published work, was not enough to reach a pH$<$5, implying a much denser structure when compared to A100/0, justifying the difference in hydraulic permeability values.

With the introduction of propyl-amine in the membrane structure, Lp decreases in current work, and increases in published work, with a difference of 4 kg/h m^2 bar between A95/5—5-05 and A90/10—5-10. The similarity between the values of hydraulic permeability may suggest that the amount of drops added in the published work, six, was enough to reach a pH<5, and close to the pH of the current work.For the last compositions there is a difference of 88, 82, and 114 kg/h m^2 bar for A80/20—5-20, A70/30—5-30, and A50/50—5-50, respectively. In the current work, with the increase of the APTES group, the amount of acid drops added to the casting solution also increased to reach a pH=2/3.This is indicative that, for molar compositions greater than 90/10, there will be a greater difficulty in protonating the amine group, since there are a greater number of NH_2 groups that can capture the H^+ ions in solution. In the published work, the number of drops added was six, as mentioned above. Keeping the number of drops equal, as the amine content increases, there will be more and more NH_2 groups available to capture ions, making the pH of the casting solution higher as the molar content of APTES increases. Consequently, for the published work, the pH reached will be close to, or higher than 10, which implies in increasingly dense structures, with the increase of NH_2, causing the linear decrease observed in the hydraulic permeability behavior. This is not verified in the current work.

As mentioned before, section 4.1.2, mechanical properties of the two works show notable differences, with the pH being the central point of difference. It becomes important, then, to see how permeation properties are affected by considering the mechanical properties, as shown in fig. 4.15.

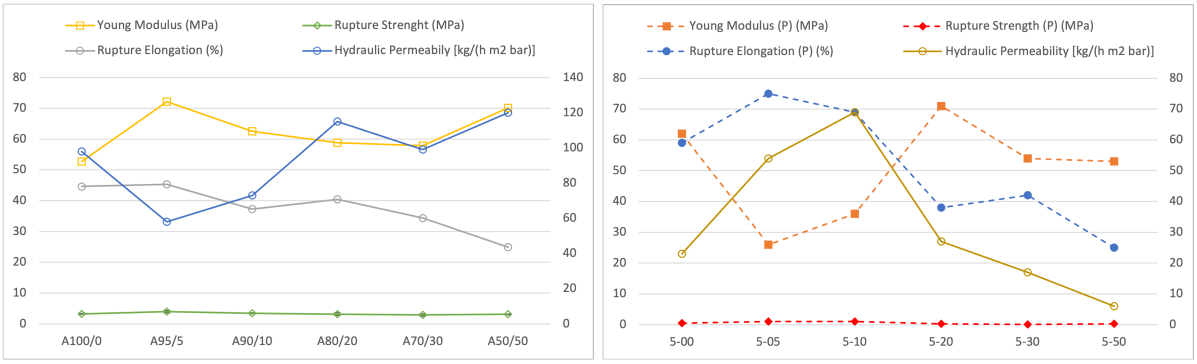

(a) Relationship between hydraulic permeability and mechanical properties of the current work

(b) Relationship between hydraulic permeability and mechanical properties of the published work

Figure 4.15: Comparison between works of the relationship of hydraulic permeability mechanical properties

In the current work, although rupture elongation remains constant, functionalization with the amine group (A100/0 to A95/5) favors an increase in Young modulus and translates into a decrease in Lp. This, and as previously mentioned, confirms that the introduction of the propylamine group forces the membrane structure to be more closed, denser, and consequently, lower uptake of water molecules. This is

also supported by the decrease in total membrane thickness by FEGSEM images. As the NH_2 group increases (from A95/5 onwards), Young's modulus decreases and presents a decreasing but stable behavior, that is, the decrease of this parameter is not very accentuated throughout the composition. Similarly, rupture elongation stably decreases. These results, once again, justify the increasing increase in hydraulic permeability, since the network produced is more extensive and with more branching.

It is important to point out that a constant pH, 2/3, for all the synthesized compositions allows us to conclude that there will not be major significant changes in the mechanical properties, and these, when present, are only justified by the increase in the APTES group. This assertion is easily supported by the comparison of the mechanical properties of the published work, whose pH becomes increasingly basic with the increase of the propylamine group. In the published work, there is an increase in the basicity of casting solution with the increase of the propylamine group. In terms of influences from mechanical properties, Young's modulus tends to increase, stabilizing for final compositions, and rupture elongation tends to decrease. Since for more basic conditions, the structure produced is denser, linear, and compact, the "approximation" of the structure may favor and indicate some cross-linking between CA chains, since carbon 3 of each glucose is available to establish cross-links between adjacent CA chains, by condensation reactions, which explains the increased membrane stiffness (by increasing the Young modulus of the membrane, and by increasing elastomer behavior seen by decreasing rupture elongation).

Taking into account what was mentioned above, the pH of the casting solution, particular with amine functionalization, is crucial for hydraulic permeability, as more acidic conditions (pH$<$5) favor this property, and for more basic conditions (pH$>$10) the opposite happens. Furthermore, a constant and acidic pH (pH$<$5) does not change the mechanical properties. The same does not happen with the increase in pH, that makes the membranes increasingly rigid and with an elastomer behavior.

Given that in all synthesized membranes there are clusters in the active layer, it is necessary to investigate their influence on the permeation level, fig. 4.16(a) and fig. 4.16(b), since the active layer plays a decisive role in the permeation properties.

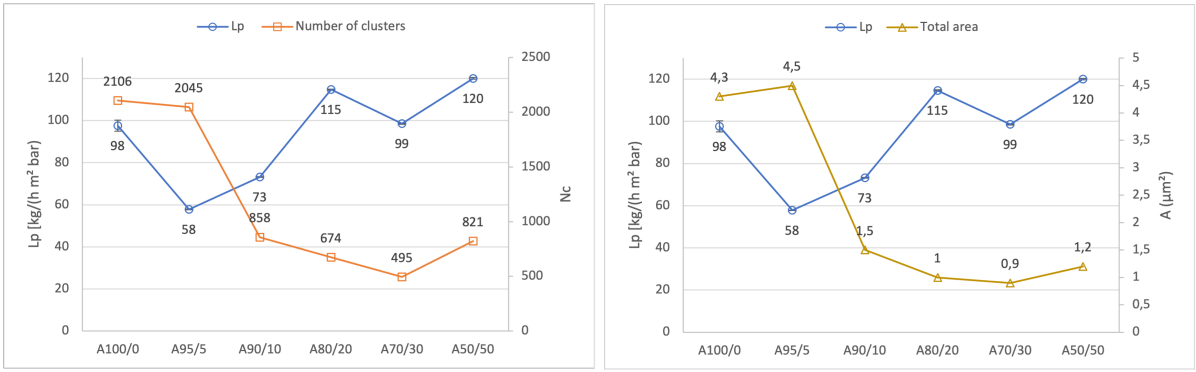

(a) Relationship between hydraulic permeability and number of clusters present in the active layer of membranes

(b) Relationship between hydraulic permeability and total area of clusters on the active layer

Figure 4.16: Relationship between hydraulic permeability and clusters' properties

Although the number of clusters decreases and the total area occupied by them increases, in the passage from A100/0 to A95/5, it is not enough to explain the Lp variation, since the decrease and increase of the mentioned properties is not significant. This implies that for CA/TEOS membranes and CA/TEOS membranes functionalized with a reduced molar amine content, the hydraulic permeability is not influenced by the presence and characteristics of these structures. For compositions above A90/10, the hydraulic permeability behavior follows the behavior of the number of clusters and the area occupied by them, apart from the A70/30 composition. This is indicative that for molar amine contents greater than 10%, the number of these structures, and their total area, decrease, thus presenting less difficulty for water molecules to cross the active layer, as if there were less impediment to mass transfer.

4.2.1.C Membrane Resistance

From the analysis of fig. 4.12, and also of the several linear regressions available in the appendix D, deionized water presents an ideal behavior, as verified in fig. 1.8. In other words, there is no decrease in flux over the permeation time, so the resistance to the mass transfer of the solvent (DI water) depends exclusively on R_m. It is important to point out that the solvent used, deionized water, presents values not higher than 5 μS/cm^2, and the presence of ionic species that can interact with the membrane is negligible. Since R_m is given by the inverse of hydraulic permeability, the mean value of the membrane resistance, taking into account the three tests for each composition and TMP, and respective standard deviation can be consulted in the following table.

Membrane	R_m x10^{-3} (h m^2 bar/kg)	std x10^{-5} (h m^2 bar/kg)
CA	24	$\pm$13
A100/0	10	$\pm$2,7
A95/5	17	$\pm$3,8
A90/10	14	$\pm$2,8
A80/20	9	$\pm$2,1
A70/30	10	$\pm$2,5
A50/50	8	$\pm$2,4

Table 4.2: Mean values of membrane resistance and respective standard deviation for tested membranes

As expected, CA has the highest membrane resistance value and consequently the lowest permeability value recorded. Membranes A100/0 with A70/30, and A80/20 with A50/50, have similar resistance values, which implies very similar permeability values. This was stated before by the analysis of fig. 4.12. Also, the higher the hydraulic permeability value, the lower the permeation resistance. Thus, membranes with better pure water permeation characteristics are A80/20 and A50/50, since they have the highest Lp and the lowest Rm.

4.2.2 Salts Rejection Coefficient

4.2.2.A Permeated Salts Fluxes

Permeation tests were carried out at TMP=1 bar and a feed rate of 150 L/h. Before any reading of the permeate concentration, three tests were performed in which the permeate mass was collected, recording the respective permeation time, for the four reference salts, for all compositions. This allowed the calculation of an average permeate flux value, for each salt, and respective standard deviation. Std never exceeded 1 kg/h m^2, except for the Na_2SO_4 salt for A100/0 composition membrane, where the highest deviation of 6 kg/h m^2 was recorded. All fluxes were corrected to 25 $^\circ$C.

The behavior in terms of permeate flux of the reference salts, fig. 4.17, follows the same behavior as the permeated DI water flux. This is expected since we are dealing with diluted solutions and, in a limiting case, consider that we are at infinite dilution. Also, and due to the similarity between salt fluxes and permeated water flux, none of the membranes were clogged, since there was no marked decrease in flux, or have pinholes, characterized by the accentuated increase in permeation flux.

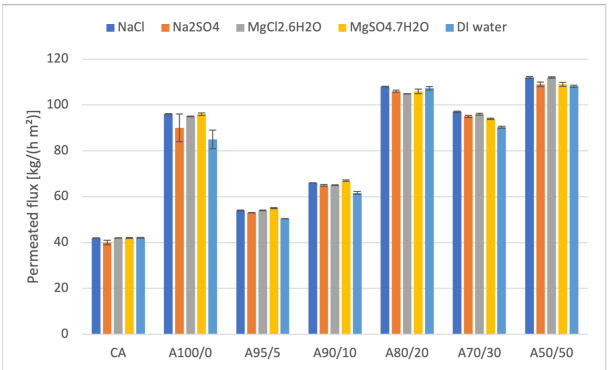

Figure 4.17: Comparison of the corrected permeate fluxes of the reference salts, obtained at TMP=1 bar and feed rate of 180 L/h, with the DI water permeate corrected fluxes obtained at TMP=1 bar and feed rate of 150 L/h

4.2.2.B Rejection Factor

The results obtained for the rejection coefficients, at 1 bar and 180 L/h, are presented in the following figure. The standard deviation never exceeds 3% except for the membrane A95/5, N_2SO_4 salt, which recorded the highest deviation, 6%.

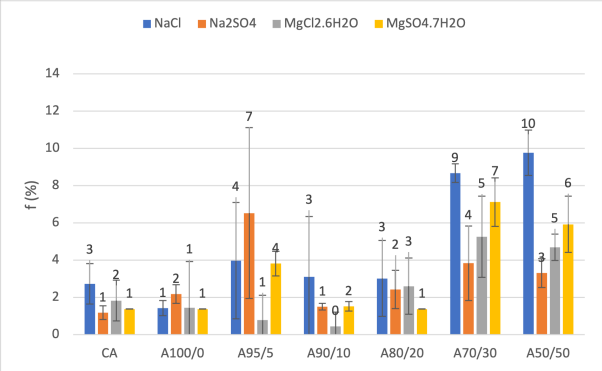

Figure 4.18: Rejection coefficients for reference salts

For the pure cellulose acetate membrane, NaCl presents the highest rejection factor, 3%, followed by $MgCl_2$, 2%, and finally Na_2SO_4 and $MgSO_4$, both with a rejection of 1%. With the introduction of the silica group, the rejection factor for NaCl decreases from 3% to 1%, $MgCl_2$ from 2% to 1%, while the rejection of Na_2SO_4 increases from 1% to 2% and that of $MgSO_4$ remains unchanged. Although the CA/TEOS functionalization promotes higher permeate salt fluxes, the rejection coefficient does not show major changes, meaning that the introduction of SiO_2, and respective structural and morphological changes caused in pure CA membranes, do not impact this property.

The shifting point of the ”stationary” behavior of the rejection coefficients changes with the introduction

of the APTES group. When changing the molar composition from A100/0 to A95/5, the rejection coefficients increase by 3% for NaCl, Na_2SO_4 and $MgSO_4$, while $MgCl_2$ remains unchanged. When changing from A100/0 to A95/5, the rejection coefficients increase by 3% for NaCl, Na_2SO_4, and $MgSO_4$, while $MgCl_2$ remains unchanged. With the increase of the amine molar composition, from A95/5 to A90/10, the rejection factor decreases to 3%, 2%, 1%, and 0%, for NaCl, $MgSO_4$, Na_2SO_4, and $MgCl_2$, respectively. Between A90/10 and A80/20 molar compositions, rejection coefficients do not show great changes, except $MgCl_2$ which shows an increase from 0% to 3%. When the amine content increases again, A70/30, all rejection coefficients increase, remaining stable for higher molar compositions, A50/50.

It should be noted that the key points for changes in the rejection factor are the passage of the pure cellulose acetate membrane (reference) to A95/5 and from A80/20 to A70/30, as for CA to A100/0, A90/10 to A80/ 20, and from A70/30 to A50/50 the rejections do not show significant changes. The size of the salt does not appear to be a decisive factor for the rejection coefficient, since NaCl is the salt with the lowest weight and has the highest rejection values for the CA, A90/10, A70/30 and A50/50 membranes.

Due to the dimensions of the salts in solution, all membranes are permeable to the reference salts. This result is expected since for UF membranes the rejection of mono and bivalent salts is theoretically null, fig. 1.4.

4.2.3 MWCO

4.2.3.A Permeated PEGs and Dextran Fluxes

To determine the MWCO it is necessary to calculate the rejection coefficient for several reference polymers, with increasing molecular weight, through permeation tests. However, and for high molecular weight polymers, clogging of pores may occur. Thus, in addition to washing the installation with DI water, and similar to the deionized water permeation fluxes, masses were weighed, and the respective permeation times were recorded to obtain the permeate flux of PEGs and Dextran. Table 4.3 summarizes the various permeation fluxes obtained. All fluxes are corrected to 25 °C.

Table 4.3: Permeate fluxes obtained at TMP=1 bar and feed rate of 180 L/h, for PEGs and Dextran, corrected for a temperature of 25ºC

Membrane	Permeated Flux [kg/(h m^2)]						
	PEG 300	PEG 3000	PEG 6000	PEG 10000	PEG 20000	PEG 35000	Dextran 40000
CA	41	41	40	39	33	28	7
A100/0	91	92	91	91	92	90	89
A95/5	52	53	50	50	53	52	53
A90/10	60	63	60	61	63	61	61
A80/20	102	108	103	92	102	104	100
A70/30	93	90	97	97	89	86	96
A50/50	114	109	110	110	104	97	92

For all compositions, with the exception of the pure CA membrane, the fluxes of PEG and Dextran are similar if we fix the same tested composition, which indicates that there are no pinholes in the membrane, as their existence would translate into an abrupt increase in the permeation flux. For each composition, an average value for the permeate flux of a polymeric solution will be considered, with weights ranging between 300 and 40000 Da, as shown in the following figure.

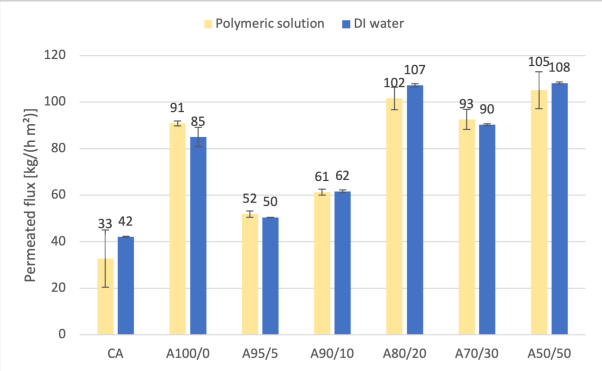

Figure 4.19: Comparison of the permeate flux of a polymer solution from 300 to 40000 Da at TMP=1 bar and feed-rate of 180 L/h, with the flow of DI water permeated at TMP=1 bar and feed-rate of 150 L/h , for the tested compositions

Figure 4.19 shows the comparison between the average permeate flux for a polymer solution and the permeate DI water flux. It is possible to conclude that there is a similar behavior between the results obtained, except for the CA membrane. In this case, between PEG 35000 and Dextran 40000, there was a sharp decrease in permeation flux. This is indicative that clogging of the pores or accumulation of polymer on the surface of the membrane that was not properly washed may have occurred, justifying the high value for std. This can be supported by the fact that for pure 100 wt.% CA a very tight polymer matrix is formed, thus the pores formed on the membrane surface will be a smaller size [64], making the passage of larger solutes more difficult.

4.2.3.B Rejection Factor for PEGs and Dextran

With the values obtained from TOC analyzer, it was possible to calculate the concentration of PEG or Dextran, in solution, with the aid of calibration lines. Thus, knowing the feed and permeate contractions, it was possible to calculate the rejection coefficients. The following figure comprises all calculated rejection factors as well as associated deviations. It is important to note that the standard deviations never exceeded 2%, with the highest value recorded being 4% for the CA membrane and PEG 35000.

Analysis of fig. 4.20 allows us to conclude that all tested membranes follow the same type of behavior except for the pure CA membrane, that is, as the molecular weight increases, the rejection factor also increases. This is expected since in ultrafiltration processes the mass transfer is done by size exclusion, which implies that larger solutes find it more difficult to pass through the pores, thus being rejected. Rejection factors obtained for the pure CA membrane are not reliable given what was said due to the clogging of the pores, preventing the solutes from being permeated and later read in the TOC analyzer. For PEG 300 Da, the rejection values are low, with the highest value recorded being 15% for A95/5. From the PEG 3000 Da onwards, a behavior is always checked. The minimum rejection factor is always for composition A50/50 and the maximum for A95/5. This is indicative that for compositions with higher silica contents it is possible to have a greater SiO_2 bond bound to the cellulose acetate structure, producing a denser three-dimensional polymer network that will hinder the passage of polymer along the membrane. In fact, as the molar content of APTES increases, the rejection value decreases, with the exception of the A70/30 membrane. Generally speaking, $f_{A95/5} > f_{A90/10} > f_{A80/20} > f_{A50/50}$.

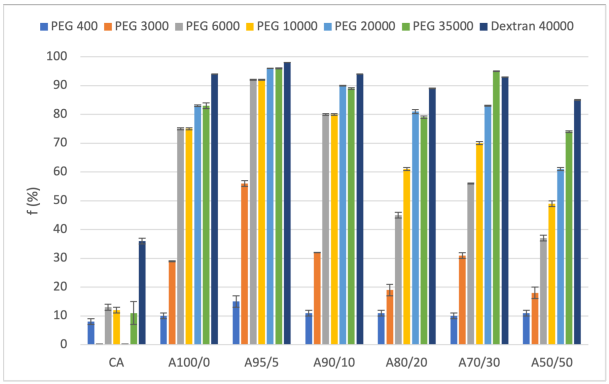

Figure 4.20: Summary of the rejection coefficients for the various solutions of PEGs and Dextran in MilliQ water for the tested compositions

4.2.3.C MWCO Determination

The determination of MWCO, for a rejection of 90%, is made by representing the molecular weights of the reference polymers as a function of the rejection coefficient, intersecting with f=90%. Sometimes,

when the rejection reaches values close to 90%, the curve tends to stabilize, making the direct reading of the chart difficult. In other situations, such as the A80/20 and A50/50 membranes, the rejection never reaches 90%, making it impossible to directly determine this property. It is possible to linearize the rejection factor in the section of the graph where the curve tends to stabilize, using the expression log[f/(1-f)] [20], and intersecting with log[0.9/(1-0.9)]=0.9542. Thus, it's achievable the determination of two MWCO: $MWCO_{exp}$ (by direct determination of the rejection factor as a function of molecular weights intersecting f=90%) and $MWCO_{lin}$ (by linearization of the rejection in the curve section intersecting with f=0.9542). The following set of images compresses the MWCO determination for the various membranes, while fig. 4.27 summarizes the results obtained for both determinations.

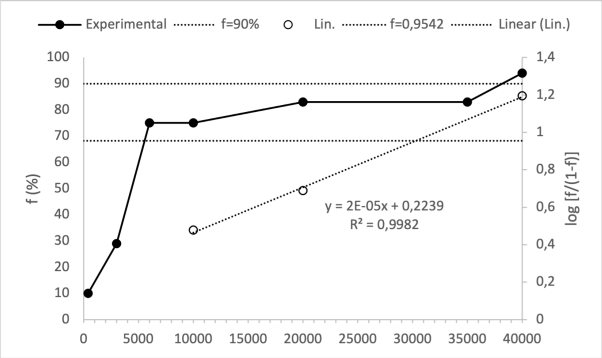

Figure 4.21: MWCO determination for A100/0

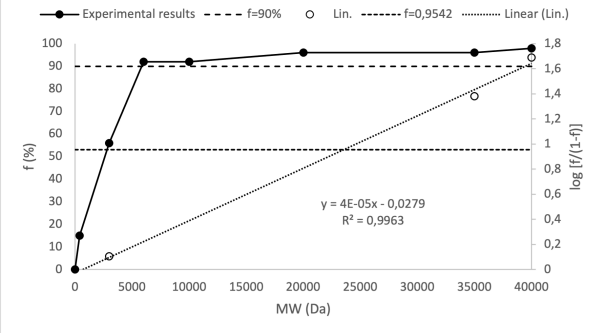

Figure 4.22: MWCO determination for A95/5

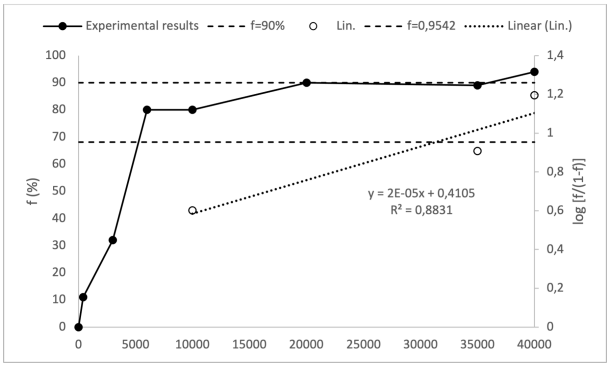

Figure 4.23: MWCO determination for A90/10

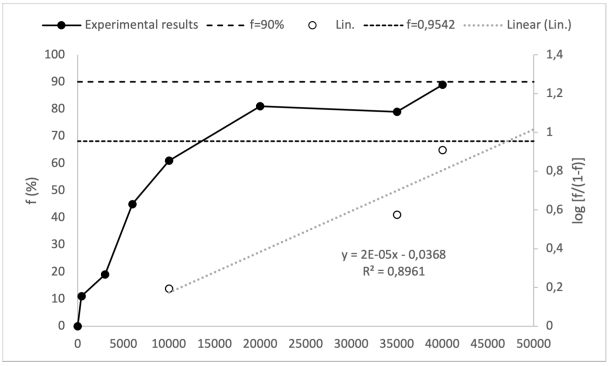

Figure 4.24: MWCO determination for A80/20

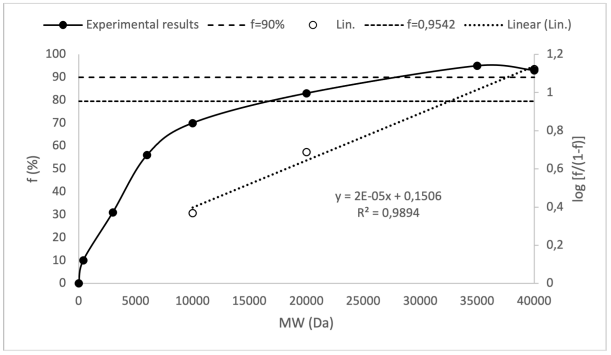

Figure 4.25: MWCO determination for A70/30

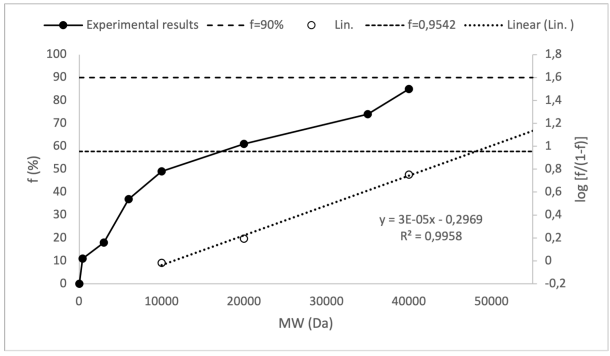

Figure 4.26: MWCO determination for A50/50

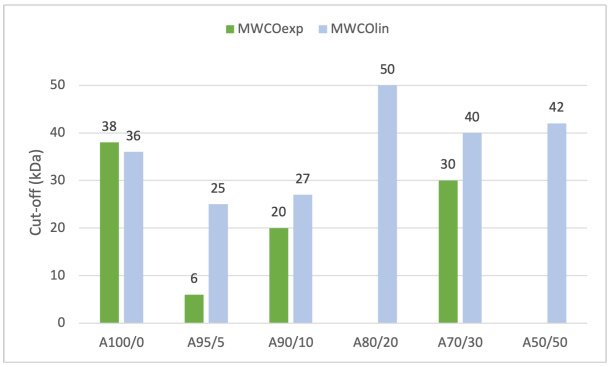

Figure 4.27: Summary of calculated MWCO values for tested membranes

For membranes of composition A80/20 and A50/50 it was not possible to determine MWCOexp, since the rejection factors do not exceed 90%. For this, it would be necessary to test higher molecular weight polymers. In this way, the MWCO will be the determined by the linearization of the rejection factors. For A100/0 and A90/10, both determined MWCOs have similar values, so the value determined by the experimental method will be considered. For A100/0 and A90/10, both determined MWCOs have similar values, so the value determined by the experimental method will be considered. In the case of A95/5 and A70/30, there is some mismatch between the calculated values. This is because there are polymers of different molecular weight with the same rejection factors, such as A95/5, and there is no increasing behavior in the rejection factor with increasing molecular weight, A70/30, since from PEG 35000 Da to Dextran 40000 Da the rejection factor decreases from 95% to 93%. For this pair of membranes, the value obtained by linearization will be considered. The following figure shows the MWCO for the tested compositions.

Figure 4.28: MWCO for the tested membranes

When going from A100/0 to A95/5, and from A95/5 to A90/10, there is a decrease of 34% and 20% in the MWCO. This decrease is to be expected, since the increase in the SiO_2 content in the CA matrix promotes the increase in MWCO [20] [43] [75]. In this case, and for this set of compositions, the molar reduction of the TEOS group promotes a decrease in the value of this property. Furthermore, for molar compositions A95/5 and A90/10, the APTES group does not make a visible contribution, as the decreasing behavior seen depends on the decrease of silica. The ”turning point” is from the A80/20 composition, as there is a notorious 150% increase in the MWCO value, from A90/10 to A80/20. This increase suggests that, despite the silica content and theoretically the MWCO value should also decrease, the molar content of APTES group introduced is sufficient to counteract this decrease. Once again, functionalization of CA-SiO2 membranes with NH_2 shows the amine's potential. However, and for compositions above A80/20, MWCO decreases, and tends to stabilize between 40 and 42 kDa. Like what happened in the above-mentioned references, starting from a given silica composition the MWCO would have a maximum value, which would decrease with the increase of the silica content. This can be indicative that for compositions around A80/20, the MWCO value will be maximum, and that for higher compositions of amine, the value tends to decrease. Despite what was mentioned, the MWCO stabilizes after the maximum value recorded, even with the increase in NH_2 and decrease in SiO_2, which suggests that for this range of compositions, the MWCO cut-off is not affected.

There are main limitations for defining MWCO [76]. First, UF membrane's pore size distribution is not constant. Second, most UF membranes being hydrophobic adsorb proteins on the surface and inside the pores due to membrane–protein interaction resulting in higher retention (a) due to reduced pore size, and (b) due to the secondary film formed on the membrane surface. Third, it is difficult to pick the 90% point on the S-shaped retention vs. molecular weight curve, and fourth, it is difficult to select the marker protein since polymers of the same molar mass have different molecular size. Despite being a commonly accepted methodology, this method is inherently deficient since the atomic mass does nothing to describe the actual size or geometry of a molecule [77]. It is a ”mere” indicator.

All synthesized membranes have a strong potential for the filtration of human blood, especially PBUTs. These toxic uremic proteins have a molecular weight $<$ 500 Da [78], which theoretically implies that they are permeated by membranes since the cut-off is greater than their molecular weight . On the other hand, these PBUTs are tightly bound, through ionic and/or hydrophobic characteristics, to albumin in the blood. Since albumin has a molecular weight of 60 kDa, all membranes would reject this protein, which is desired. However, it is necessary to test whether the amine group will intervene and break this strong bond between PBUT-Albumin, which is only possible through permeation tests to these toxins. These set of affirmations are mere hypotheses.

4.3 Pore Size

Despite the limitations presented in the determination of MWCO, there are empirical correlations that allow relating the cut-off of a given membrane with the pore diameter (d_p), in nm, eq. (4.1) [79]

$$d_p = 0.09(MWCO)^{0.44} \tag{4.1}$$

being $MWCO$ in Da. The following figure encompasses the results obtained at the expense of the aforementioned equation.

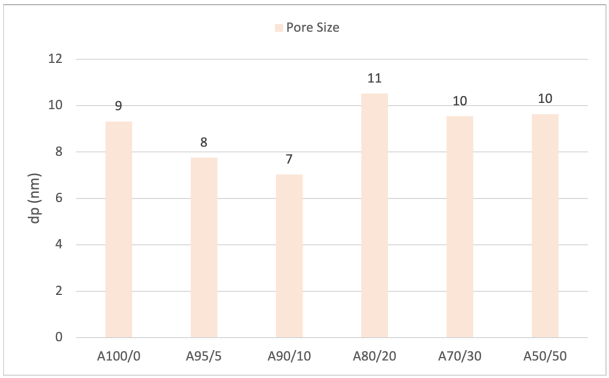

Figure 4.29: Size pore determination based on the MWCO

By analyzing the figure above, the reduction of the SiO_2 group and the introduction of the NH_2 group promotes a linear decrease in pore size. However, for higher amine contents, A80/20, the pore size increases, remaining stable for higher compositions, showing the amine functionalization alters the properties of the membrane, since in this same range it is where the increase, and the highest values, of hydraulic permeability are registered. All synthesized membranes have typical pore diameter values for UF membranes, ranging from 2 to 50 nm [70].

5

Conclusion

Contents

5.1 Future Work Proposals 71

Pure cellulose acetate membrane, cellulose acetate silica membrane and amine functionalized silica and cellulose acetate membranes were prepared and synthesized by the phase inversion method. Silica and amine were added to the cellulose acetate polymer matrix, *in-situ*, via the sol-gel process, by the addition of precursors, TEOS (silica precursor) and APTES (amine precursor), so that the process of hydrolysis and condensation would occur, to promote the chemical bond between silica and amine with the polymer.

Morphological analysis via FEGSEM allowed us to conclude that the functionalization of CA/SiO_2 membranes with amine leads to a linear increase in the total membrane thickness with the increase in the molar content of the amine, once for conditions of pH$<$5 condensation only occurs after total hydrolysis of the precursors, which implies extensive branching and less dense/compact structures. Images of the active and bottom layers reveal the presence of clusters in all membranes functionalized with SiO_2 and SiO_2-$NH2$. Regarding the top layer, the number of clusters remains stable for reduced molar amine contents, A100/0 and A95/5, drastically reducing for higher molar compositions. This behaviour repeats for the total area of these structures. Concerning the bottom layer, the number of clusters and the area occupied by them decreases with increasing molar content of the APTES precursor, and for TEOS/APTES equimolar compositions, both properties increase. There is a clear deviation from this behaviour , regarding the number of clusters, in the transition from A100/0-A95/5-A-A90/10. This deviation can be explained by the presence of large O-ring-shaped structures in A95/5 membrane. Images of the cross sections allowed the identification of two layers: the active dense layer (top layer) and a porous layer (bot layer). Functionalization with the APTES precursor reveals that there is no kind of interference in the asymmetrical character in the synthesized membranes.

In terms of mechanical properties, with the introduction of the propylamine group in the functionalized membrane of CA/SiO_2 (A100/0 to A95/5), the Young modulus increases from 53 MPa to 72 MPa. As the molar content of APTES increases, this parameter has a strictly decreasing behaviour, except for A50/50 membrane composition. This behaviour is also verified for rupture elongation, except the first two tested compositions whose value is constant. Tensile strength results are almost in line with the elongation results. This is expected since for the same Young modulus, the larger is the elongation at rupture point, the larger might be the rupture tensile strength. Generally speaking, as the amine content increases, membranes become less rigid and less ductile. Furthermore, clusters present on the bottom layer do not explain any variations on the mechanical properties. When compared to published works, pH of the casting solution has a great impact on mechanical properties. A constant pH (and lower than 5) does not cause any differences on these properties, while an increase of basicity of the casting solution translates into the decrease of the Young modulus and decreases of the rupture elongation, making

the overall network more close and dense.

Regarding the permeation of pure water, when compared to the pure cellulose acetate membrane, the introduction of silica in the membrane matrix translates into a 133% increase in the hydraulic permeability value, as expected. The introduction of the NH_2 group in the CA/SiO_2 matrix translates into a 41% decrease in the Lp value, revealing that the chemical complexity of the membrane surface is such that it negatively affects this permeation property. However, with increasing molar amine content, there is an increase of 26% and 58% from A95/5 to A90/10, and from A90/10 to A80/20. For higher molar compositions, hydraulic permeability values tend to stabilize. The determination of the Lp value reveals that the functionalization with the APTES precursor results in an improvement of the hydraulic permeability when compared to the pure CA and CA/SiO_2 membrane. When CA/SiO_2/NH_2 membranes are compared with published result values, it is concluded that the pH of the casting solution has a direct impact on the permeation properties. For casting solutions at pH$<$5, the Lp value is favoured, while for more basic pH, the three-dimensional mesh structures produced are more compact, which leads to a decrease in the hydraulic permeability value with an increase in the molar content of NH_2. When the values of Lp, in the present work, are related to the properties of the clusters, there is a tendency for an increase in permeability with a decrease in the number of these structures and a decrease in the total area occupied by them, as the NH_2 increases. Mechanical properties do explain permeation results, since the decrease of the Young modulus and rupture elongation, as propylamine groups increases, translates into an opening of the overall structure that justifies the increase of hydraulic permeability.

About the rejection of reference salts, the membranes are permeable, an expected result since UF membranes are permeable to mono and divalent salts. There is no behaviour that explains the increase or decrease in the rejection of salts, but, in general terms, the rejection coefficients tend to increase with the increase in the molar amine content, and that the molecular weight of the salts has no effect on this permeation property.

In determining the molecular exclusion rate for a 90% rejection, the introduction of the amine group reveals itself in a decrease in the MWCO of the membranes, which decreases from 38 to 25 kDa, and from 25 kDa to 20 kDa, between A100/0 for A95/5 and from A95/5 to A90/10, respectively. When the molar amine composition is greater than A90/10, the cut-off MWCO increases by 150%, then decreases by 20% from A80/20 to A70/30. From A70/30 onwards, the value of this property stabilizes. Through empirical correlations it was possible to estimate the pore size of the membranes. There is a linear decrease in pore size between compositions A100/0 and A90/10. However, pore size increases considerably to A80/20, and remains constant for higher compositions. All synthesized membranes have pores

in the range of UF membranes.

In summary, amine functionalization of membranes under pH$<$5 conditions translate into an increase in hydraulic permeability when compared to traditional cellulose acetate membranes and cellulose acetate and silica membranes. These membranes, in addition to the high permeation fluxes, permeate reference salts. In terms of applicability, particularly in blood purification treatments, synthesized membranes have great potential. However, in terms of mechanical properties, membranes are less rigid and elastomer than CA/SiO_2/NH_2 membranes synthesized in basic media.

5.1 Future Work Proposals

Following the work developed during this master's dissertation:

- Synthesis of membranes by another experimental method. Instead of putting it all together in the reaction vessel, do it in stages. For example, add the matrix of solvents, leave it to stir, and add the precursors, properly mixed, to the casting solution.
- Use a mechanical stirrer with arms that promote mixing at all possible angles, rather than just the axial angle as is the case with magnetic stirring.
- ATR/FTIR (Attenuated Total Reflection) spectroscopy to study the chemical composition of membranes, bond types and compounds present.
- EDS (Energy dispersive X-ray) on the surface of the active layer in order to prove the presence, or not, of the added precursors. The XPS (X-ray photoelectron spectroscopy) technique may also be workable.
- Gas permeation tests and heavy metals, for example, in order to verify the application of membranes in other areas.
- Synthesis of membranes, without a coagulation bath, in order to synthesize a single active layer that can be studied via BET (Brunauer-Emmett-Teller) to check for porosity.
- NMR (Nuclear magnetic resonance) to determine the structure of organic molecules in solution and study molecular physics
- Hemocompatibility and anti-fouling tests in order to ascertain the possibility of applying membranes to the treatment of human blood.
- Urea, creatine and PBUT permeation tests to confirm the potential of these membranes in blood purification treatments.

Bibliography

[1] T. Quarterly, "Population Growth and Technological Change : One Million B . C . to 1990 Author (s): Michael Kremer Source : The Quarterly Journal of Economics , Vol . 108 , No . 3 (Aug ., 1993), pp . 681-716," vol. 108, no. 3, pp. 681–716, 2014.

[2] M. Takht Ravanchi, T. Kaghazchi, and A. Kargari, "Application of membrane separation processes in petrochemical industry: a review," *Desalination*, vol. 235, no. 1-3, pp. 199–244, 2009. [Online]. Available: http://dx.doi.org/10.1016/j.desal.2007.10.042

[3] Kaushik Nath, "MEMBRANE SEPARATION PROCESSES - KAUSHIK NATH - Google Books," p. 3, 2017. [Online]. Available: https://books.google.com/books?hl=en&lr=&id=1VrWDQAAQBAJ&oi=fnd&pg=PP1&dq=membrane+separation+processes&ots=GbcnYgzFod&sig=IeQ5fR0NxqUbozxeLbAMMaJmS3E#v=onepage&q=membraneseparationprocesses&f=false%0Ahttps://books.google.com.my/books?id=1VrWDQAAQBAJ&prin

[4] E. Gomes de Azevedo and A. Maria Alves, *Engenharia de Processos de Separação*, 2nd ed., IST - Instituto Superior Técnico, Ed. Lisboa: IST - Instituto Superior Técnico, 2013.

[5] A. M. Alves and D. Afonso, *Processos de Separação II. Apontamentos de membranas*. Lisboa: IST - Instituto Superior Técnico.

[6] M. Mulder, *Basic Principle of Membrane Technology*, 2nd ed., Springer, Ed. Center of Membrane Science and Tecnhology University of Twente, The Netherlands, 2013, vol. 53, no. 9.

[7] K. C. Khulbe, F. C.Y., and T. Matsuura, *Synthetic Polymeric Membranes- Characterization by Atomic Force Microscopy*, 1st ed., I. Alig, J. Janca, and W.-M. Kulicke, Eds. Ottawa, Canada: Springer Laboratory Manuals in Polymer Science, 2008.

[8] GRAND VIEW RESEARCH, "Membrane Separation Technology Market Size, Share Trends Analysis Report By Technology (Microfiltration, Ultrafiltration, Nanofiltration), By Application, By Region, And Segment Forecasts, 2020 - 2027," p. 143. [Online]. Available: https://www.grandviewresearch.com/industry-analysis/membrane-separation-technology-market

[9] MARKETS AND MARKETS, “Membrane Separation Technology Market by Application (Water Wastewater Treatment, Food Beverage, Medical Pharmaceutical, Industrial Processing), Technology (RO, UF, MF, NF), and Region - Global Forecast to 2022.”

[10] A. Afzali, S. Maghsoodlou, and B. Noroozi, *Nanoporous Polymer/Carbon Nanotube Membrane Filtration: The ”How-to” Guide to Computational Methods*, 2015, no. May 2016.

[11] “Membrane Separation Technology Primer.” [Online]. Available: https://www.asahi-kasei.co.jp/membrane/microza/en/kiso/kiso_1.html

[12] X. Qiu and S. Hu, ““smart” materials based on cellulose: A review of the preparations, properties, and applications,” *Materials*, vol. 6, no. 3, pp. 738–781, 2013. [Online]. Available: https://www.mdpi.com/1996-1944/6/3/738

[13] T. Uragami, *Science and Technology of Separation Membranes*, 2017.

[14] R. Singh, “Chapter 1 - introduction to membrane technology,” in *Membrane Technology and Engineering for Water Purification (Second Edition)*, second edition ed., R. Singh, Ed. Oxford: Butterworth-Heinemann, 2015, pp. 1–80. [Online]. Available: https://www.sciencedirect.com/science/article/pii/B978044463362000001X

[15] M. C. Andrade, J. C. Pereira, N. de Almeida, P. Marques, M. Faria, and M. C. Gonçalves, “Improving hydraulic permeability, mechanical properties, and chemical functionality of cellulose acetate-based membranes by co-polymerization with tetraethyl orthosilicate and 3-(aminopropyl)triethoxysilane,” *Carbohydrate Polymers*, vol. 261, p. 117813, 2021. [Online]. Available: https://www.sciencedirect.com/science/article/pii/S0144861721002009

[16] S. I. I. W. A, “Neue Bucher / New Books,” vol. 36, no. 8, p. 1990, 1990.

[17] O. Kutowy and S. Sourirajan, “Cellulose acetate ultrafiltration membranes,” *Journal of Applied Polymer Science*, vol. 19, no. 5, pp. 1449–1460, 1975.

[18] S. Beisl, S. Monteiro, R. Santos, A. S. Figueiredo, M. G. Sánchez-Loredo, M. A. Lemos, F. Lemos, M. Minhalma, and M. N. de Pinho, “Synthesis and bactericide activity of nanofiltration composite membranes – cellulose acetate/silver nanoparticles and cellulose acetate/silver ion exchanged zeolites,” *Water Research*, vol. 149, pp. 225–231, 2019. [Online]. Available: https://www.sciencedirect.com/science/article/pii/S0043135418309242

[19] J. Wu and Q. Yuan, “Gas permeability of a novel cellulose membrane,” *Journal of Membrane Science*, vol. 204, no. 1, pp. 185–194, 2002. [Online]. Available: https://www.sciencedirect.com/science/article/pii/S0376738802000376

[20] M. Faria, C. Moreira, T. Eusébio, P. Brogueira, and M. N. de Pinho, “Hybrid flat sheet cellulose acetate/silicon dioxide ultrafiltration membranes for uremic blood purification,” *Cellulose*, vol. 27, no. 7, pp. 3847–3869, 2020.

[21] M. Sasaki, N. Hosoya, and M. Saruhashi, “Vitamin E modified cellulose membrane,” *Artificial Organs*, vol. 24, no. 10, pp. 779–789, 2000.

[22] J.-J. Qin, Y. Li, L.-S. Lee, and H. Lee, “Cellulose acetate hollow fiber ultrafiltration membranes made from CA/PVP 360 K/NMP/water,” *Journal of Membrane Science*, vol. 218, no. 1, pp. 173–183, 2003. [Online]. Available: https://www.sciencedirect.com/science/article/pii/S0376738803001704

[23] J. Su, Q. Yang, J. F. Teo, and T.-S. Chung, “Cellulose acetate nanofiltration hollow fiber membranes for forward osmosis processes,” *Journal of Membrane Science*, vol. 355, no. 1, pp. 36–44, 2010. [Online]. Available: https://www.sciencedirect.com/science/article/pii/S0376738810002115

[24] W. Gao, H. Liang, J. Ma, M. Han, Z.-l. Chen, Z.-s. Han, and G.-b. Li, “Membrane fouling control in ultrafiltration technology for drinking water production: A review,” *Desalination*, vol. 272, no. 1, pp. 1–8, 2011. [Online]. Available: https://www.sciencedirect.com/science/article/pii/S0011916411000622

[25] Y. Orooji, M. Faghih, A. Razmjou, J. Hou, P. Moazzam, N. Emami, M. Aghababaie, F. Nourisfa, V. Chen, and W. Jin, “Nanostructured mesoporous carbon polyethersulfone composite ultrafiltration membrane with significantly low protein adsorption and bacterial adhesion,” *Carbon*, vol. 111, pp. 689–704, 2017. [Online]. Available: https://www.sciencedirect.com/science/article/pii/S0008622316309174

[26] J. Wang, Y. Wang, Y. Zhang, A. Uliana, J. Zhu, J. Liu, and B. Van Der Bruggen, “Zeolitic Imidazolate Framework/Graphene Oxide Hybrid Nanosheets Functionalized Thin Film Nanocomposite Membrane for Enhanced Antimicrobial Performance,” *ACS Applied Materials and Interfaces*, vol. 8, no. 38, pp. 25 508–25 519, 2016.

[27] S. S. Shojaie, T. G. Rials, and S. S. Kelley, “Preparation and characterization of cellulose acetate organic/inorganic hybrid films,” *Journal of Applied Polymer Science*, vol. 58, no. 8, pp. 1263–1274, 1995.

[28] J. [U+FFFD]uval, A. J. Kemperman, B. Folkers, M. H. Mulder, G. Desgrandchamps, and C. A. Smolders, “Preparation of zeolite filled glassy polymer membranes,” *Journal of Applied Polymer Science*, vol. 54, no. 4, pp. 409–418, 1994.

[29] L. Kwang-Il, S. Il-Wun, and H. Sun-Tak, “The effects of transition metal complexes on the permeation of small gas molecules through cellulose acetate membranes,” *Journal*

of Membrane Science, vol. 60, no. 2, pp. 207–218, 1991. [Online]. Available: https://www.sciencedirect.com/science/article/pii/S0376738800815355

[30] N. M. Barkoula, B. Alcock, N. O. Cabrera, and T. Peijs, "Flame-Retardancy Properties of Intumescent Ammonium Poly(Phosphate) and Mineral Filler Magnesium Hydroxide in Combination with Graphene," *Polymers and Polymer Composites*, vol. 16, no. 2, pp. 101–113, 2008.

[31] S. K. Young, G. C. Gemeinhardt, J. W. Sherman, R. F. Storey, K. A. Mauritz, D. A. Schiraldi, A. Polyakova, A. Hiltner, and E. Baer, "Covalent and non-covalently coupled polyester–inorganic composite materials," *Polymer*, vol. 43, no. 23, pp. 6101–6114, 2002. [Online]. Available: https://www.sciencedirect.com/science/article/pii/S0032386102005153

[32] J. Dasgupta, S. Chakraborty, J. Sikder, R. Kumar, D. Pal, S. Curcio, and E. Drioli, "The effects of thermally stable titanium silicon oxide nanoparticles on structure and performance of cellulose acetate ultrafiltration membranes," *Separation and Purification Technology*, vol. 133, pp. 55–68, 2014. [Online]. Available: https://www.sciencedirect.com/science/article/pii/S1383586614003839

[33] A. M. Estrada, M. Faria, G. J. Labrada Delgado, M. N. de Pinho, and M. G. Sánchez Loredo, "Synthesis of calcium fluoride ultrafine particles for the preparation of integral asymmetric cellulose acetate/calcium fluoride membranes," *Journal of Membrane Science and Research*, vol. 6, no. 2, pp. 147–157, 2020.

[34] X.-L. Zhang, H. Yamada, T. Saito, T. Kai, K. Murakami, M. Nakashima, J. Ohshita, K. Akamatsu, and S.-i. Nakao, "Development of hydrogen-selective triphenylmethoxysilane-derived silica membranes with tailored pore size by chemical vapor deposition," *Journal of Membrane Science*, vol. 499, pp. 28–35, 2016. [Online]. Available: https://www.sciencedirect.com/science/article/pii/S0376738815301885

[35] R. Nooney, C. O'Connell, S. Roy, K. Boland, G. Keegan, S. Kelleher, S. Daniels, and C. McDonagh, "Synthesis and characterisation of far-red fluorescent cyanine dye doped silica nanoparticles using a modified microemulsion method for application in bioassays," *Sensors and Actuators B: Chemical*, vol. 221, pp. 470–479, 2015. [Online]. Available: https://www.sciencedirect.com/science/article/pii/S0925400515300290

[36] P. D. Castrillo, D. Olmos, D. R. Amador, and J. González-Benito, "Real dispersion of isolated fumed silica nanoparticles in highly filled PMMA prepared by high energy ball milling," *Journal of Colloid and Interface Science*, vol. 308, no. 2, pp. 318–324, 2007.

[37] L. P. Singh, S. K. Bhattacharyya, R. Kumar, G. Mishra, U. Sharma, G. Singh, and S. Ahalawat, "Sol-Gel processing of silica nanoparticles and their applications," *Advances*

in Colloid and Interface Science, vol. 214, pp. 17–37, 2014. [Online]. Available: https://www.sciencedirect.com/science/article/pii/S0001868614002802

[38] M. T. Veciana-Nogués, A. Mariné-Font, and M. C. Vidal-Carou, "Biogenic Amines as Hygienic Quality Indicators of Tuna. Relationships with Microbial Counts, ATP-Related Compounds, Volatile Amines, and Organoleptic Changes," *Journal of Agricultural and Food Chemistry*, vol. 45, no. 6, pp. 2036–2041, 1997. [Online]. Available: https://doi.org/10.1021/jf960911l

[39] Tanganov B.B., "About sizes of the hydrated salt ions - the components of sea water," *European Journal of Natural History*, vol. 1, no. 1, pp. 36–37, 2013. [Online]. Available: https://world-science.ru/pdf/2013/1/15.pdf

[40] O. S. Serbanescu, A. M. Pandele, F. Miculescu, and S. I. Voicu, "Synthesis and characterization of cellulose acetate membranes with self-indicating properties by changing the membrane surface color for separation of Gd(III)," *Coatings*, vol. 10, no. 5, 2020.

[41] A. A. Taha, Y. na Wu, H. Wang, and F. Li, "Preparation and application of functionalized cellulose acetate/silica composite nanofibrous membrane via electrospinning for Cr(VI) ion removal from aqueous solution," *Journal of Environmental Management*, vol. 112, pp. 10–16, 2012.

[42] B. Marek, K. Nalan, R. Bernabe L., and B. Jochen, *Innovative Materials and Methods for Water Treatment-Solutions for Arsenic and Chromium Removal*, 1st ed. London: CRC Press, 2016.

[43] G. Mendes, "Novas Membranas Assimétricas de Matriz Mista de Acetato de Celulose e Sílica," 2016.

[44] C.J. Brinker; G. W. Scherer, "Sol-Gel Science: The physics and chemistry of sol-gel processing," p. 462, 1990.

[45] M. Faria and M. N. de Pinho, "Challenges of reducing protein-bound uremic toxin levels in chronic kidney disease and end stage renal disease," *Translational Research*, vol. 229, pp. 115–134, 2021.

[46] S. Lekawanvijit, A. R. Kompa, and H. Krum, "Protein-bound uremic toxins: A long overlooked culprit in cardiorenal syndrome," *American Journal of Physiology - Renal Physiology*, vol. 311, no. 1, pp. F52–F62, 2016.

[47] A. S. Levey and J. Coresh, "Chronic kidney disease," *The Lancet*, vol. 379, no. 9811, pp. 165–180, 2012. [Online]. Available: http://dx.doi.org/10.1016/S0140-6736(11)60178-5

[48] N. K. Foundation, "Estimated Glomerular Filtration Rate (eGFR)," 2018. [Online]. Available: https://www.kidney.org/atoz/content/gfr

[49] K. Mistry, "Chronic kidney disease," *Clinical Pediatric Nephrology: Third Edition*, pp. 601–626, 2016.

[50] I. S. o. N. (ISN) and C. network (i3C), "No Title." [Online]. Available: https://www.theisn.org/initiatives/what-is-ckdu/ckdu-network-i3c/

[51] B. Bikbov, C. A. Purcell, and A. S. Levey, "Global, regional, and national burden of chronic kidney disease, 1990–2017: a systematic analysis for the Global Burden of Disease Study 2017," *The Lancet*, vol. 395, no. 10225, pp. 709–733, 2020.

[52] K. J. Jager, C. Kovesdy, R. Langham, M. Rosenberg, V. Jha, and C. Zoccali, "A single number for advocacy and communication-worldwide more than 850 million individuals have kidney diseases," *Nephrology Dialysis Transplantation*, vol. 34, no. 11, pp. 1803–1805, 2019.

[53] K. J. Foreman and N. Marquez, "Forecasting life expectancy, years of life lost, and all-cause and cause-specific mortality for 250 causes of death: reference and alternative scenarios for 2016–40 for 195 countries and territories," *The Lancet*, vol. 392, no. 10159, pp. 2052–2090, 2018. [Online]. Available: http://dx.doi.org/10.1016/S0140-6736(18)31694-5

[54] P. R. Loubeau, J. M. Loubeau, and R. Jantzen, "The economics of kidney transplantation versus hemodialysis," *Progress in Transplantation*, vol. 11, no. 4, pp. 291–297, 2001.

[55] R. Mehrotra, O. Devuyst, S. J. Davies, and D. W. Johnson, "The current state of peritoneal dialysis," *Journal of the American Society of Nephrology*, vol. 27, no. 11, pp. 3238–3252, 2016.

[56] Usrds, "Chapter 9: Transition of Care in Chronic Kidney Disease," vol. 1, pp. 1–60, 2019.

[57] N. U. Afsar, D. Yu, C. Cheng, K. Emmanuel, L. Ge, B. Wu, A. N. Mondal, M. I. Khan, and T. Xu, "Fabrication of cation exchange membrane from polyvinyl alcohol using lignin sulfonic acid: Applications in diffusion dialysis process for alkali recovery," *Separation Science and Technology (Philadelphia)*, vol. 52, no. 6, pp. 1106–1113, 2017. [Online]. Available: http://dx.doi.org/10.1080/01496395.2017.1279629

[58] J. Luo, C. Wu, T. Xu, and Y. Wu, "Diffusion dialysis-concept, principle and applications," *Journal of Membrane Science*, vol. 366, no. 1-2, pp. 1–16, 2011. [Online]. Available: http://dx.doi.org/10.1016/j.memsci.2010.10.028

[59] H. D. Humes, W. H. Fissell, and K. Tiranathanagul, "The future of hemodialysis membranes," *Kidney International*, vol. 69, no. 7, pp. 1115–1119, 2006. [Online]. Available: http://dx.doi.org/10.1038/sj.ki.5000204

[60] B. Kunst and S. Sourirajan, "An approach to the development of cellulose acetate ultrafiltration membranes," *Journal of Applied Polymer Science*, vol. 18, no. 11, pp. 3423–3434, 1974.

[61] I. Peixoto, M. Faria, and M. C. Gonçalves, “Synthesis and characterization of novel integral asymmetric monophasic cellulose–acetate/silica/titania and cellulose–acetate/titania membranes,” *Membranes*, vol. 10, no. 9, pp. 1–26, 2020.

[62] R. Fischer, J. Aguirre, A. Herrera-estrella, and L. M. Corrochano, “The Complexity of Fungal Vision,” *The Fungal Kingdom*, pp. 441–461, 2017.

[63] A. R. Costa and M. N. de Pinho, “Performance and cost estimation of nanofiltration for surface water treatment in drinking water production,” *Desalination*, vol. 196, no. 1-3, pp. 55–65, 2006.

[64] G. Arthanareeswaran, T. K. Sriyamuna Devi, and M. Raajenthiren, “Effect of silica particles on cellulose acetate blend ultrafiltration membranes: Part I,” *Separation and Purification Technology*, vol. 64, no. 1, pp. 38–47, 2008.

[65] ABB Group, “Manual del Usuario,” *Manual del usuario, operación y mantenimiento de transformadores de potencia*, p. 20, 2007.

[66] O.-l. T. O. C. Analyzer, T. Organic, and C. Analyzer, “ON-LINE TOC-V CSH.”

[67] J. Brandi and L. Wilson-Wilde, “Standard Methods,” *Encyclopedia of Forensic Sciences: Second Edition*, pp. 522–527, 2013.

[68] A. Lui, F. D. Talbot, A. Fouda, T. Matsuura, and S. Sourirajan, “Studies on the solvent exchange technique for making dry cellulose acetate membranes for the separation of gaseous mixtures,” *Journal of Applied Polymer Science*, vol. 36, no. 8, pp. 1809–1820, 1988.

[69] M. Andrade, J. Pereira, N. Almeida, P. Marques, M. Faria, and M. C. Gonçalves, “Improving hydraulic permeability, mechanical properties, and chemical functionality of cellulose acetate-based membranes by co-polymerization with tetraethyl orthosilicate and 3-(aminopropyl)triethoxysilane,” *Carbohydrate Polymers*, vol. 261, p. 117813, 02 2021.

[70] F. P. Cuperus and C. A. Smolders, “Characterization of UF membranes. Membrane characteristics and characterization techniques,” *Advances in Colloid and Interface Science*, vol. 34, no. C, pp. 135–173, 1991.

[71] R. E. Kesting and A. Menefee, “The role of formamide in the preparation of cellulose acetate membranes by the phase inversion process,” *Kolloid-Zeitschrift Zeitschrift für Polymere*, vol. 230, no. 2, pp. 341–346, 1969.

[72] Z. D. JASTRZEBSKI, *Nature and properties of engineering materials*, 1st ed. John Wiley Sons, 1959.

[73] M. Fan and F. Fu, “1 - Introduction: A perspective – natural fibre composites in construction,” in *Advanced High Strength Natural Fibre Composites in Construction*, M. Fan and F. Fu, Eds. Woodhead Publishing, 2017, pp. 1–20. [Online]. Available: https://www.sciencedirect.com/science/article/pii/B9780081004111000017

[74] C. Brinker and G. Scherer, *Sol-Gel Science: The Physics and Chemistry of Sol-Gel Processing*. United States: Elsevier Inc., Oct. 2013.

[75] G. Mendes, M. Faria, A. Carvalho, M. C. Gonçalves, and M. N. de Pinho, “Structure of water in hybrid cellulose acetate-silica ultrafiltration membranes and permeation properties,” *Carbohydrate Polymers*, vol. 189, pp. 342–351, 2018. [Online]. Available: http://dx.doi.org/10.1016/j.carbpol.2018.02.030

[76] R. Singh, “Chapter 1 - Introduction to membrane technology,” in *Hybrid Membrane Systems for Water Purification*, R. Singh, Ed. Amsterdam: Elsevier Science, 2005, pp. 1–56. [Online]. Available: https://www.sciencedirect.com/science/article/pii/B9781856174428500026

[77] X. Li and J. Li, “Encyclopedia of Membranes,” *Encyclopedia of Membranes*, 2020.

[78] W. R. Clark, N. L. Dehghani, V. Narsimhan, and C. Ronco, “Uremic Toxins and their Relation to Dialysis Efficacy,” *Blood Purification*, vol. 48, no. 4, pp. 299–314, 2019.

[79] S. Lentsch, P. Aimar, and J. L. Orozco, “Separation albumin–PEG: Transmission of PEG through ultrafiltration membranes,” *Biotechnology and Bioengineering*, vol. 41, no. 11, pp. 1039–1047, 1993.

A

Membrane Selection

The choice of membranes to cut is essential for permeation tests, such as in the drying process which aims to characterize them. At the time of casting the membranes, each casting solution can produce between 5 to 8 films with dimensions 20 cm (width) x 30 cm (height) each. The edges of the synthesized films, fig, should not be considered for the cut, as there may be a smaller or larger accumulation of casting solution, as these zones coincide with the terminal zones of the knife.

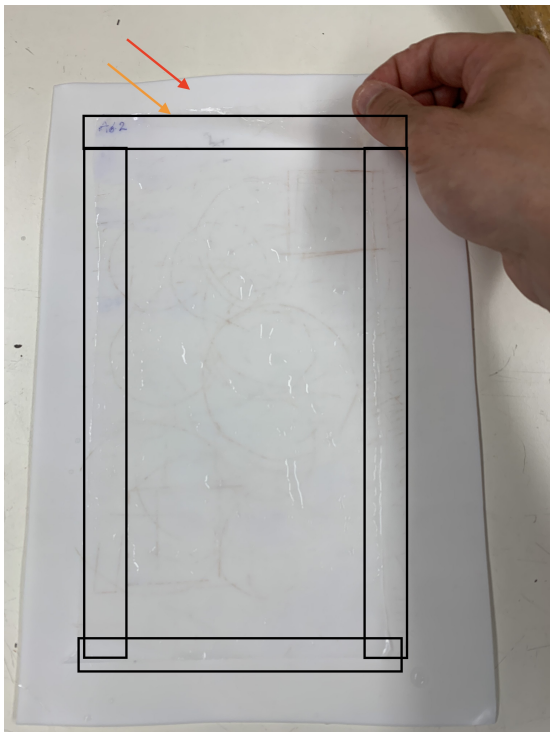

Figure A.1: Representation of the active layer facing top (orange arrow), with a protective surface (red arrow) and areas that should be excluded from the cut (boxes in black)

Then, with your hands properly washed or with gloves on, carefully pick up the flat-sheet membrane and point it towards a light source. This technique allows detecting 3 things: a) the presence of pinholes (holes), b) areas where the manual casting was not done uniformly and c) an area with greater or lesser accumulation of polymer.

- a) Pinholes are circular structures, usually white in color, and represent holes in the membrane. This should be avoided, as it interferes with permeation tests (sudden increase in fluxes obtained).

- b) At the time of manual casting, if the vertical movement (top to bottom) with the knife is not made at the same speed and uniformly, there is an accumulation of solution in the area where there was a change in speed, or inclination of the knife. This situation is easily identified by the presence of a dense, white line.

- c) Differences in color indicate a greater (if is whiter) or lesser (less white) homogeneity. This happens when there isn't a good mixing, of some section, of the casting solution

Both situation a), b) and c) are represented on the following image.

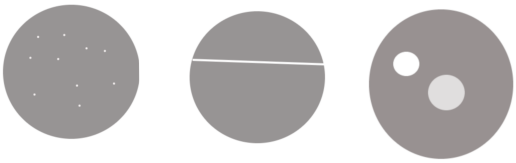

Figure A.2: Representation a), b) and c) scenarios, respectively

B

Pump Calibration

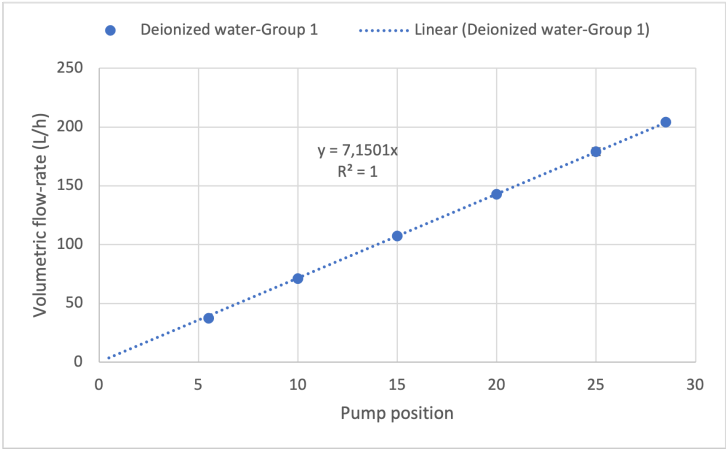

Figure B.1: Pump Calibration for membranes CA, A100/0-1-1, A95/5-1-2, A90/10-1-4 and A80/20-1-4, together with filter paper, using DI water

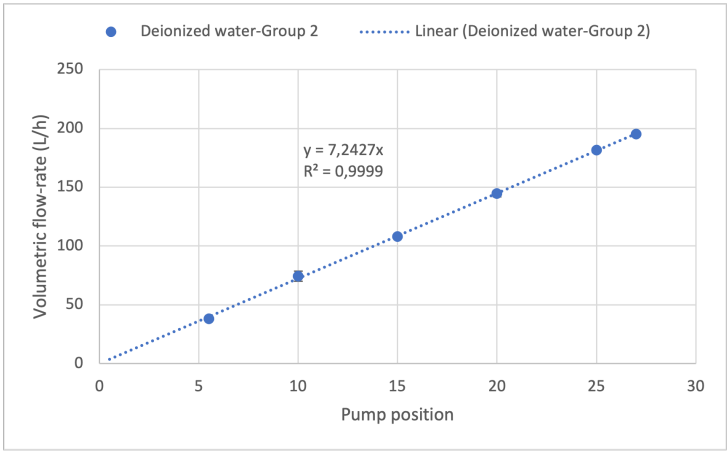

Figure B.2: Pump Calibration for membranes A70/30-1-5 and A50/50-1-6, together with filter paper, using DI water

C

Temperature Correction of the Permeate Fluxes

Since all prepared solutions used in the permeation experiments were sufficiently dilute, they can be considered as water. At a temperature of 25ºC the density, ρ, viscosity, μ, of water are:

ρ = 99,077 kg m^{-3} μ = 0,8949 $\times 10^{-3}$ kg m^{-1} s^{-1}

The viscosity, in 10^{-3} kg m^{-1} s^{-1}, can be described by as a function of the temperature by the following correlation [68]:

$ln(\mu) = -6,96 + \frac{2044}{T} (r = 0.99978)$ 287,15<T(K)<308,15

Given that, on eq. (3.1), neither ΔP and L_p are temperature dependent and the density is the same, experimental mass flux and temperature, J_{m1} and T_1, can be corrected to the temperature of 25ºC, J_{m2} and T_2, through the next relationship:

$$J_{m1}\mu_1 = J_{m2}\mu_2$$

D

Linear Regressions to Calculate Hydraulic Permeability

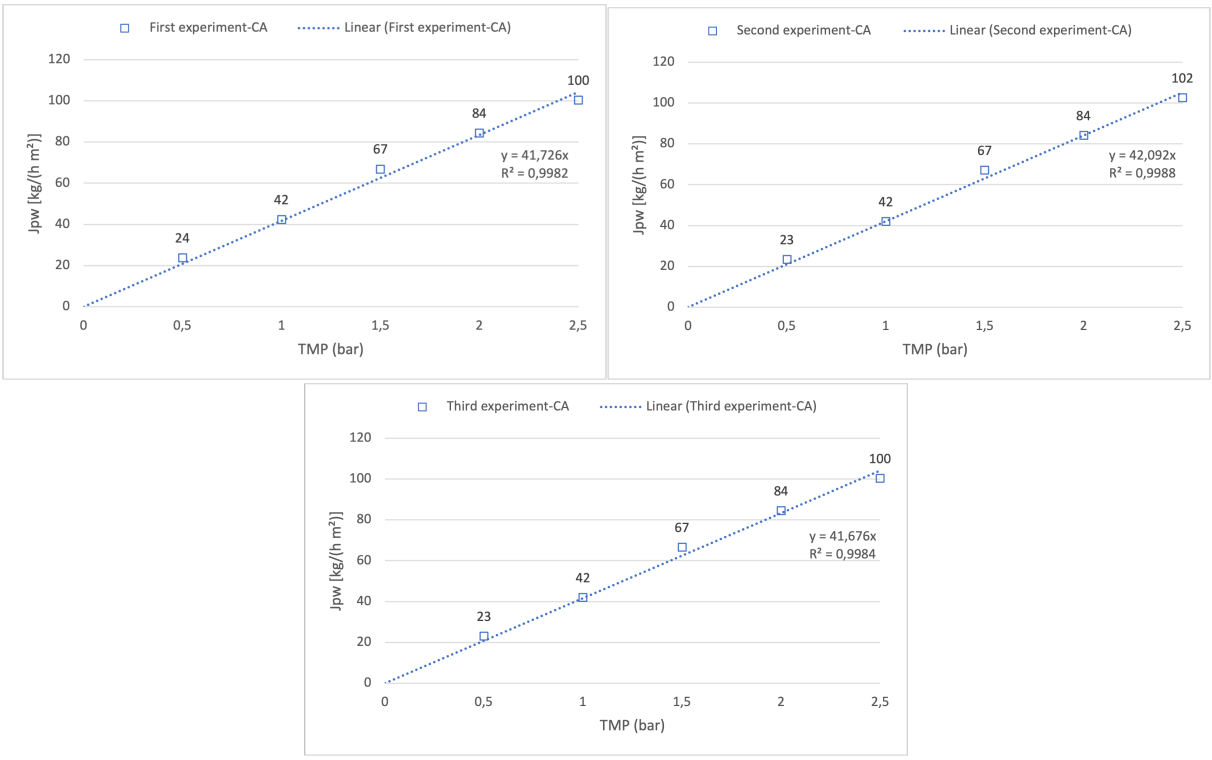

Figure D.1: J_{pw} as a function of TMP, for the first, second and third experiment, for the CA membrane

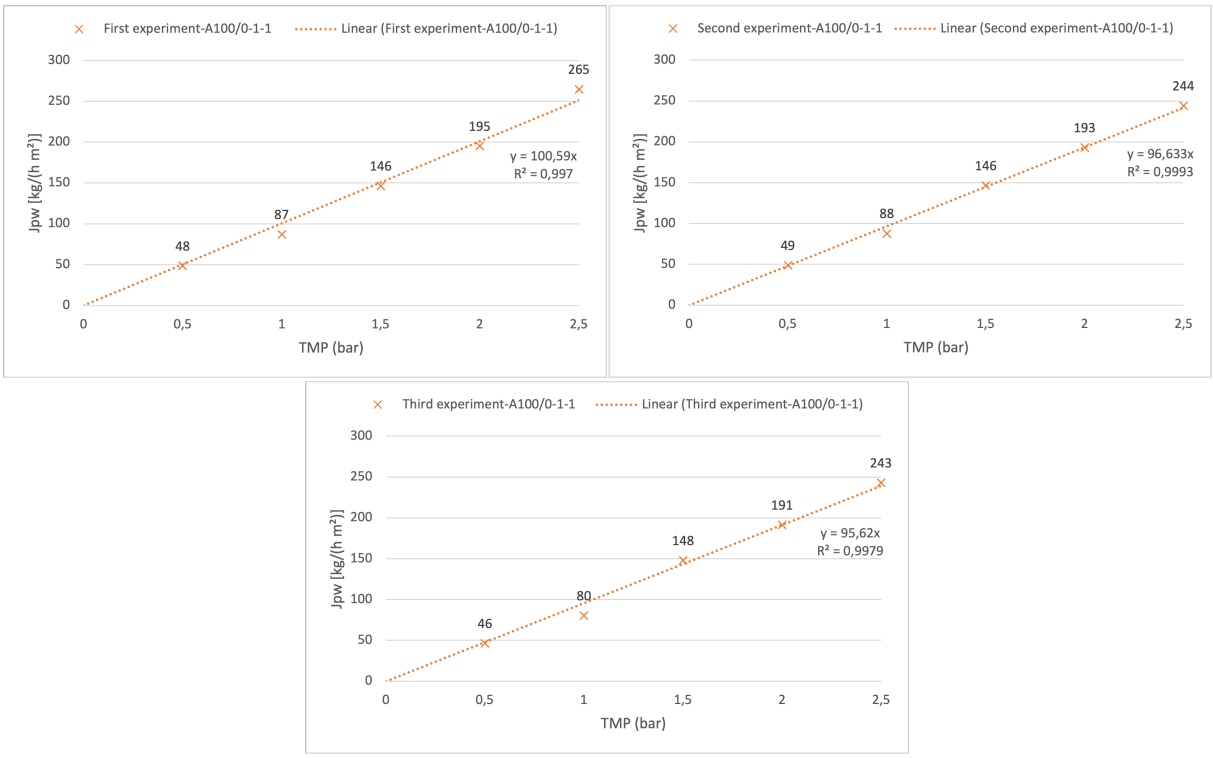

Figure D.2: J_{pw} as a function of TMP, for the first, second and third experiment, for the A100/0-1-1 membrane

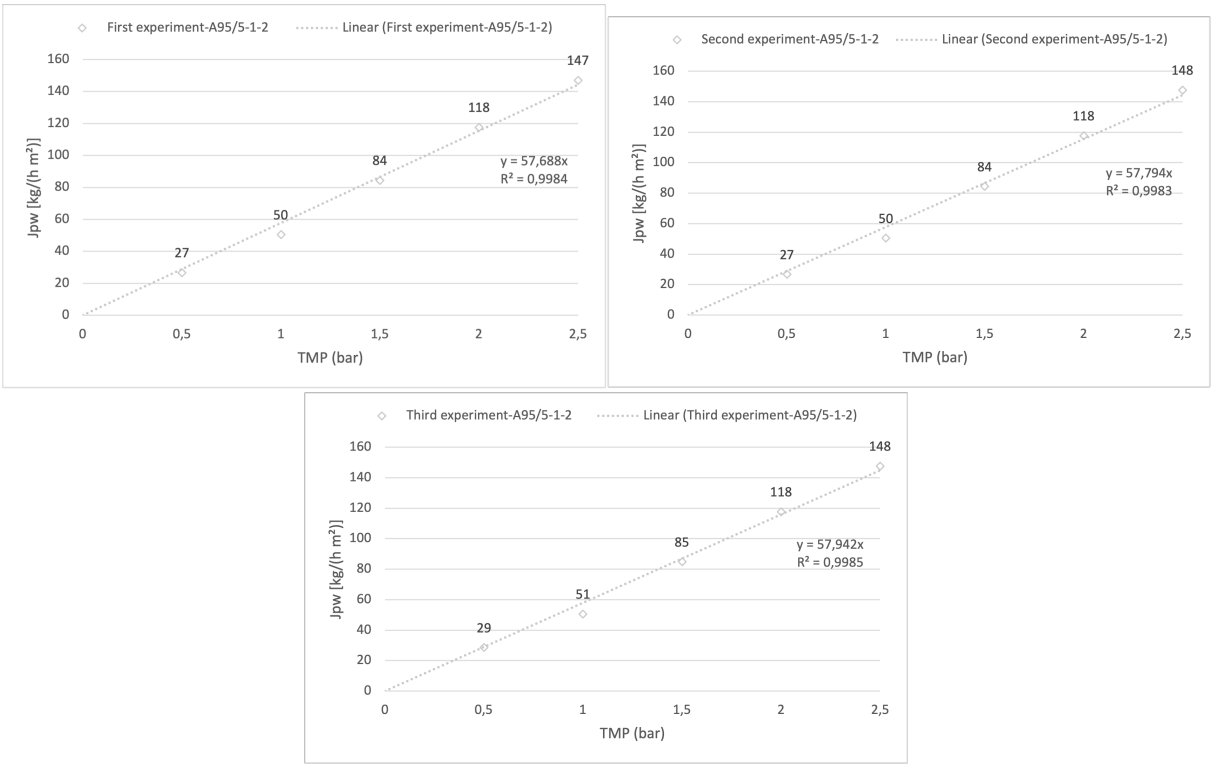

Figure D.3: J_{pw} as a function of TMP, for the first, second and third experiment, for the A95/5-1-2 membrane

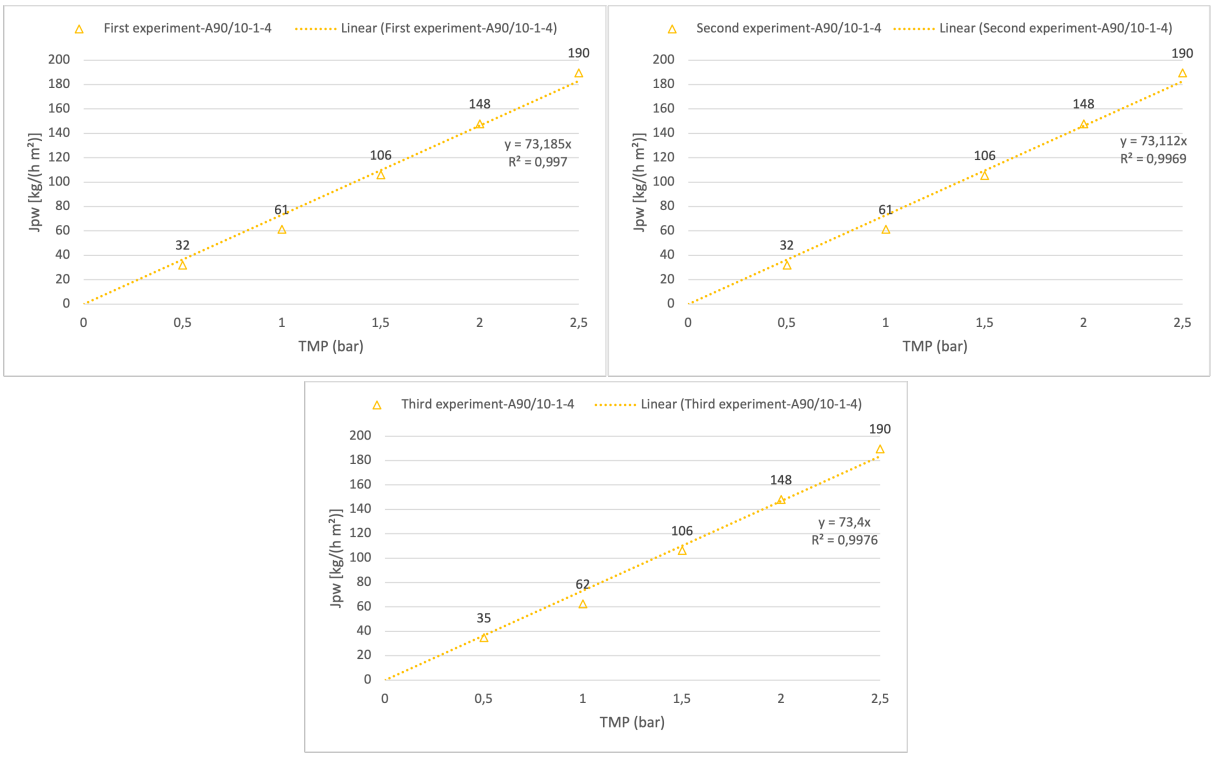

Figure D.4: J_{pw} as a function of TMP, for the first, second and third experiment, for the A90/10-1-4 membrane

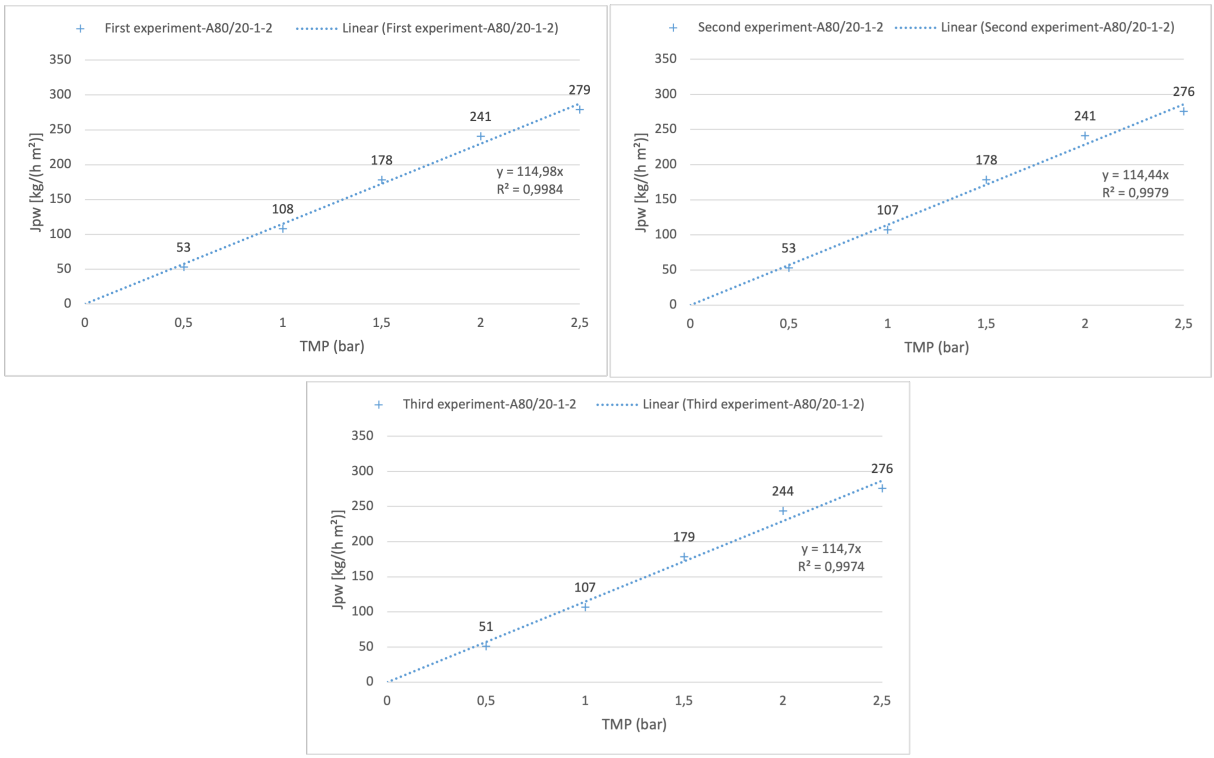

Figure D.5: J_{pw} as a function of TMP, for the first, second and third experiment, for the A80/20-1-2 membrane

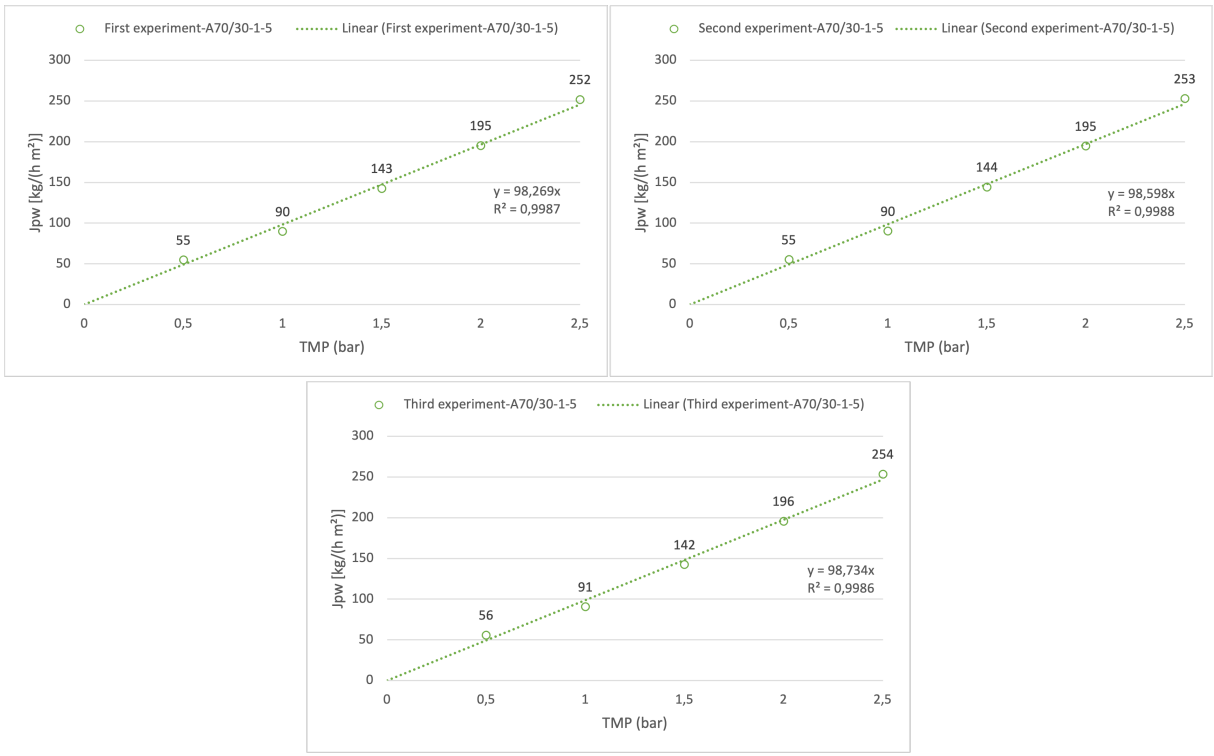

Figure D.6: J_{pw} as a function of TMP, for the first, second and third experiment, for the A70/30-1-5 membrane

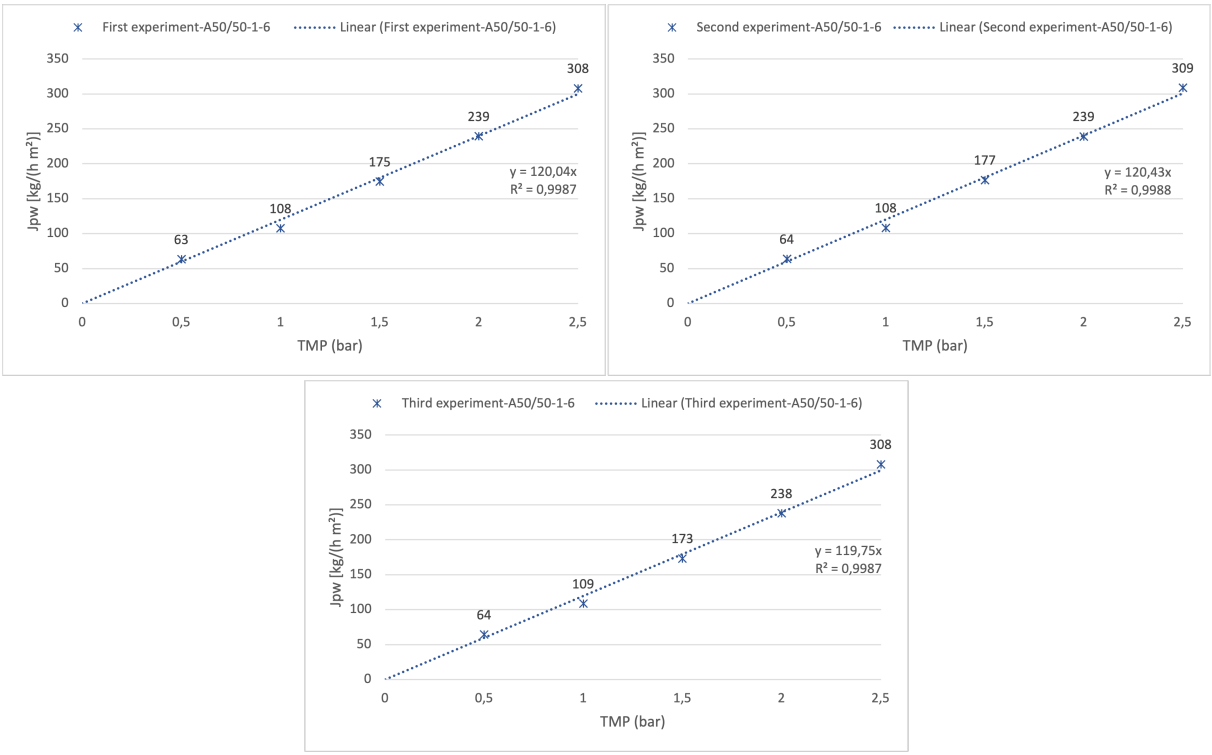

Figure D.7: J_{pw} as a function of TMP, for the first, second and third experiment, for the A50/50-1-6 membrane

E

Salts Concentration Measurement Calibration Lines

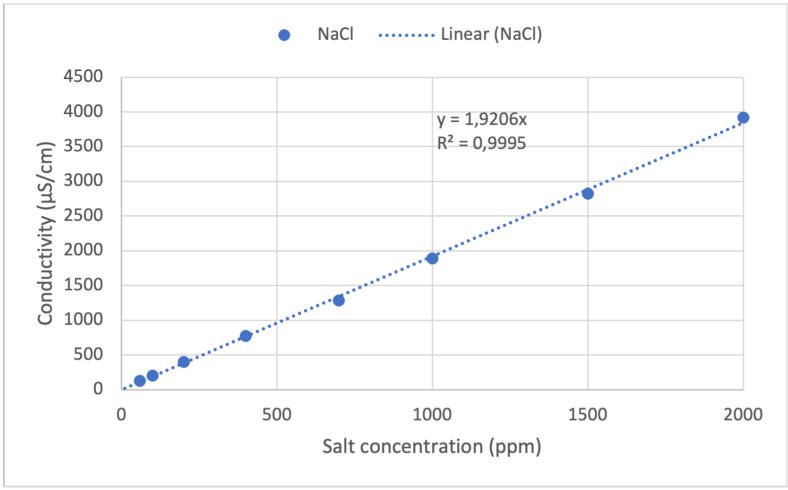

Figure E.1: NaCl conductivity as a function of the concentration calibration line

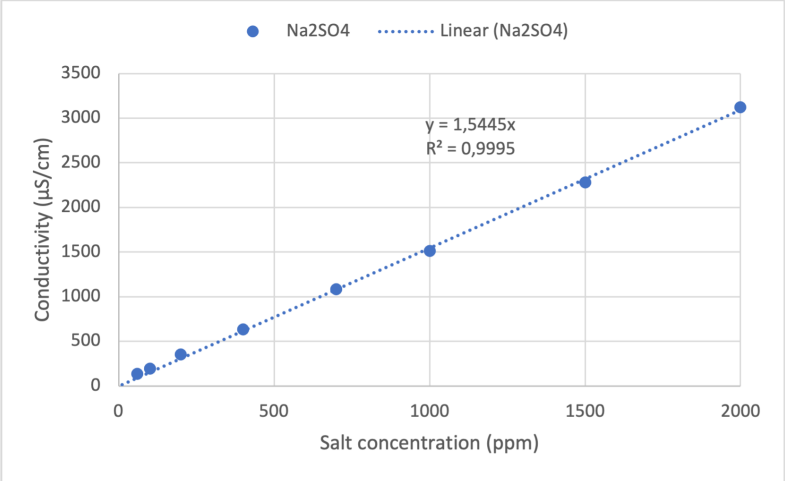

Figure E.2: Na_2SO_4 conductivity as a function of the concentration calibration line

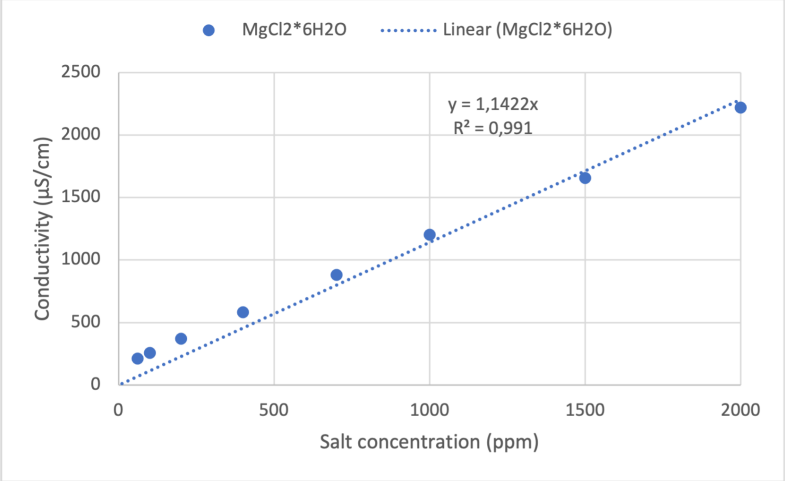

Figure E.3: $MgCl_2$*$6H_2O$ conductivity as a function of the concentration calibration line

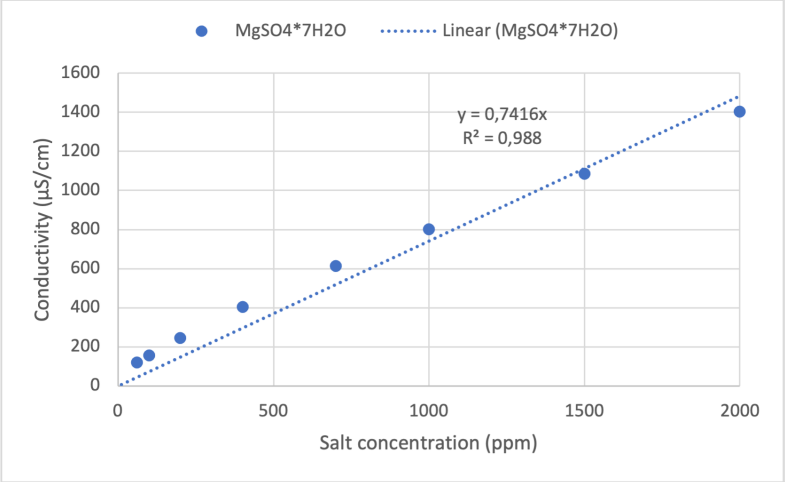

Figure E.4: $MgSO_4$*$7H_2O$ conductivity as a function of the concentration calibration line

F

Total Organic Carbon Calibration Lines

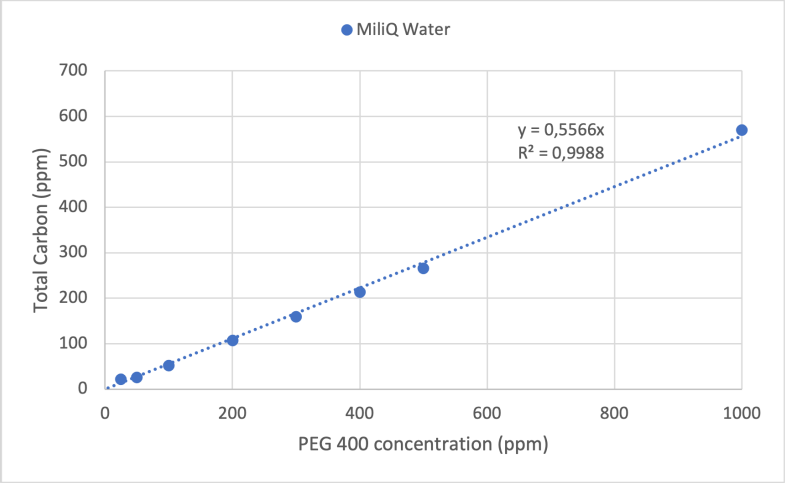

Figure F.1: PEG 400 Total Carbon as a function of the concentration

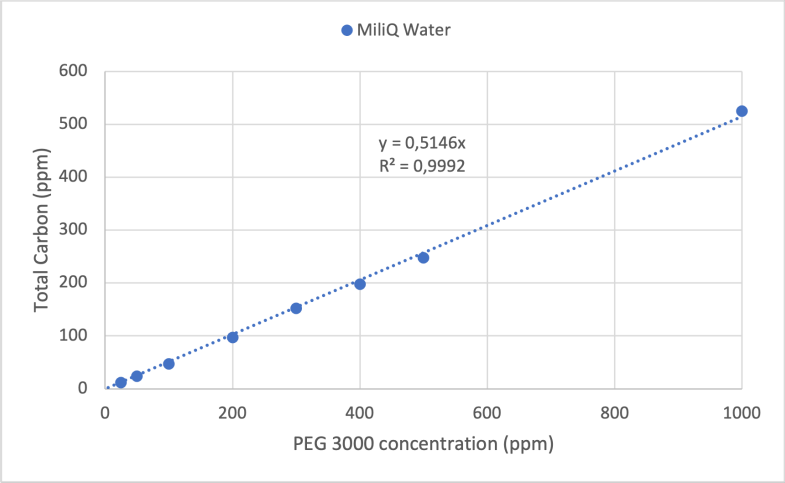

Figure F.2: PEG 3000 Total Carbon as a function of the concentration

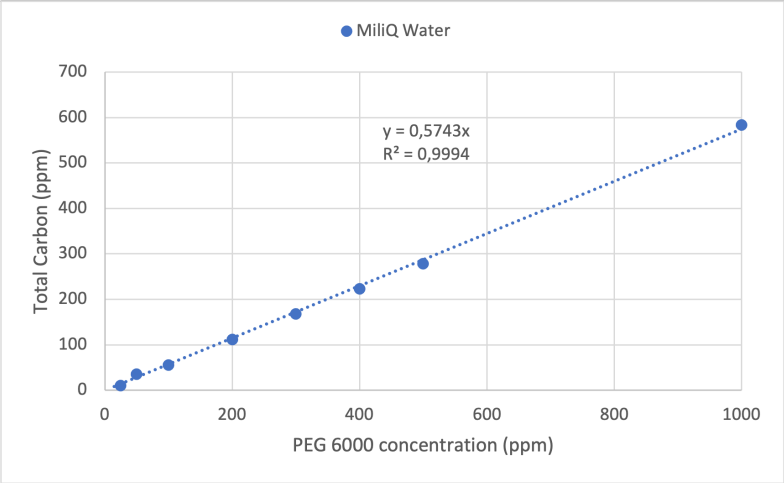

Figure F.3: PEG 6000 Total Carbon as a function of the concentration

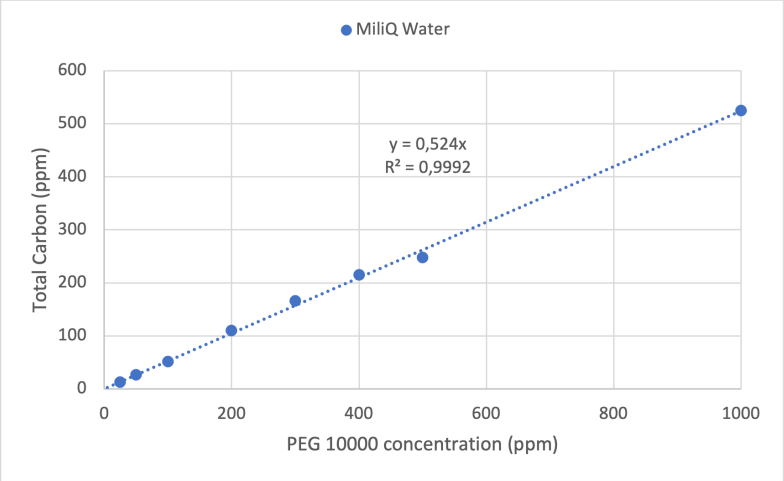

Figure F.4: PEG 10000 Total Carbon as a function of the concentration

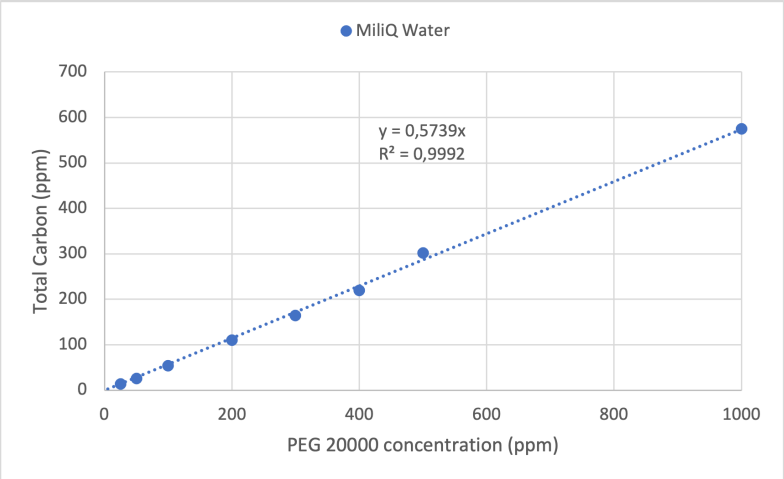

Figure F.5: PEG 20000 Total Carbon as a function of the concentration

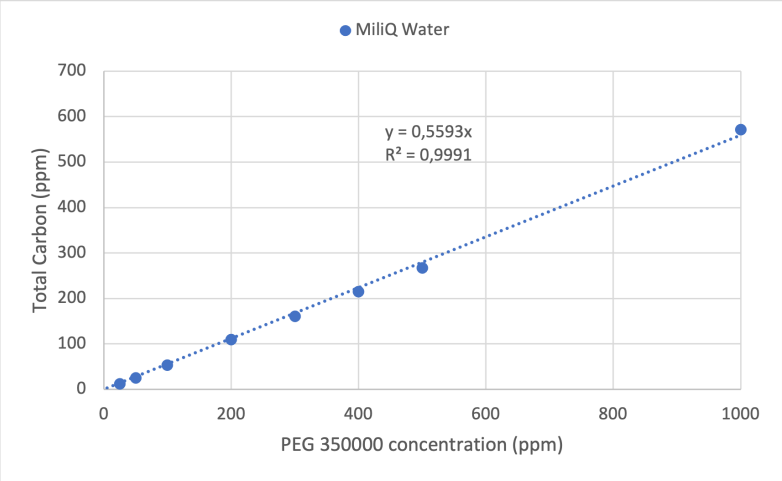

Figure F.6: PEG 350000 Total Carbon as a function of the concentration

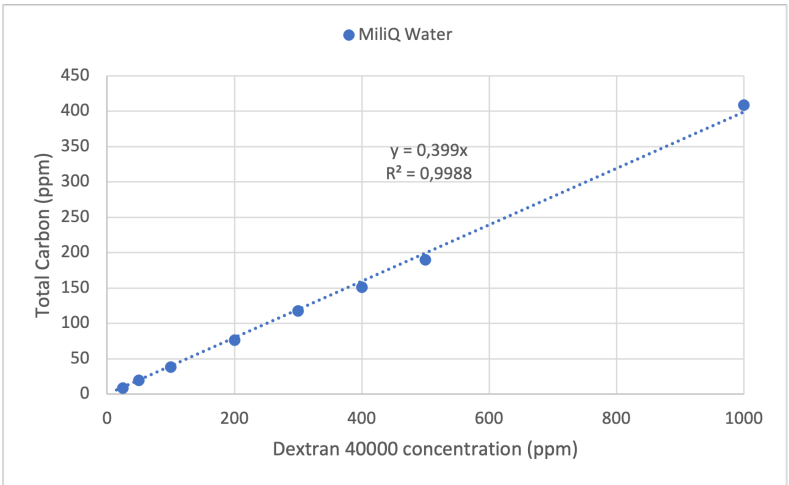

Figure F.7: Dextran 40000 Total Carbon as a function of the concentration